NICKELOCENE, FERROCENE, AND BENZENE ADSORBED ON SILICA AND ACTIVATED CARBON: A SOLID-STATE NMR STUDY

A Dissertation

by

JORDON WILLIAM BENZIE

Submitted to the Office of Graduate and Professional Studies of
Texas A&M University
in partial fulfillment of the requirements for the degree of

DOCTOR OF PHILOSOPHY

Chair of Committee,	Janet Bluemel
Committee Members,	James Batteas
	Sarbajit Banerjee
	Terry Creasy
Head of Department,	Simon North

December 2020

Major Subject: Chemistry

ABSTRACT

The ultimate goal of this thesis was to explore a new strategy for creating a nickel single atom catalyst (SAC) on a silica or activated carbon surface. It has been demonstrated in a preliminary experiment earlier that SAC formation might be possible by reducing nickelocene that had been dispersed on silica in a monolayer, with hydrogen. A Ni(0) catalyst had been obtained that was active for the cyclotrimerization of acetylenes. In order to explore this venue in detail, the objective of this thesis was to thoroughly investigate dynamic processes on silica surfaces that involve the supported molecular nickel complex nickelocene. As models for the paramagnetic and moderately sensitive nickelocene, benzene and the diamagnetic ferrocene have been employed. The studies relied mostly on solid-state NMR analyses because a plethora of different insights can be gained by this technique, especially with respect to molecular motions on surfaces. Dynamic processes do not only occur when catalysts immobilized covalently via linkers are suspended in a solvent. It has been discovered previously that metal complexes adsorbed via van der Waals interactions can also display different modes of mobility on diverse surfaces within pores, even in the absence of a solvent. Benzene and ferrocene can easily be obtained as deuterated species, which allow deuterium solid-state NMR analyses of their orientation on surfaces and their dynamics. Ferrocene can additionally be investigated as representative for all metallocenes and in particular for nickelocene that is slightly more reactive. For benzene, slow exchange between semi-bound and stationary, firmly adsorbed states has been found. In contrast to intuition, ferrocene is mostly adsorbed lying sideways on the surface. Nickelocene in comparison shows similar behavior, but a more robust interaction with the surface. When ferrocene and nickelocene are adsorbed in a sub-monolayer on the same surface they mix on the molecular level. This could be determined by analyzing the proton wideline signal halfwidths and relaxation times of both components at variable temperatures. The strong interactions between nickelocene and ferrocene on the support surface might even allow one to create well-defined dual Ni/Fe atom catalysts on the surface. The results described in this thesis enhanced the fundamental knowledge about how to create and characterize precursors for well-defined, atom-efficient, recyclable, supported catalysts which can lead to more sustainable processes in the future.

ACKNOWLEDGEMENTS

I would like to thank my committee chair, Dr. Janet Bluemel, and my committee members, Dr. Sarbajit Banerjee, Dr. James Batteas, and Dr. Terry Creasy, for their guidance and support throughout the course of this research, as well as Dr. Vladimir Bakhmutov for showing me how to use the solid-state NMR.

I would like to give special thanks to my friends who have been a reliable support network throughout my time in graduate school here at Texas A&M University, in particular my former housemates Chris Delaney, Chris Mallis, and Andrew Jeffries, who helped me through practice presentations and exam preparation in the early years of the program.

Thanks also go to my colleagues and mentees in the Bluemel group, past and present, as well as Valerie and Sandy, all whom have made me feel welcomed from day one at Texas A&M University.

I would also like to acknowledge and thank the GSAC 2019-2020 executive committee, and all of those that put their trust in me and allowed me to develop my leadership skills outside of the lab as the former GSAC President.

Finally, thanks to my parents, Anne and Allan, for their encouragement and support through undergraduate and graduate school, and to Kelly for her patience, kindness and love.

CONTRIBUTORS AND FUNDING SOURCES

Contributors

The research described in this thesis was supervised by the committee chair, Dr. Janet Bluemel, and supported by the committee members, Dr. Sarbajit Banerjee, Dr. James Batteas of the Department of Chemistry, and Dr. Terry Creasy of the Department of Materials Science and Engineering. Dr. Vladamir Bakhmutov assisted in using the solid-state NMR spectrometer for sample analyses, simulations of spectra and data evaluation. All other work conducted for the thesis was completed by the student independently.

Funding Sources

This work was supported by the National Science Foundation (CHE 1900100).

TABLE OF CONTENTS

Page

LIST OF FIGURES

LIST OF TABLES

Page

CHAPTER I

INTRODUCTION

Overview

Solid-state nuclear magnet resonance (NMR) spectroscopy has increasingly become a more mainstream form of analysis across academia and industry. Modern techniques allow the analysis of a large variety of compounds and materials in the solid state. Classical applications are found in polymers, regardless of nature, be that organic, organic-inorganic hybrid, or organometallic. One can investigate the purity, tacticity and dynamics of polymers, and, for example, distinguish between crystalline and amorphous regions. Characteristics of solid materials such as phase transitions or defects in the crystal lattice can also be studied conveniently by solid-state NMR. Important insights about structures and processes on surfaces can be gained, in particular those of solid immobilized and heterogeneous catalysts, such as zeolites. All amorphous and insoluble substances, and compounds that would be destroyed upon solution, like self-assembly materials and clathrates, can be investigated by solid-state NMR.

Bulk characteristics of materials in solution and in diverse solid states can be compared readily. For example, a coordination compound might display a different arrangement of ligands around the metal center in solution than in the solid state, when crystal packing forces are dominant. Often solid-state NMR provides the decisive clue about a disordered crystalline substance, so that a challenging X-ray structure can finally be solved with this additional piece of information because both methods are complementary. Finally, for the research discussed in this thesis it is important to know that even in the solid state dynamic processes take place that can be analyzed with solid-state NMR. In host-guest assemblies, like substances adsorbed on the surface within pores of a support material, the adsorbate can often display several different modes of mobility, including but not limited to translational movements. Rotational processes of functional groups and substituents are also found in crystalline compounds. For example, a methyl group always rotates about the threefold $-CH_3$ axis at ambient temperature, while trimethylsilyl groups rotate about the threefold $-SiMe_3$ axis. The same is true for cyclopentadienyl (Cp) ligands in metallocenes that rotate about the fivefold metal−(Cp center) axis. This dissertation will focus on the use of different solid-state NMR spectroscopic techniques to study the molecular motions of benzene, ferrocene, and nickelocene adsorbed on the surfaces of silica and activated carbon.

The first chapter of this body of work will cover the adsorption and mobility of benzene and cyclohexane on activated carbon (**AC**). Benzene-d_6 and cyclohexane-d_{12} have been adsorbed on the surface within the pores of high-surface area active **AC**. Their molecular motions have been characterized by variable-temperature ^2H and ^{13}C solid-state NMR spectroscopy. Three different states of benzene molecules on the **AC** surface have been found: isotropically moving molecules, bound molecules and intermediates between these states. In contrast to cyclohexane, benzene assumes stationary states that are stabilized by π - p interactions with the **AC** surface. Hereby, fast in-plane C_6 rotations take place. The adsorption enthalpy $-\Delta H^0$ for benzene on the surface of **AC** within the pores was determined as 4.6 ± 0.3 kcal/mol. The strongly adsorbed molecules undergo slow exchange with isotropically moving, liquid-like molecules. In contrast to this, exchange between the molecules in a liquid-like state with benzene in semi-bound states (T-complexes) is very fast, requiring only low activation energies E_{act} and $\Delta H^{\ddagger}$ of 3.1 and 2.7 kcal/mol, respectively.

The second section of this document explores the adsorption of nickelocene on the surface of silica within the pores by dry grinding in the absence of a solvent at room temperature. While the dry adsorption and translational mobility of nickelocene within the pores are already established visually, there is little systematic understanding of the surface site-to-site motions of the nickelocene molecules and their orientation with respect to the surface. In this chapter, silica is used as support material. Using paramagnetic variable temperature ^1H solid-state NMR and T_1 relaxation time measurements, the dynamics of nickelocene on the surface of silica within the pores has been quantitatively characterized on the molecular scale. The obtained data indicate that nickelocene molecules show a liquid-like behavior on the surface. Fast exchange between isotropically moving molecules and surface-attached molecular states of nickelocene has been found in a sample with sub-monolayer surface coverage.

The final portion of this body of work further explores the themes of the previous section. Again, utilizing paramagnetic variable temperature ^1H solid-state NMR and T_1 relaxation time measurements, the dynamics of nickelocene on the surface of silica within the pores has been quantitatively characterized on the molecular scale. Using samples with additionally adsorbed ferrocene, it could be proven that both metallocenes mix on the molecular level on the surface. The phase states of both components can be described as highly viscous liquids.

Solid-State Nuclear Magnetic Resonance

A recurring theme in all chapters of this dissertation are the analysis of anisotropic interactions that are probed via the use of solid-state NMR spectroscopy. Anisotropic interactions are cumulative in the solid state, and they can be described in the form of their corresponding Hamiltonians.[18,19]

$$\widehat{H} = \widehat{H}z + \widehat{H}_{\mathrm{Q}} + \widehat{H}_{\mathrm{D}} + \widehat{H}_{\mathrm{g}} + \widehat{H}_{\mathrm{CS}} + \widehat{H}_{\mathrm{J}}.$$

Of these Hamiltonian expressions, only $\widehat{H}_{\mathrm{z}}$, the Zeeman interaction, is isotropic and determined by the external magnetic field. The remainder of the interactions when regarding their size and presence, are defined by the sample material. The typical maximal values for H_{z} and the anisotropic interactions are given in Table 1, and the values listed are indicative of how broad the signals can become in a solid-state NMR spectrum when these particular interactions are present.

Anisotropy is a property of substances, in this dissertation the nuclei of the compounds being studied through solid-state NMR, to exhibit variations in physical properties along different axes. These interactions are directional in space and as such manifest in the solid-state, whereas in a liquids NMR these interactions are reduced through random tumbling of molecules in a solution which will average out by giving these nuclei a “spherical” shape. A crucial point in the following chapters will be that probing the anisotropic interactions under various conditions allows to determine mobilities in the solid state. For example, a reduction of the chemical shift anisotropy (CSA) and therewith the signal width when transitioning from polycrystalline to adsorbed substances indicates that a certain degree of reorientation of the molecules occurs on the surface. Using multinuclear and variable-temperature solid-state NMR techniques then allows to disentangle different modes of mobility.

Table 1. Interactions in the solid state, their dependence on the external magnetic field B_o, and the typical values found for static samples.

$\widehat{H}z$	**Zeeman** interaction	(splitting of spin energy levels in B_o)	~ B_o	**50 000 000 Hz** (50 MHz)
$\widehat{H}_{\mathrm{Q}}$	**Quadrupolar** interactions	only for $I > 1/2$	1st order H_Q independent of B_o, 2nd order $H_Q \sim 1/B_o$	**5 000 000 Hz** (5 MHz)
$\widehat{H}_{\mathrm{D}}$	**Dipolar** interactions	Direct Homo- and Hetero-nuclear couplings	independent of B_o	**100 000 Hz** (0.1 MHz)
$\widehat{H}_{\mathrm{g}}$	Interactions with **electron spins**	Paramagnetic samples	dependent on B_o (complex)	**100 000 Hz** (100 kHz)
$\widehat{H}_{\mathrm{CS}}$	**Chemical Shift** interactions	Chemical Shift Anisotropy (CSA)	~ B_o	**20 000 Hz** (20 kHz)
$\widehat{H}_{\mathrm{J}}$	**Scalar Couplings**	Indirect *J* couplings	independent of B_o	**100 Hz**

Magic Angle Spinning (MAS)

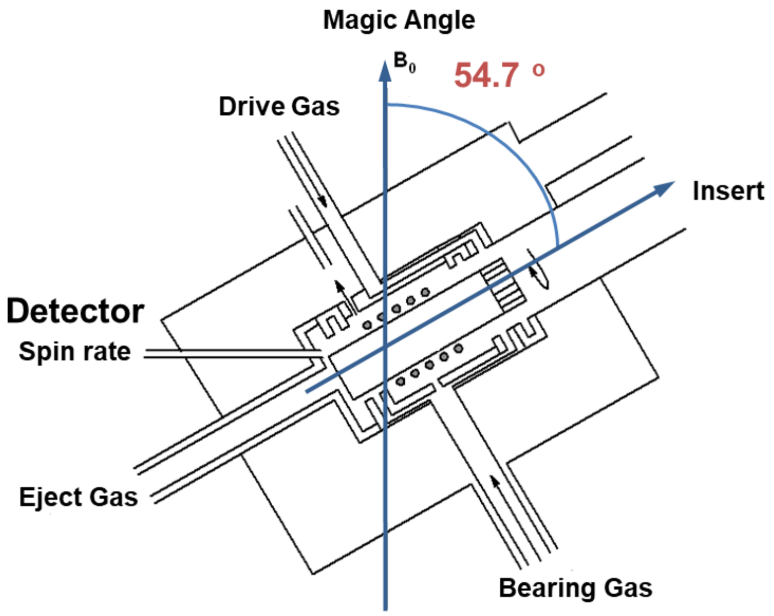

Figure 1. Depiction of the internal components of a solid-state probe and rotor.

To deal with the anisotropic nature of solid-state NMR samples, spinning at the “Magic Angle” is required to reduce most of the interactions and allow narrower signals that are more representative of liquids measurements to be viewed in the spectrum. A solid-state NMR probehead will be equipped with a Magic Angle Spinning (MAS) unit to enable rotation about the magic angle, 54.7° (Figure 1), in respect to the magnetic field, and this serves to simplify the Hamiltonian of the CSA tensor in equation (**1**) by reducing the ($3\cos^2\theta$-1) term to zero. Ultimately, this results in a spectrum that contains only the isotropic chemical shift of the desired substance being measured.

$$\textbf{(1)}\quad \widehat{H}_{CSA} = \underbrace{\gamma h \sigma_{iso} B_0 \hat{I}_z}_{\text{Isotropic chemical shift } (\delta_{iso})} + \gamma h B_0 \hat{I}_z \tfrac{1}{2} \left[(3\cos^2\theta\text{-}1)(\sigma_{33} - \sigma_{iso}) + \underbrace{(\sin^2\theta \cos^2\psi(\sigma_{22} - \sigma_{11}))]}_{\text{Rotational Sidebands}}\right.$$

Chemical Shift Anisotropy (CSA)

It was previously highlighted that the orientation of the molecule in space is of significant importance in the solid-state, and that the chemical shift anisotropy (CSA) of a signal can be used as an analytical tool to determine the mobility of a molecule on a surface. An example of this, is seen in previous work by the Bluemel group whereby a comparison can be drawn between a sample of triphenylphospine in its polycrystalline form and when it is adsorbed on the surface of a material such as silica gel. In the bottom spectrum of Figure 2, it can be seen that polycrystalline triphenylphosphine has a large ^{31}P CSA with a span of ~60 ppm, and that when spinning is applied with an increasing frequency from 2 to 4 kHz that rotational sidebands can be seen, which are indicative of residual CSA (Top, Figure 2).

A significant change in the CSA can be seen when the triphenylphosphine is adsorbed onto the surface of silica through solvent free dry grinding as a sub-monolayer. Without rotation it can be seen that there is a single isotropic chemical shift that corresponds to the triphenylphosphine in solutions NMR (Figure 3). While the signal appears to still be somewhat broad at 4 kHz spinning, it should be noted that no rotational sidebands have been generated, and that the signal width is reduced when compared to the static sample, this is indicative of solution-like reorientation of the molecules on the surface and in the pores of silica.

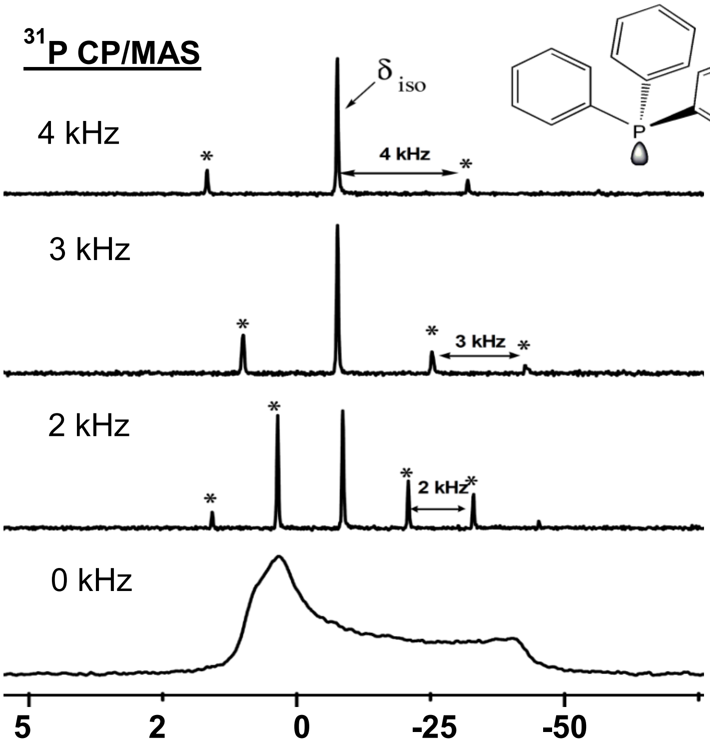

Figure 2. ^{31}P CP/MAS spectra of polycrystalline triphenylphosphine at different rotational speeds.[20]

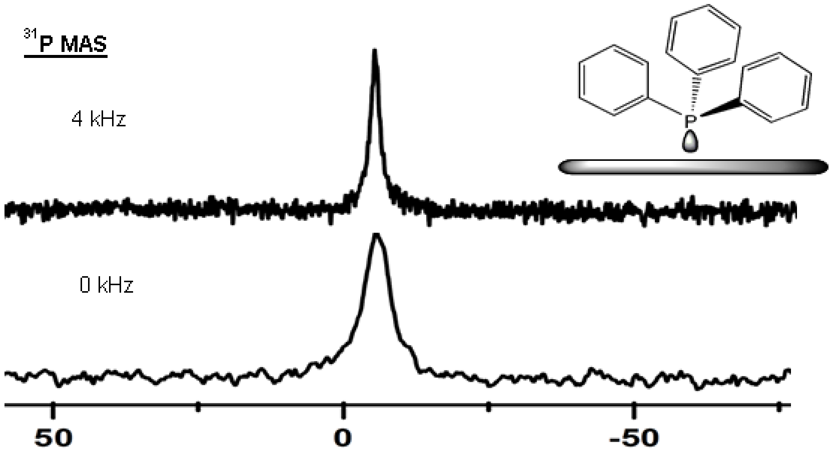

Figure 3. ^{31}P MAS spectra of triphenylphosphine adsorbed on silica.[20]

Quadrupolar Interactions

Nuclei with as spin quantum number I > ½ have a non-spherical distribution of charge in the nucleus, which gives rise to a quadrupole moment. The quadrupole moment occurs due to unsymmetrical distribution of charge within the nuclei, which gives rise to two different non-spherical nuclei; prolate and oblate. Prolate nuclei are longer in the direction of their nuclear spin angular momentum, possessing a cigar-type shape with a Q > 0. Oblate nuclei bulge near their "equator" and possess a Q < 0.

In solutions NMR the fast isotropic tumbling and reorientation of molecules will result in the averaged out quadrupolar interactions, thus deconvolution of the resulting NMR spectrum will be seen and these types of nuclei can be easily measured. The half width in solution, $\nu_{1/2}$, is given in equation (**2**).[18]

$$\textbf{(2)}\quad \Delta\nu_{1/2} = 3/10 \cdot \pi \cdot (2I+3)/[I^2(2I-1)] \cdot (e^2Qq/h)^2 \cdot \tau_c$$

Here τ_c is the correlation time, q the electric field gradient, and (e^2Qq/h) is the quadrupolar coupling constant, Q_C.

From this equation it follows that the quadrupolar coupling constant can be obtained from measuring the halfwidth of a signal. The lines in the spectrum can be made narrower by reducing the correlation time, or in simpler terms, making the molecules in solution more mobile. It is important for this purpose to ensure that the solvent used is as non-viscous and as dilute as possible, and that the temperature of measurement is as high as possible. Smaller molecules will have smaller correlation times, thus the resulting half-width will be smaller too. This is the reason why ^{14}N is an often favoured nucleus for measuring small organic and organometallic molecules, whilst in proteins and soluble polymers it is not competitive to the spin ½ nucleus ^{15}N.

As mentioned previously the quadrupolar interactions are mostly cancelled out by the rapid reorientation of the molecules when they are in solution, in the solid state they can be rather prominent. First order quadrupolar interactions result when the quadrupolar coupling constant is relatively small as compared to the Zeeman interaction. If there are only first order quadrupolar interactions, then the line shapes of the spectrum should be realtively simple as well as predicatable, and should be easy to interpret and simulate. In the case of second order quadrupolar interations, the situation is rather different, leading to complicated and unpredictable spectra.

Deuterium is an easy to measure quadrupolar nucleus with mostly first order quadrupolar interactions and a spin of 1. These features render it an excellent candidate for solid-state NMR studies. A typical Pake pattern is shown in the deuterium spectrum of Cp_2Fe-d_2 in Figure 4.

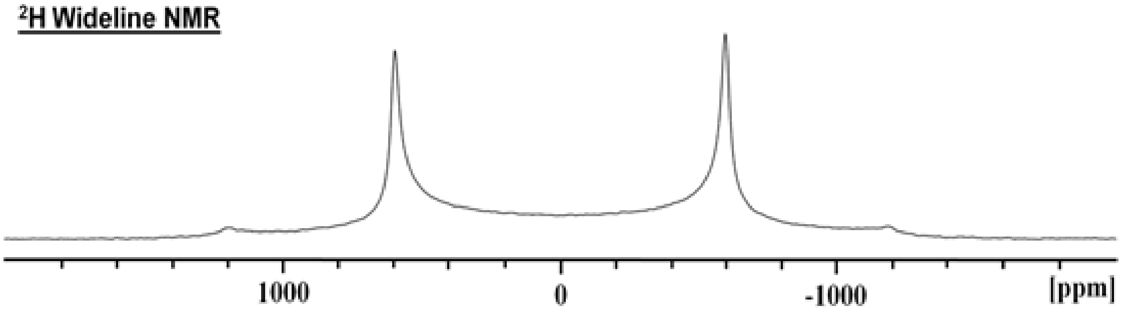

Figure 4. ^{2}H Wideline spectrum of Cp_2Fe-d_2.

From this spectrum the quadrupolar coupling constant can be derived using equation (**3**)[18] based on the distance between the two inner peaks $\Delta\nu_i$ in Hz. Furthermore, the isotropic chemical shift for the deuterium Pake patterns is found at the center of the signal. Therefore, from the Pake pattern one can obtain δ_{iso}, as well as the characteristic quadrupolar coupling constant Q_C.

$$\textbf{(3)}\quad \Delta\nu_i = 3/4\ (e^2qQ/h)$$

Paramagnetic Nuclear Magnetic Resonance

Compounds that contain unpaired electrons are paramagnetic. The unpaired electron can be part of an organic framework, such as in organic radicals, or they can be attached to a metal atom. Transition metals are most likely to have paramagnetic forms, as the shift of electrons between energy levels is relatively easy. Examples of these complexes are porphyrins, metallocenes, and chemical shift reagents such as chromium (III) acetylacetonate.

When conducting paramagnetic NMR it is essential to understand the basic characteristics that stand it apart from measuring diamagnetic NMR samples, and the characteristics that the target nuclei should possess to make this easier to analyze. A general rule of thumb is that the nuclei directly bound to the paramagnetic center cannot be recorded as the relaxation process is too fast. It can be recorded on a conventional NMR spectrometer, adjusting the parameters accordingly to see the desired signals of the sample in question, provided that the electronic spin relaxation time, τ_e, is in the region of 10^{-9} to 10^{-13} seconds. If the electronic spin relaxation is slower than this electronic paramagnetic resonance spectroscopy (EPR) may be employed instead. The chemical shift range is much larger, for a typical paramagnetic ^{13}C NMR sample this range spans from -200 to +1500 ppm, and the signals that are observed are typically broader with halfwidths reaching the kHz scale, it is worth noting that as the nuclei get closer to the paramagnetic center the signals they produce get broader, as well as further shifter from the diamagnetic region. It is important that the sample temperature remain consistent for the duration of the measurement, as the chemical shifts are very dependent on temperature, and the higher the temperature the more likely the signal is to migrate towards the diamagnetic region.

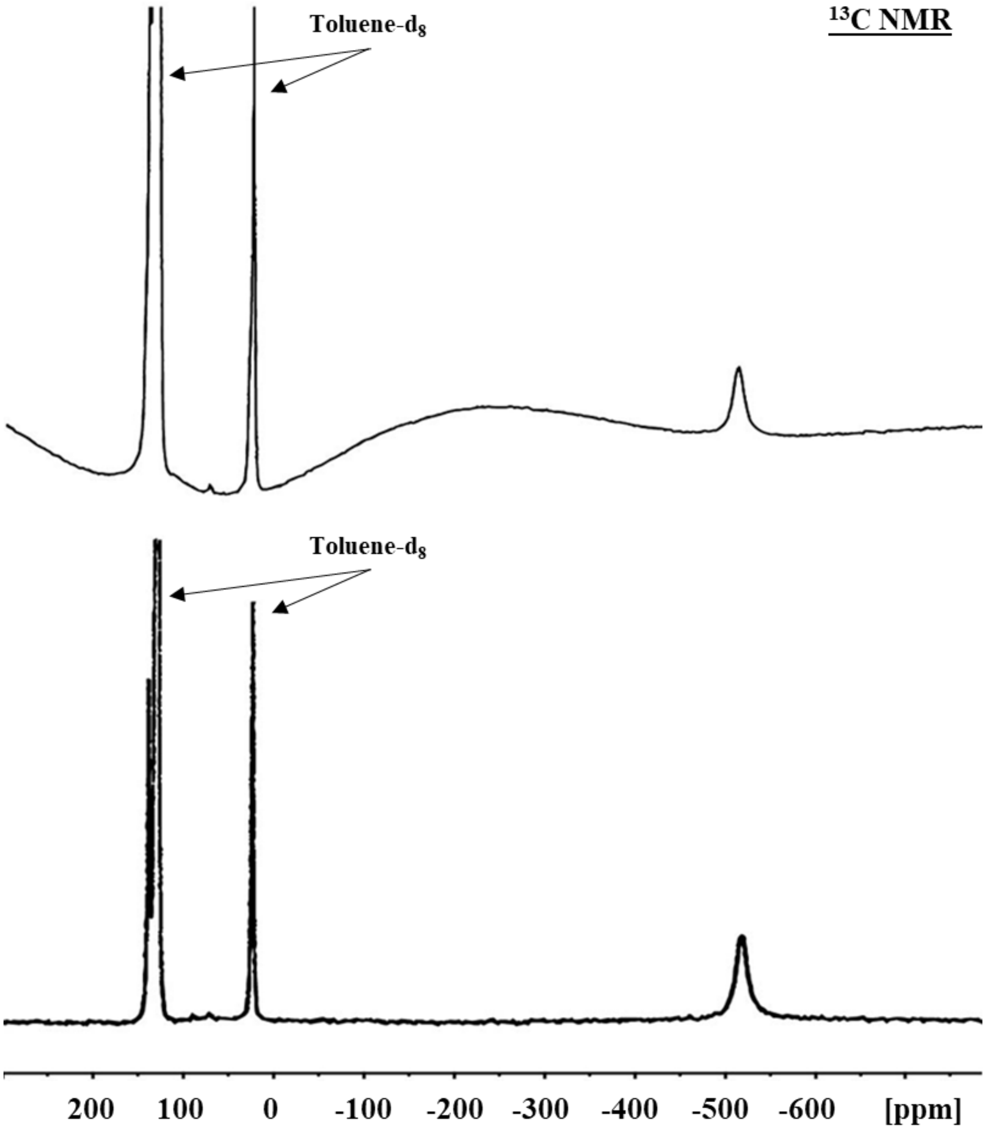

Figure 5 ^{13}C NMR of vanadocene. Bottom trace has a reduced deadtime compared to the top trace to allow for simpler first order phase corrections.

When measuring samples in practice there are many different things to consider when compared to diamagnetic NMR. The solution of the sample should be as concentrated as possible, in contrast to what is desired in diamagnetic sample, as the linewidths will be decreased. Deuterated solvents should be employed, although locking and shimming are not needed, and the high concentration allows for the sample to show up as visibly as possible without being engulfed by the solvent signal or causing "dynamic range" issues, that is, the signal would be below the threshold for digitalization. To further add to this a dominant solvent signal may pose issues for any first order phase corrections. Solvent signals can be reduced further by applying "dummy scans", where RF pulses are applied to the sample without recording the spectrum. This allows the solvent to reach saturation of its magnetization, before continuing RF pulses with data collection ("real" scans). In short, concentrated samples are highly coveted in paramagnetic NMR.

The T_1 and T_2 parameters for paramagnetic compounds are approximately equal, and within the millisecond range, therefore one can use short pulse delays between 100 and 200 ms without loss of signal intensity. The longitudinal and transverse relaxation times can be estimated from the linewidths of the signal according to the equation **4**.

$$\textbf{(4)}\quad \Delta^{\mathrm{exp.}} = 1/(\pi T_2) \approx 1/(\pi T_1)$$

Surface Coverage and Adsorbates

A recurring theme amongst the following chapters in this dissertation is determining the maximal amount of a compound that can be adsorbed onto a given surface in sub-monolayer, monolayer, and excess coverages. The question posed here can be addressed in a number of ways, but the simplest and most straightforward is to rationalize the footprint of the adsorbate as a 2D projection on the adsorbent surface, treated in a planar fashion. A depiction of this can be seen in Figure 6.

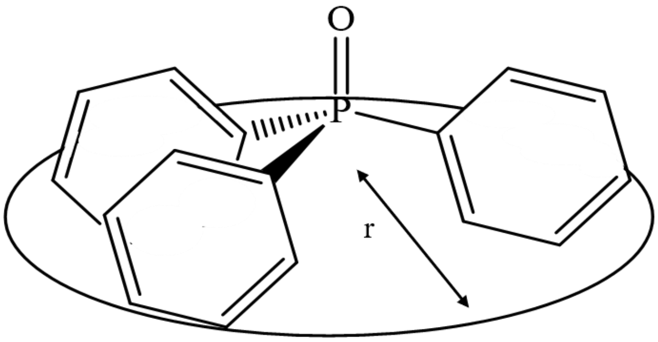

Figure 6. 2D Projection of **1** used to calculate its footprint on an idealized surface.

The proposed view of the adsorbate allows determination based on surface area occupied by each molecule, using the Van der Waals radius obtained from the molecule's crystal structure. This footprint can be used with the known surface area of the support material adsorbent to estimate the desired surface coverage, which once the details of radii and surface coverage are known a gravimetric approach can be taken. As already mentioned, there are three main types of surface coverage scenarios that are utilized in this dissertation, all of which are depicted in Figure 7.

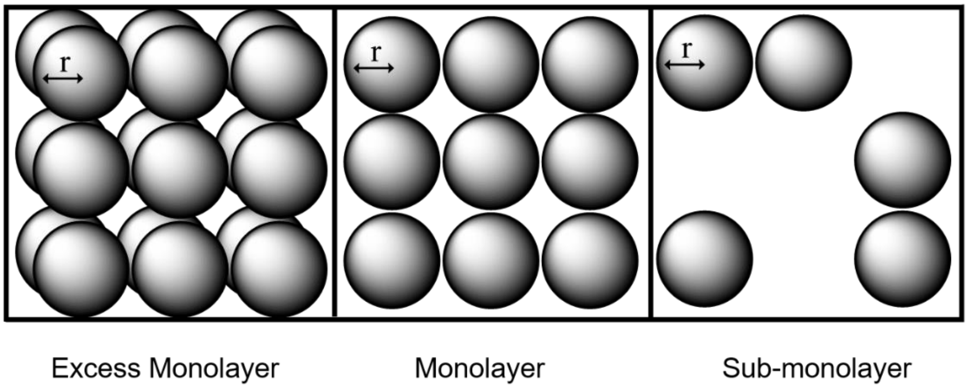

Figure 7. Three possible loadings of molecules on a surface**.**

Metallocenes

Metallocenes are organometallic "sandwich" complexes that are termed such due to a metal ion being placed between two cyclopentadienyl rings with η^5-coordination, or similar extended aromatic ring systems.[43] The first metallocene, ferrocene, was characterized by single X-ray diffraction in 1951, and Geoffrey Wilkinson and Ernst Otto Fischer shared the 1973 Nobel Prize in Chemistry for this discovery.

The Bluemel group discovered recently that metallocenes of the type Cp_2M (Cp = cyclopentadienyl, C_5H_5) can be adsorbed on silica by dry grinding of the components in the absence of solvents.[46-48] However, some metallocenes, like vanadocene and chromocene, react rather quickly with the surface after the adsorption step. By reacting with silica, chromocene forms the important heterogeneous Union Carbide catalyst that is utilized in industry for olefin polymerization under mild conditions in the absence of a co-catalyst.[49,51] Despite the importance and scale of utility of this particular catalyst, very little is actually known about the structure of it on oxide surfaces. The commonly accepted partial structure of the catalytically active species consists of a CpCr(III) moiety that must be bound to a surface siloxide anion, as determined mostly by solid-state NMR,[48] and XPS and IR studies.[50,51]

In our endeavors to identify the complete structure of the surface-bound chromium species, chromocene has been dry-ground with silica in the absence of solvent or any other chemicals that could influence the outcome of the surface reaction. However, it was seen that without a solvent that the reaction took place too quickly to allow for a sufficient time window to study the initial reaction steps that occur via solid-state NMR or other methods. Due to this, efforts were shifted towards another metallocene, ferrocene, which is less reactive and stable under inert conditions for a much longer timescale. Obtaining a deeper insight into the mechanisms and structure of ferrocene on different surfaces, parallel conclusions should be able to be drawn to chromocene as they are structurally identical with exception to the metal ion. Of great importance in these studies is the orientation of ferrocene on the surface of silica, as the reaction that would occur between the surface silanol groups and the metallocene can only proceed through the metal ion and not through the Cp ring. In short, a sideways orientation of ferrocene must occur at some point to facilitate the reaction between the metal and the surface. Ferrocene when adsorbed on the surface, and also in the presence of oxygen will react to produce a blue colored material instead of the usual orange color, this is indicative of ferrocenium salts being generated at the surface silanol sites,[23e] and therefore, it can be anticipated that a sideways orientation of ferrocene will have occurred at some stage of immobilization.

Nickelocene is another metallocene of interest in these quantitative studies investigating the interactions between these organometallic compounds and surfaces as it can be utilized as a precursor for single atom catalysts (SAC). However the approach in analyzing it is complicated due to its high instability in air and its paramagnetic nature.

Volatile Organic Compounds (VOCs)

Volatile organic compounds (VOCs) are a class of organic compounds that have a high vapor pressure, even at room temperature. Volatility is a measure of how easily a compound vaporizes. A common misconception regarding VOCs is that they are always in a liquid state. This however is untrue as solid materials such as benzoic acid have a high vapor pressure at room temperature, and are also considered a VOC.

The World Health Organization (WHO) estimated that air pollution was responsible for more than seven million deaths in a study conducted in 2012.[52] Street vendors in Bankok, Thailand, reported respiratory issues,[53] and flight crews for aircrafts are exposed to numerous VOCs on a daily working basis causing potentially significant health problems.[54] VOCs are not limited to polluted cities and workplaces, but also in households.[55] These examples are just a small portion of the health issues that we face from VOCs on a daily basis.

Due to the toxic nature of VOCs, a plethora of research involving remedial means to combat them in the environment. There are three major materials utilized in adsorption of VOCs: activated carbon, zeolites and hypercrosslinked polymeric resins.[56] Activated carbon has received significant attention in its ability to adsorb VOCs due to its incredibly large surface area per gram of material and the simplicity it has in being modified for targeted adsorption. [56-60]

Through collaboration with a local waste management company, we have been working to apply our knowledge of adsorption to aid in the design of a new air purification system for the removal of noxious VOCs in waste receptacles. In addition to this a study into the new activated carbon materials and their ability to retain VOCs over a significant period of time was conducted.

Silica and Activated Carbon as Support Materials

Heterogeneous catalysis makes use of all sorts of inorganic oxides and ceramic materials. Silica and Alumina are used extensively in the Bluemel group because they are the most favorable supports for immobilized homogeneous catalysts,[23,61] and adsorbates.[1,2i,5,6,37,46-48] When compared to polymers, silica and alumina have numerous advantages,[65] most important of these is that the oxide supports are both chemically and thermally inert, and available in neutral forms when considering pH. Mechanically they are stable and robust, being able to endure stirring with a stir bar for days without being broken down into finer particulates, this is important when considering the reusability and separation when used as a support for a catalyst, as the supernatant of the reaction can be decanted easily once the material has settles post stirring. The most favorable particle size for the purposes of this dissertation are 0.0063-0.200 mm, which corresponds to large grains that will settle fast (in approximately 5 minutes) in organic solvents. This particle size also allows for easy handling under a nitrogen stream or in a glove box, as well as filling the rotors for solid-state NMR samples. Suppliers offer a large selection of well-defined silica and alumina with different characteristic pore sizes or specific surface areas depending on the function intended for its use. It is important to note that the pore sizes must be big enough to accommodate catalysts, substrates, or adsorbates to enter and exit with the ability to move around freely without any noteworthy diffusion delays. The most powerful tool utilized in this dissertation is moderately sensitive solid-state NMR,[18,19,23,62,63] it is essential to have the largest possible specific surface area that allows for maximal loading of adsorbate or catalyst, with minimal adsorbent possible, that can be handled easily. Silica with an average pore size of 40 Å and a specific surface area of 750 m^2/g has proven to be the optimal choice over decades of research in the Bluemel group and was therefore chosen as the metallocene adsorbent utilized for all work presented in this dissertation. To create consistently reproducible results, and maintain the same quality of adsorbent, the silica is treated before used by drying at 200 ^{o}C for 2 days *in vacuo* to remove any water and condense the silanol surface groups as much as possible. When utilizing activated carbon it does not need to be treated in this way as it does not readily soak up water or moisture from the atmosphere.

It should be noted that the other popular porous materials listed previously are simply not viable for adsorbing metallocenes. Zeolites and metal organic frameworks (MOFs) have too small pore sizes, and MOFs in particular do not have a contiguous surface area that is required for adsorbate-adsorbent interactions and mobility on the surface. In addition to this, all supports utilized are available from chemical suppliers in bulk with certification attesting to the physical qualities they have, as well as being relatively inexpensive and environmentally benign.

Conclusion

In conclusion, the work presented in this thesis has deepened the understanding of adsorption processes and the mobility behaviors of metallocenes and organic compounds on support surfaces in the absence of solvents. The benzene-d_6 molecular motion in the pores of **AC** have been characterized for the first time. Isotropically moving and stationary molecules, as well as molecules in the intermediate states in exchange with isotropically moving molecules, have been identified. The molecular dynamics of nickelocene on silica have been demonstrated to be similar to those of ferrocene on silica and triphenylphosphine oxide on alumina, in spite of differences in the surface-molecule interactions. The co-adsorption of diamagnetic ferrocene and paramagnetic nickelocene on silica has provided important insights into the dynamic processes on the surface, with these adsorbed metallocene molecules mixing on the surface at a molecular level, and ultimately exhibiting characteristics that can be described as highly viscous liquids.

References

1. C. R. Hilliard, N. Bhuvanesh, J. A. Gladysz, J. Blümel, *Dalton Trans.* **2012**, *41*, 1742.

2. **(a)** J. Blümel, *Coord. Chem. Rev.* **2008**, *252*, 2410-2423. **(b)** J. Guenther, J. Reibenspies, J. Blümel, *Adv. Synth. Catal*. **2011**, *353*, 443-460. **(c)** R. Silbernagel, A. Diaz, E. Steffensmeier,A. Clearfield, J. Blümel, *J. Mol. Catal. A* **2014**, *394*, 217-223. **(d)** C. Merckle, J. Blümel, *Adv. Synth. Catal.* **2003**, *345*, 584-588. **(e)** C. Merckle, J. Blümel, *Top. Catal.* **2005**, *34*, 5-15. **(f)** J. C. Pope, T. Posset, N. Bhuvanesh, J. Blümel, *Organometallics* **2014**, *33*, 6750-6753. **(g)** T. Posset, J. Blümel, *J. Am. Chem. Soc.* **2006**, *128*, 8394-8395. **(h)** T. Posset, J. Guenther, J. Pope, T. Oeser, J. Blümel, *Chem. Commun.* **2011**, *47*, 2059-2061. **(i)** K. J. Cluff, N. Bhuvanesh, J. Blümel, *Chem. Eur. J.* **2015**, *21*, 10138-10148. **(j)** J. H. Baker, N. Bhuvanesh, J. Blümel, *J. Organomet. Chem*. **2017**, *847*, 193-203.

3. R. Yerushalmi, J. C. Ho, Z. Fan, A. Javey, *Angew. Chem. Int. Ed*. **2008**, *47*, 4440.

4. **(a)** A. R. Wilmsmeyer, W. O. Gordon, E. D. Davis, B. A. Mantooth, T. A. Lalain, J. R. Morris, *Rev. Sci. Instrum*. **2014**, *85*, 014101. **(b)** J. Kemsley, *Chem. Eng. News* **2014**, *92*, 29.

5. S. Kharel, T. Jia, N. Bhuvanesh, J. H. Reibenspies, J. Blümel, J. A. Gladysz, *Chem. Asian J.* **2018**, *13*, 2632-2640.

6. C. R. Hilliard, S. Kharel, K. J. Cluff, N. Bhuvanesh, J. A. Gladysz, J. Blümel, *Chem. Eur. J.* **2014**, *20*, 17292-17295.

7. **(a)** T. Kovacs, G. Keglevich, *Curr. Org. Chem*. **2017**, *21*, 569-585. **(b)** D. Herault, D. H. Nguyen, D. Nuel, G. Buono, *Chem. Soc. Rev*. **2015**, *44*, 2508-2528. **(c)** M. D. Fletcher, *Organophosphorus Reagents*, **2004**, 171-214. **(d)** H. R. Hays, D. J. Peterson, *Org. Phosphorus Compounds*, **1972**, *3*, 341-500. **(e)** H. Adams, R. C. Collins, S. Jones, C. J. A. Warner, *Org. Lett*. **2011**, *13*, 6576-6579.

8. K. J. Cluff, J. Blümel, *Organometallics* **2016**, *35*, 3939−3948.

9. K. J. Cluff, M. Schnellbach, C. R. Hilliard, J. Blümel *J. Organomet. Chem*. **2013**, *744*, 119-124.

10. H. Marsh, F. Rodriguez-Reinoso, *Activated Carbon* (Oxford: Elsevier), **2006**.

11. S. Bubanale, Shivashankar, M. History, *Intern. J. Engin. Research & Technol.* **2017**, *6*, 495-497.

12. N. Wibowo, L. Setyadhi, D. Wibowo, J. Setiawan, S, Ismadji, *J. Hazard. Materials* **2007**, *146*, 237–242.

13. M. M. Dubinin, N. S. Polyakov, L. I. Kataeva, *Carbon* **1991**, *29*, 481-488.

14. H. L. Chiang, C. P. Huang, P. C. Chiang, *Chemosphere* **2002**, *46*, 143-152

15. H. Hindarso, S. Ismadji, F. Wicaksana, N. Mudjijati, H. Indraswati, *J. Chem. Eng. Data* **2001**, *46*, 788–791.
16. M. C. Basso, A. L. Cukierman, D. Arundo, *Chem. Res*. **2005**, *44*, 2091–2100.
17. Y. Xu, T. Watermann, H.-H. Limbach, T. Gutmann, D. Sebastianib, G. Buntkowsky, *Chem. Phys*. **2014**, *16*, 9327- 9336.
18. C. A. Fyfe, C.F.C. Press, Guelph, Canada, **1983**.
19. T. M. Duncan, T. M. Farragut, Press: Chicago, IL, **1990**.

20. Y. Yang, Dissertation, University of Heildelberg, **2007**.

21. S. Kharel, T. Jia, N. Bhuvanesh, J. H. Reibenspies, J. Blümel, J. A. Gladysz, *Chem. Asian J.* **2018**, *13*, 2632-2640.

22. **(a)** J. Chrzanowski, D. Krasowska, J. Drabowicz, *Heteroatom Chem*. **2018**, *29*, e21476. **(b)** T. Kovacs, G. Keglevich, *Curr. Org. Chem*. **2017**, *21*, 569-585. **(c)** D. Herault, D. H. Nguyen, D. Nuel, G. Buono, *Chem. Soc. Rev*. **2015**, *44*, 2508-2528. **(d)** M. D. Fletcher, *Organophosphorus Reagents*, **2004**, 171-214. **(e)** H. R. Hays, D. J. Peterson, *Org. Phosphorus Compounds*, **1972**, *3*, 341-500. **(f)** H. Adams, R. C. Collins, S. Jones, C. J. A. Warner, *Org. Lett*. **2011**, *13*, 6576-6579. **(g)** K. C. K. Swamy, N. N. B. Kumar, E. Balaraman, K. V. P. P. Kumar, *Chem. Rev.* **2009**, *109*, 2551-2651. **(h)** R. H. Beddoe, K. G. Andrews, V. Magne, J. D. Cuthbertson, J. Saska, A. L. Shannon-Little, S. E. Shanahan, H. F. Sneddon, R. M. Denton, *Science* **2020**, *365*, 910-914. **(i)** D. W. Stephan, *Science* **2016**, *354*, 1248. **(j)** J. M. Bayne, D. W. Stephan, *Chem. Soc. Rev.* **2016**, *45*, 765-774. **(k)** X. Cai, S. Majumdar, G. C. Fortman, L. M. Frutos, M. Temprado, C. R. Clough, C. C. Cummins, M. E. Germain, T. Palluccio, E. V. Rybak-Akimova, B. Captain, C. D. Hoff, *Inorg. Chem*. **2011**, *50*, 9620-9630.

23. Selected references: **(a)** J. Blümel, *Coord. Chem. Rev.* **2008**, *252*, 2410-2423. **(b)** J. Guenther, J. Reibenspies, J. Blümel, *Adv. Synth. Catal*. **2011**, *353*, 443-460. **(c)** R. Silbernagel, A. Diaz, E. Steffensmeier, A. Clearfield, J. Blümel, *J. Mol. Catal. A*, **2014**, *394*, 217-223. **(d)** J. H. Baker, N. Bhuvanesh, J. Blümel, *J. Organomet. Chem*. **2017**, *847*, 193-203. **(e)** J. C. Pope, T. Posset, N. Bhuvanesh, J. Blümel, *Organometallics* **2014**, *33*, 6750-6753. **(f)** T. Posset, J. Guenther, J. Pope, T. Oeser, J. Blümel, *Chem. Commun.* **2011**, *47*, 2059-2061. **(g)** K. J. Cluff, N. Bhuvanesh, J. Blümel*, Chem. Eur. J.* **2015, *21*, 10138-10148.**

24. J. Guenther, J. Reibenspies, J. Blümel, *Mol. Catal*. **2019**, *479*, 110629.

25. **(a)** A. Zheng, S.-B. Liu, F. Deng, *Chem. Rev.* **2017**, *117*, 12475−12531. **(b)** R. Yerushalmi, J. C. Ho, Z. Fan, A. Javey, *Angew. Chem. Int. Ed.* **2008**, *47*, 4440-4442. **(c)** J. P. Osegovic, R. S. Drago, *J. Phys. Chem. B*, **2000**, *104*, 147-154. **(d)** S. Hayashi, K. Jimura, N. Kojima, *Bull. Chem. Soc. Jpn.* **2014**, *87*, 69-75. **(e)** S. Machida, M. Sohmiya, Y. Ide, Y. Sugahara, *Langmuir* **2018***, 34,* 12694−12701.

26. **(a)** A. R. Wilmsmeyer, W. O. Gordon, E. D. Davis, B. A. Mantooth, T. A. Lalain, J. R. Morris, *Rev. Sci. Instrum*. **2014**, *85*, 014101. **(b)** J. Kemsley, *Chem. Eng. News* **2014**, *92*, 29-30.

27. P. J. Hubbard, J. W. Benzie, V. I. Bakhmutov, J. Blümel, *J. Chem. Phys*. **2020**, *152*, 054718.

28. S. Kharel, K. J. Cluff, N. Bhuvanesh, J. A. Gladysz, J. Blümel, *Chem. Asian J.* **2019**, *14*, 2704-2711.

29. C. R. Hilliard, S. Kharel, K. J. Cluff, N. Bhuvanesh, J. A. Gladysz, J. Blümel, *Chem. Eur. J.* **2014**, *20*, 17292-17295.

30. **(a)** A. E. Stross, G. Iadevaia, C. A. Hunter, *Chem. Sci.* **2016**, *7*, 94-101. **(b)** G. Iadevaia, A. E. Stross, A. Neumann, C. A. Hunter, *Chem. Sci.* **2016**, *7*, 1760-1767. **(c)** R. Cuypers, E. J. R. Sudhölter, H. Zuilhof, *Chem. Phys. Chem.* **2010**, *11*, 2230-2240.

31. D. Nunez-Villanueva, C. A. Hunter, *Chem. Sci*. **2017**, *8*, 206-213.

32. N. A. Bewick, A. Arendt, Y. Li, S. Szafert, T. Lis, K. A. Wheeler, J. Young, R. Dembinski, *Curr. Org. Chem*. **2015**, *19*, 469-474.

33. S. J. Pike, C. A. Hunter, *Org. Biomol. Chem*. **2017**, *15*, 9603-9610.

34. N. J. Burke, A. D. Burrows, M. F. Mahon, J. E. Warren, *Inorg. Chim. Acta* **2006**, *359*, 3497-3506.

35. R. Joshi, S. P. Pasilis, *J. Mol. Liquids* **2015**, *209*, 381-386.

36. F. F. Arp, N. Bhuvanesh, J. Blümel, *Dalton Trans*. **2019**, *48*, 14312-14325.

37. S. Kharel, N. Bhuvanesh, J. A. Gladysz, J. Blümel, *Inorg. Chim. Acta* **2019**, *490*, 215-219.

38. **(a)** E. Y. Tupikina, M. Bodensteiner, P. M. Tolstoy, G. S. Denisov, I. G. Shenderovich, *J. Phys. Chem. C* **2018**, *122*, 1711-1720. **(b)** G. Begimova, E. Y. Tupikina, V. K. Yu, G. S. Denisov, M. Bodensteiner, I. G. Shenderovich, *J. Phys. Chem. C* **2016**, *120*, 8717-8729.

39. F. F. Arp, S. H. Ahn, N. Bhuvanesh, J. Blümel, *New J. Chem*. **2019**, *43*, 17174-17181.

40. S. H. Ahn, K. J. Cluff, N. Bhuvanesh, J. Blümel, *Angew. Chem*. **2015**, *127*, 13539-13543.

41. S. H. Ahn, N. Bhuvanesh, J. Blümel, *Chem. Eur. J.* **2017**, *23*, 16998-17009.

42. S. H. Ahn, D. Lindhardt, N. Bhuvanesh, J. Blümel, *ACS Sustainable Chem. Eng.* **2018**, *6*, 6829-6840.

43. R. Peters, D. F. Fischer, S. Jautze, *Top. Organomet. Chem.* **2011**, *33*, 139-175.

44. A. Fihri, P. Meunier, J.-C. Hierso, *Coord. Chem. Rev.* **2007**, *251*, 2017-2055.

45. L. Qiao, X. Zhou, X. Li, W. Du, A. Yu, S. Zhang, W. Wu, *Talanta* **2017**, *163*, 94-101.

46. K. J. Cluff, M. Schnellbach, C. R. Hilliard, J. Blümel, *J. Organomet. Chem.* **2013**, *744*, 119-124.

47. K. J. Cluff, J. Blümel, *Organometallics* **2016**, *35*, 3939-3948.

48. K. J. Cluff, J. Blümel, *Chem. Eur. J.* **2016**, *22*, 16562-16575.

49. M. Schnellbach, J. Blümel, F. H. Köhler, *J. Organomet. Chem.* **1996**, *520*, 227-230.

50. W. P. McKenna, S. Bandyopadhyay, E. M. Eyring, *Applied Spectrosc*. **1984**, *38*, 834-837.

51. F. J. Karol, G. L. Karapinka, C. Wu, A. W. Dow, R. N. Johnson, W. L. Carrick, *J. Polym. Sci. A1* **1972**, *10*, 2621.

52. P. M. Mannucci, M. Franchini, *Int. J. Environ. Res. Public Health* **2017**, *14,* 1048.

53. P. Kongtip, W. Thongsuk, W. Yoosook, S. Chantanakul, *Atmos. Environ.* **2006**, *40*, 7138-7145.

54. Y. Otsuka, Y. Mizohata, A. Kobayashi, S. Okubo, T. Nakadate, *The Showa Univ. J. of Med. Sci.* **2017**, *29*, 231-240.

55. P. Harb, N. Locoge, F. Thevenet, *Chem. Eng. J.* **2020**, *380*, 122525.

56. X. Li, L. Zhang, Z. Yang, P. Wang, Y. Yan, J. Ran, *Sep. Purif. Technol.* **2020**, *235*, 116213.

57. K. Vikrant, K.-H. Kim, W. Peng, S. Ge, Y. Sik Ok, *Chem. Eng. J.* **2020**, *387*, 123943.

58. L. Ma, M. He, P. Fu, X. Jiang, W. Lv, Y. Huang, Y. Liu, H. Wang, *Sep. Purif. Technol.* **2020**, *235*, 116146.

59. W. Qiu, K. Dou, Y. Zhou, H. Huang, Y. Chen, H. Lu, *Chin. J. Chem. Eng.* **2018**, *26*, 81-88.

60. G. Wang, B. Dou, Z. Zhang, J. Wang, H. Liu, Z. Hao, *J. Environ. Sci.* **2015**, *30*, 65-73.

61. a) P. Barbaro, F. Liguori, Eds., *Heterogenized Homogeneous Catalysts for Fine Chemicals Production*, Springer: Heidelberg, 2010. b) F. R. Hartley, *Supported Metal Complexes*; Reidel, D. Publ. Co.: Dordrecht, The Netherlands, 1985. c) D. E. DeVos, I. F. J. Vankelecom, P. A. Jacobs, Eds., *Chiral Catalyst Immobilization and Recycling*: Wiley-VCH: Weinheim, 2000. d) G. Rothenberg, *Catalysis: Concepts and Green Applications*; Wiley-VCH, Weinheim, 2008.

62. C. Merckle, J. Blümel, *Chem. Mater*. **2001**, *13*, 3617-3623.

63. **(a)** A. T. Bell, *NMR Techniques in Catalysis*. Taylor & Francis: 1994. **(b)** S. Reinhard, J. Blümel, *Magn. Reson. Chem.* **2003**, *41*, 406-416.

CHAPTER II

PORE SURFACE INTERACTIONS AND MOLECULAR MOTIONS OF ADSORBED BENZENE ON ACTIVATED CARBON[*]

Introduction

Activated carbon (**AC**), featuring a high surface area and porosity, attracts great attention in diverse fields of chemistry as an inexpensive and indispensable material. **AC** is of enormous importance for applications in chemistry, medicine and industry, for example, for gas and water purifications, metal extractions, and many others.[1,2] During the past decades, diverse carbon materials have been studied by different physicochemical methods,[3-18] including NMR spectroscopy,[3-5,16-19] thermal analysis,[5-7,14,15] X-ray[10,12] and neutron diffraction,[7] and FTIR.[5] Additionally, theoretical calculations[8,9,11,13] and thermochemical studies of simple organic molecules, adsorbed on **AC** surfaces from vapors and solutions (benzene, toluene, ethyl chloride, carbon tetrachloride and many others), have been performed.[20-24]

In spite of the many results obtained so far, currently there is only limited knowledge about the molecular dynamics of adsorbates and their interactions with the surface in AC pores.[25] Even for benzene only limited information has been reported, although it often serves as a reference molecule in adsorption studies. For example, benzene molecules on

---

[*] Reproduced with permission from “Benzene Adsorbed on Activated Carbon: A Comprehensive Solid-State Nuclear Magnetic Resonance Study of Interactions with the Pore Surface and Molecular Motions”, Jordon W. Benzie, Vladimir I. Bakhmutov, and Janet Blümel, *Journal of Physical Chemistry C* **2020**, *124,* 21532-21537. DOI: 10.1021/acs.jpcc.0c06225. Copyright 2020 American Chemical Society.

nonporous graphitized carbon black have been characterized by low-temperature ^2H T_1 relaxation time measurements[26] interpreted by low-energy hexad axis benzene reorientations (fast in-plane C_6 rotations). Similar results have been obtained for ^{13}C-enriched benzene adsorbed on the surface of charcoal when it was probed by ^{13}C solid-state NMR spectroscopy.[27]

Recently, ferrocene $(C_5H_5)_2Fe$) has been adsorbed on silica and activated carbon surfaces.[19,28] Although ferrocene is an organometallic compound that obviously differs from benzene, it features aromatic cyclopentadienyl rings as ligands. Each cyclopentadienyl ring is planar and contains six π electrons, in analogy to benzene. On **AC** surfaces within the pores ferrocene showed liquid-like behavior with fast exchange between isotropically moving molecules and surface-attached horizontally oriented ferrocene molecules.[28] The adsorption enthalpy ΔH^0 has been determined to be in the range of −8.4 to −7.0 kcal/mol.[28] In the surface-attached state, the C_5H_5 rings display fast rotation and they are perpendicular to the pore surface. Since the in-plane C_6 rotating benzene molecules are oriented parallel to the surface on nonporous graphitized carbon black[26,27] and perpendicular to a graphite surface,[29] the characteristics of benzene in the pores of **AC** is of great interest in order to gain a deeper insight into the general factors that determine its surface orientation and dynamics.

Activated carbon (charcoal) consists of non-graphitic carbon with complex surface characteristics and ranges of pore sizes from 2 nm to > 50 nm.[2] In addition, depending on the manufacturing processes and starting materials, **AC** can contain different surface groups, impurities and irregularities.[20] Therefore, the precise atomic structure of **AC** is still unknown.[30] In addition, **AC** is a paramagnetic material and active in EPR,[31,32] thus complicating the application of NMR techniques for probing the adsorbate dynamics of benzene. Although paramagnetic solid-state NMR has successfully been applied, for example, to surface-adsorbed metallocenes[33,34] and aromatic compounds on a graphitic surface,[29] the paramagnetism of **AC** might have deterred chemists from applying this method. However, solid-state NMR spectroscopy has been successfully used for studies of molecular dynamics in diamagnetic systems, for example, in the case of ferrocene on silica mentioned above.[28] Finally, only for small molecules investigations have been performed using theoretical molecular dynamics simulations to describe, for example, the translational and rotational diffusion of methane molecules in carbon nanotubes.[35,36]

In this contribution we report the comprehensive solid-state NMR study of a commercial **AC** (DARCO),[37] containing 370 mg and 620 mg of benzene-d_6 per 1 g of **AC** (materials **AC-C_6D_6-370** and **AC-C_6D_6-620**, respectively), and 55 mg of cyclohexane-d_{12} (sample **AC-C_6D_{12}-55**). The choice of the adsorbents was dictated by their similar molecular sizes, albeit different electronic features, and also by the fact that the dynamics of benzene on the surface of selected porous materials is well established.[38-44]

Results and Discussion

The **AC** sample showed an intense sharp EPR signal at a field of 3348 G and a g-factor of 2.0021[31,32] (Figure S1), proving the presence of unpaired electrons. Therefore, a single pulse sequence with high-power decoupling was applied first for measuring a ^{13}C solid-state NMR spectrum of a static sample. However, this leads to the appearance of ^{13}C background signals from standard NMR probe heads. Unfortunately, spin-echo experiments could not be used to suppress the signal originating from the probehead, because it also removes the signal of the benzene on the AC. Therefore, to identify the ^{13}C NMR resonances of the sample **AC-C_6D_6-370**, its static ^{13}C{^{1}H} NMR spectrum was recorded at 295 K (Figure 8, middle). The background signal was obtained by measuring the empty rotor in the NMR probe head under identical conditions (Figure 8, bottom). Subtracting the background signal resulted in a broad signal and a narrow resonance residing on top of it (Figure 8, top). The sharp peak at $\delta(^{13}C) = 126$ ppm belongs to the isotropically moving liquid-like benzene molecules. The very broad resonance with a shape similar to that observed for graphite[18] stems from the **AC** support. Deconvolution of these signals allows the determination of their relative integrals and the benzene content in the sample. The same approach has been used to characterize **AC-C_6D_6-620** and **AC-C_6D_{12}-55** (Figure S2). For the latter, the corresponding static spectrum shows the isotropically moving molecules of cyclohexane-d_{12} ($\delta = 23.4$ ppm).

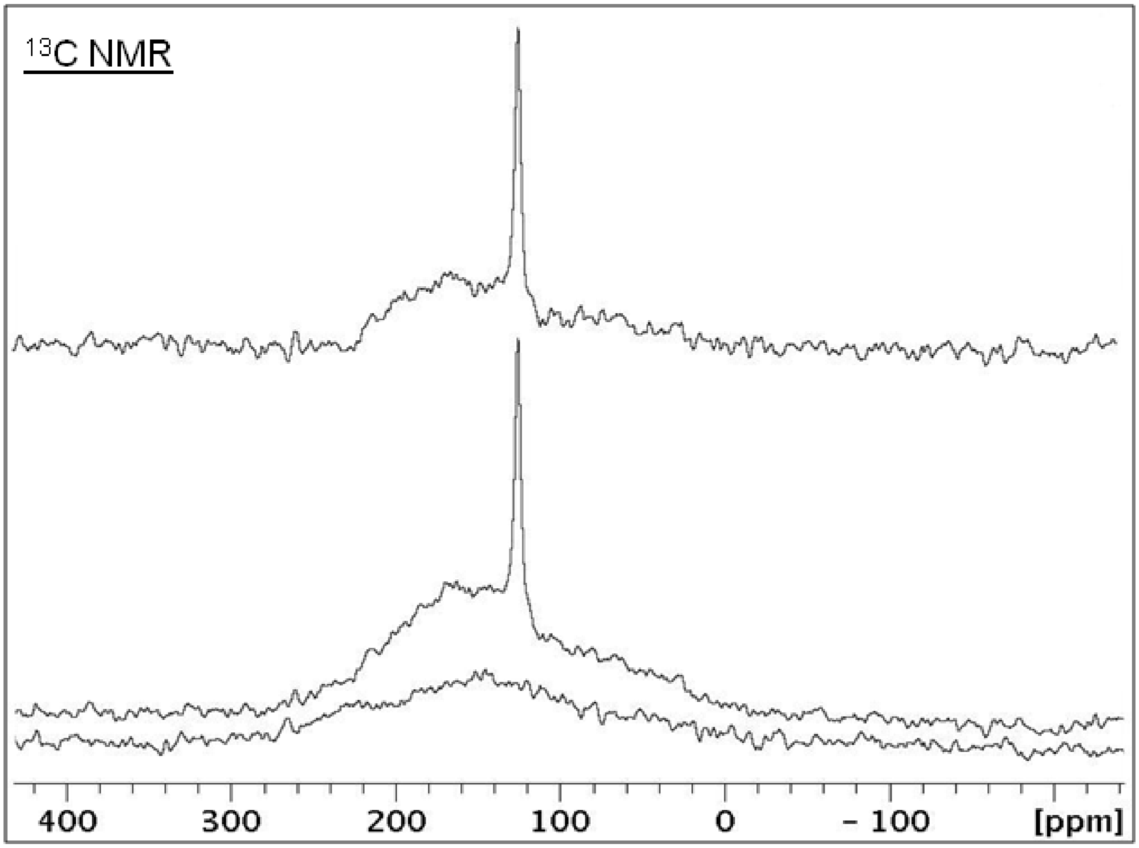

Figure 8. Static $^{13}C\{^1H\}$ solid-state NMR spectra recorded under identical conditions for **AC-C_6D_6-370** (middle) and the empty rotor (bottom) at 295 K. The top trace shows the difference spectrum.

The Hahn-echo ^2H NMR spectra of the static samples **AC-C_6D_6-370** and **AC-C_6D_6-620** were measured at temperatures between 175 and 295 K (Figure 9 and S3). In accord with ^{13}C NMR (Figure 9, bottom), at 295 K only the ^2H resonance with Lorentzian lineshape is observed that is characteristic for the isotropically moving benzene molecules of **AC-C_6D_6-370**. Upon cooling, the signal remains liquid-like even at 175 K, which is a temperature significantly lower than the benzene melting point (278 K). This effect is caused by the well-known melting point depression which depends on pore sizes.[42]

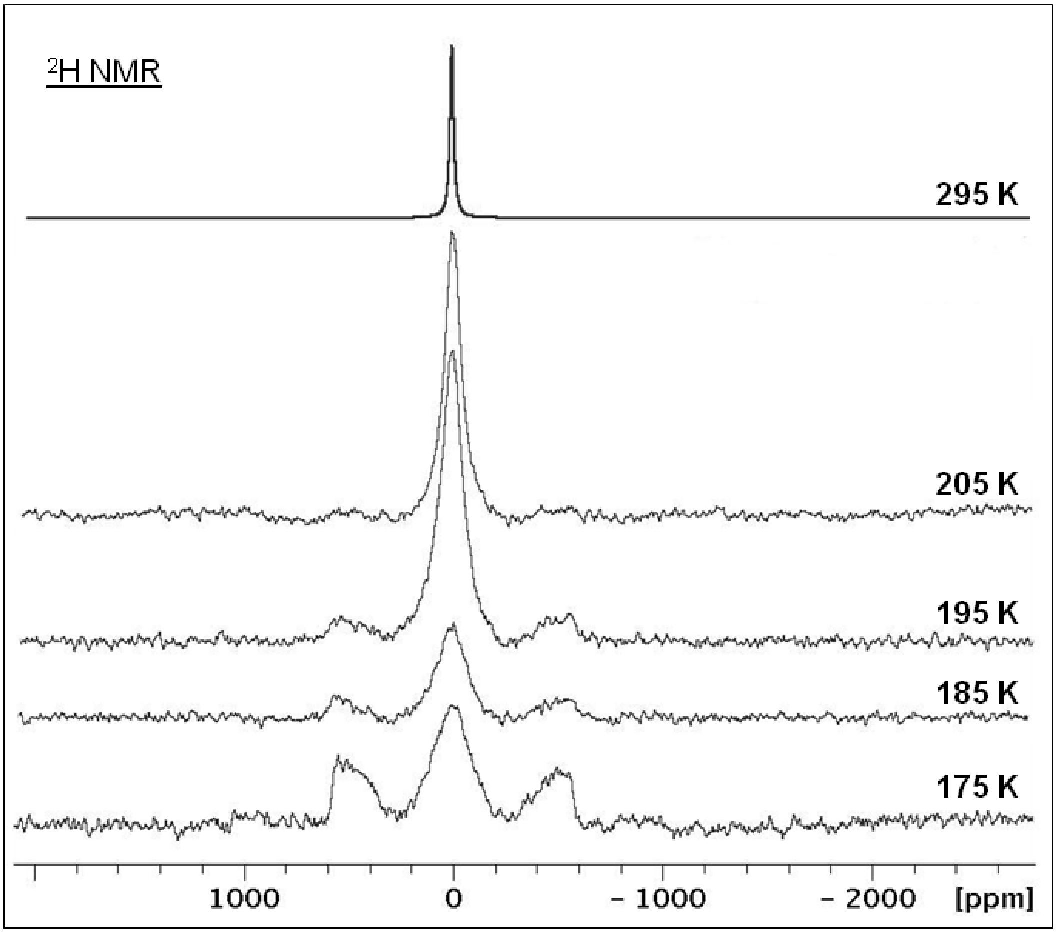

Figure 9. Hahn-echo ^{2}H NMR spectra of the static sample **AC-C_6D_6-370** at the indicated temperatures.

As Figure 9 shows, the isotropic resonance experiences spectral evolution and at 175 K the quadrupolar Pake pattern[42-44] manifests while the broadened central component is still present. The Pake pattern obviously belongs to adsorbed benzene molecules that are no longer translationally mobile, but located at a specific site on the **AC** surface. These "stationary" molecules are depicted in (Figure 10, left). The Pake patterns are identical for

AC-C_6D_6-370 and **AC-C_6D_6-620** (Figure S4) and can be simulated with a quadrupolar coupling constant (C_Q) of 92 ± 3 kHz. This value is characteristic for Pake patterns of C_6D_6 molecules on surfaces of other porous systems,[37-41] where they are oriented parallel to the surface and perform fast in-plane C_6 rotation (Figure 10, left). This is in accordance with the NMR data obtained for nonporous graphite[26] and charcoal[27] as support materials. The parallel orientation of the benzene ring to the surface was also suggested earlier for a graphite support based on X-ray diffraction studies.[10]

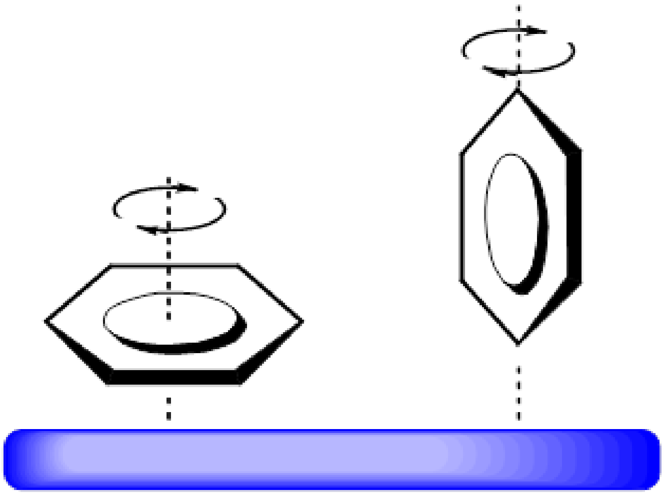

Figure 10. Surface-adsorbed benzene molecules experiencing fast in-plane C_6 rotation (left) and semi-bound molecules (right).

Recent TEM (transmission electron microscopy) experiments have demonstrated that hexagonal and pentagonal rings, as in fullerene-type structures, are present in activated carbon.[30] Both five- and six-membered rings will promote π - p interactions[25] as a driving force for benzene adsorption.

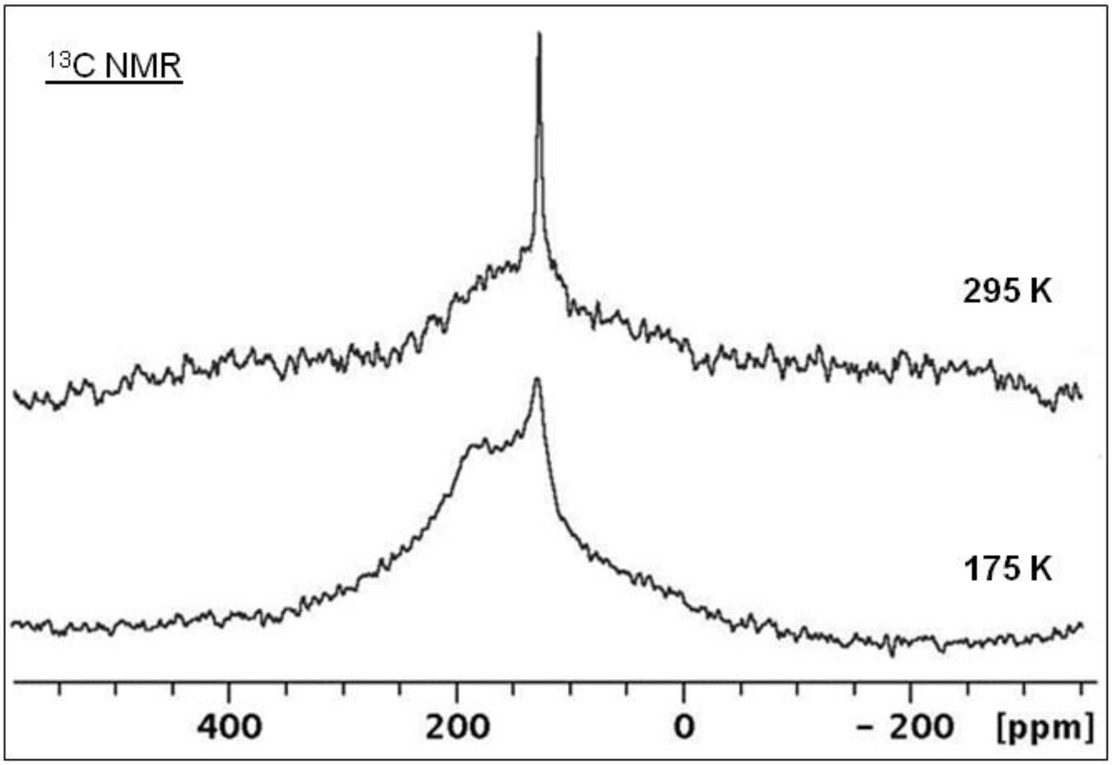

Figure 11. $^{13}C\{^1H\}$ NMR spectra of a static sample of **AC-C_6D_6-370** at 295 K (top) and 175 K (bottom).

Importantly, these π - p interactions constitute a direct mechanism which affects the ^{13}C NMR resonance of benzene molecules located on the paramagnetic **AC** surface. In fact, even at room temperature the ^{13}C NMR resonance of the isotropically moving C_6D_6 molecules exhibits a ^{13}C T_1 relaxation time of 0.63 s, which is unusually short even for liquids. The $^{13}C\{^1H\}$ static NMR spectra of **AC-C_6D_6-370** were recorded under the same conditions at 295 and 175 K (Figure 9). In both spectra, the probe head background is obviously present. Therefore, comparison of the spectra in Figure 8 and Figure 9 allows to identify a broad line with a maximum at about 160-180 ppm (instead of the axially symmetric pattern observed in ref. 27), which obviously belongs to stationary molecules (Scheme 1, left). We believe that this dramatic broadening, caused by ^{13}C nucleus/electron dipolar coupling of benzene with the paramagnetic pore surface of **AC** strongly proves their π - p interactions.

The chemical exchange between *stationary* and *isotropically moving* C_6D_6 molecules is slow on the deuterium NMR time scale in the temperature range from 175 to 295 K (Figure 9 and S3). Therefore, relative populations of these molecular states can easily be determined under these conditions. The mole fractions of stationary (P_{stat}) and isotropically moving, mobile benzene molecules (P_{mob}), determined for **AC-C_6D_6-370** at different temperatures, are given in Table 2.

Table 2. The temperature dependence of stationary (P_{stat}) and mobile (P_{mob}) mole fractions of **AC-C_6D_6-370** and the corresponding equilibrium constants K_{eq}. The averaged values obtained by two independent experiments are reported.

T (K)	P_{stat}	P_{mob}	K_{eq}
205	0.12	0.88	0.14
195	0.18	0.81	0.23
185	0.36	0.64	0.57
175	0.46	0.54	0.86

The fraction P_{stat} grows upon cooling and results in a straight line when $\ln(K_{eq})$ is plotted versus 1/T. This line corresponds to a free enthalpy (ΔH^0) value of -4.2 ± 0.3 kcal/mol, which characterizes the benzene-surface interactions. This value has been determined for the first time by NMR spectroscopy. It should be noted that the absolute value, accepted as the adsorption enthalpy of benzene on **AC**, is close to the lowest enthalpy (−4.97 kcal/mol) reported for benzene adsorption on activated carbons, ranging from −4.97 to −10.7 kcal/mol in thermochemical experiments.[22] We assume that the ΔH^0 value determined here by NMR characterizes the surface π - p interactions of benzene with the **AC** surface better. It is furthermore remarkable that the found enthalpy is larger than the fusion enthalpy of benzene (2.4 kcal/mol), and closer to the range of values (2.87 to 4.73 kcal/mol) obtained by MP2 calculations for π - π interactions in benzene dimers with parallel-displaced and sandwich orientations.[45]

In contrast to benzene that displays surface π - p interactions, cyclohexane-d_{12} in the sample **AC-C_6D_{12}-55** does not show a stationary state in the ^{2}H NMR spectra (Figure S5). Even at the lowest temperatures only one signal with Lorentzian lineshape is observed. In accordance with this result, no ^{13}C NMR resonance of stationary cyclohexane is detected at 175 K (Figure S6). The resonance observed is not even broadened by the paramagnetic nature of the **AC** surface. It is obvious that the cyclohexane/**AC** surface energy is significantly lower.

One spectral effect observed in this study remains to be clarified. The central component in the ^{2}H NMR spectra of **AC-C_6D_6-370** and **AC-C_6D_6-620** broadens substantially upon cooling (Figure 9 and S3, and Table S1) although the chemical exchange between stationary and mobile C_6D_6 molecules is slow on the ^{2}H NMR time scale. In analogy, a broadening effect is also observed for the ^{2}H resonance of cyclohexane in **AC-C_6D_{12}-55** (Table S1). However, the broadening is much less pronounced, as the halfwidth of the central component ($\Delta\nu$) equals nearly 12.6 kHz in the case of **AC-C_6D_6-370** at 175 K, while it is only 4.7 kHz for **AC-C_6D_{12}-55**. Since the large value of 12.6 kHz cannot be explained by the ^{2}H relaxation, the broadening of the central component might be the consequence of a fast chemical exchange between the isotropically moving C_6D_6 molecules and an additional mode of mobility, called here a ‘semi-bound’ state (Figure 12). In this case, the magnitude of $\Delta\nu$ will depend on an exchange rate constant k_{exch}.[46]

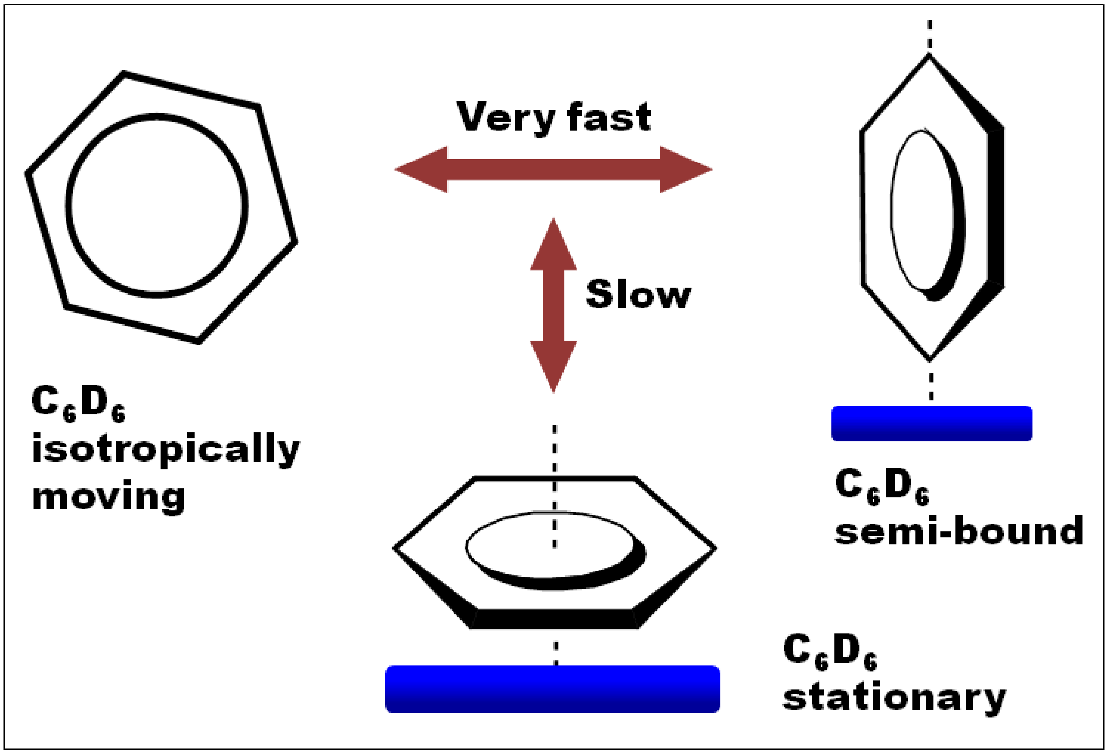

Figure 12. Exchange between isotropically moving, semi-bound, and stationary C_6D_6 molecules adsorbed on activated carbon.

In general, the nature of the semi-bound state is unclear. Nevertheless, the experiments show that this state actually has to exist as an intermediate in the exchange between isotropically moving and stationary molecules. The most likely scenario for this intermediate state of adsorbed benzene is represented by the molecules being oriented perpendicular to the surface and rotating around the $C_1 \cdots C_4$ axis as shown in Scheme 1.[29] In fact, according to calculations performed by different methods, sandwich and T-complexes in benzene dimers are energetically almost identical, with a slight preference of T-complexes.[47-50] Regarding ^2H NMR, this fast rotation will not affect the static C_Q of

180 kHz for the C−D bonds lying on this axis, while the other C−D bond vectors, defining an angle of 60° with the rotational axis, will reduce C_Q to 23 kHz via equation **(5)**.

$$\textbf{(5)}\ \Delta\nu(\text{splitting}) = \tfrac{3}{4}\ 180\ (\text{kHz})(3\cos^2\theta - 1)/2$$

Here, $\Delta\nu$ stands for the quadrupolar splitting ($\Delta\nu = 3/4\ C_Q$).[51,52]

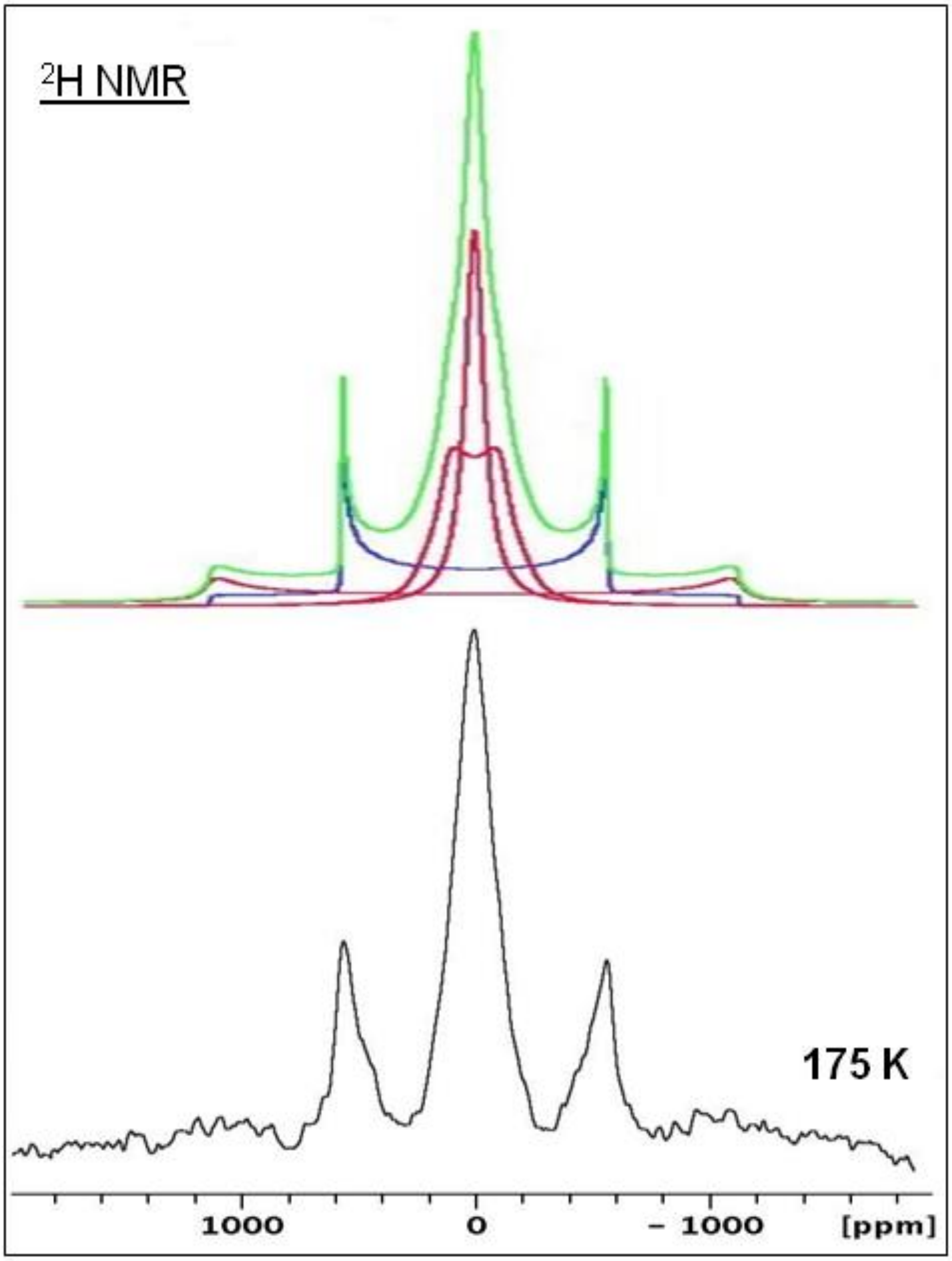

Figure 13. The ^{2}H static NMR spectrum **AC-C_6D_6-620** at 175 K (bottom) and simulation of this spectrum using four different spectral patterns (top), $C_Q(1)$ = 187.0 kHz with η = 0.15 (two deuterium atoms located on the rotation axis at $\theta = 0°$), $C_Q(2)$ = 20 kHz with η = 0.15 (four deuterium atoms at $\theta = 60°$), $C_Q(3)$ = 95 kHz with η = 0.05 (C_6–rotation) and $C_Q(4)$ = 0 (isotropic motions).

To support this assumption, the ^{2}H NMR spectrum of the static sample **AC-C_6D_6-620**, containing the largest amount of C_6D_6, was recorded at 175 K with 3000 scans. Figure 13 (bottom) shows this spectrum after careful phase and baseline corrections have been performed. The signal pattern can accurately be simulated with four sub-spectra (Figure 13, top) in the agreement with the proposed surface-binding models for C_6D_6 (Figure 10 and Figure 12). Hereby, the pattern with a C_Q of 93 kHz is not broadened, while the other signals require large linewidths of about 6 kHz because of the chemical exchange described above (Figure 12). In the limits of this exchange, the decrease of the linewidth of the central component in the ^{2}H NMR spectra of **AC-C_6D_6-370** when heating the sample from 193 to 253 K is caused by the acceleration of the exchange between the semi-bound and isotropically moving benzene states (Figure 12). The exchange has been approximated by a three-chenter exchange model, where the frequency distance of the outer peaks was taken as 15 kHz (the distance between two main singularities of the pattern with C_Q of 20 kHz) and the central resonance belongs to the isotropically moving benzene molecules. The three-center fitting procedures lead to the rate constants k_{exch} summarized in Table 3. The corresponding temperature dependence in the coordinates $\ln(k_{exch})$ versus 1/T (Figure S7) results in an activation energy, E_{act}, of 3.1 ± 0.3 kcal/mol and enthalpy and entropy changes, $\Delta H^{\ddagger}$ and $\Delta S^{\ddagger}$, of 2.7 ± 0.3 kcal/mol and –21 e.u., respectively. We believe that the relatively large negative magnitude of $\Delta S^{\ddagger}$ is caused by the approximated character of the line shape analysis.

Table 3. Rate constants k_{exch} obtained for the chemical exchange between the semi-bound and free benzene molecules (Figure 12).

T (K)	k_{exch} ($10^3 \cdot s^{-1}$)
193	68
203	89
213	120
233	230
253	480

Conclusion

In summary, molecular motions of benzene-d_6, surface-adsorbed within the pores **AC**, have been characterized for the first time by solid-state NMR. Isotropically moving and stationary molecules, as well as molecules in intermediate states in exchange with isotropically moving molecules, have been identified. The stationary molecules, stabilized by π - p interactions with the AC surface experience fast in-plane C_6 rotations. Benzene molecules in semi-bound states, similar to T-complexes in benzene dimers, rotate perpendicular to the surface as depicted in Scheme 1. The adsorption enthalpy $-\Delta H^0$ for benzene on the pore surface of **AC** has been determined as 4.6 ± 0.3 kcal/mol. This value is larger than the binding π - π interactions in benzene dimers calculated for the gas phase,[44-47] but it is smaller than the adsorption enthalpy found for the horizontally oriented molecules of ferrocene on the pore surface of AC.[27] Finally, the exchange between semi-bound and isotropically moving benzene molecules is fast, requiring only a low activation energy.

Experimental Section

Materials. Activated carbon (**AC**, DARCO KB-G) was purchased from Sigma-Aldrich and used without further treatment. It has a specific surface area of 1700 m^2/g and pore volumes for micro-, meso- and macropores of 0.28, 0.3, and 0.4 mL/g, respectively. A sample of **AC** was immersed in liquid benzene-d_6 (Sigma-Aldrich) for 30 minutes and was then placed into a drying oven at 150 °C for 30 minutes. The resulting dry, black powder gained 620 mg of weight per g of **AC** and is designated **AC-C_6D_6-620**. Then, a sample of **AC-C_6D_6-620** was placed into a drying oven at 150 °C for an additional 30-minute heating period, which resulted in a weight gain of 370 mg with respect to 1 g of the original **AC**. This material is labelled **AC-C_6D_6-370**. In order to adsorb cyclohexane-d_{12} (Sigma-Aldrich), a sample of **AC** was immersed in liquid cyclohexane, then placed into a drying oven (150 °C) and heated for 45 minutes (**AC-C_6D_{12}-55**).

EPR Spectroscopy. The ESR spectrum of **AC** was recorded with a Bruker ELEXSYS II E 500 spectrometer operating at 9.75 GHz (X-band) and using the Xepr software. Since the aim of the EPR experiment was the observation of paramagnetic species, it has been performed only at room temperature.

NMR Measurements. All NMR experiments were carried out with a Bruker Avance-400 solid-state NMR spectrometer (400 MHz for ^{1}H nuclei) equipped with two-channel 7 mm and 4 mm MAS probe heads. The ^{13}C{^{1}H} NMR spectra with high-power decoupling were referenced to external TMS. They were obtained by direct excitation of ^{13}C nuclei with pulse lengths of 2.5 μs (50°), 1400 scans, and recycle delays of 5-8 s which afforded full nuclear relaxation. The ^{2}H NMR spectra of static samples were obtained using the Hahn-echo (90°-τ-180°-τ) pulse sequence ($\tau = 50$ μs) with a 90° pulse length of 5.25 μs, a recycle delay of 1-3 s, and a number of scans between 300 and 400. The variable temperature NMR experiments were performed with a thermocouple calibrated using the ^{1}H NMR spectra of liquid methanol ($\Delta\delta = \delta(OH) - \delta(CH_3)$) placed into a static MAS NMR rotor. Following a change in the temperature setting, a delay of 15 to 20 minutes was used before the acquisition in order to allow for thermal stabilization.

Simulations of quadrupolar patterns have been performed with a standard Bruker package program of the solid-state NMR spectrometer.

The chemical exchange was approximated with a three-center exchange model. The frequency distance of the outer resonances was taken as 15 kHz (the distance between two main singularities of the pattern with a C_Q of 20 kHz). The central resonance belongs to the free benzene molecules. The three-center fitting procedures were performed using the Bruker program Dynamics.

References

1. Marsh, H.; Rodriguez-Reinoso, F., *Activated Carbon* (Oxford: Elsevier), **2006**

2. Bubanale, S.; Shivashankar, M. History, Method of Production, Structure and Applications of Activated Carbon. *Intern. J. Eng. Res. & Technol.* **2017**, *6*, 495-497

3. Turov, V. V.; Leboda, R. ^{1}H NMR Chemical shifts of adsorbed molecules on the carbon surface. *Adsorpt. Sci. Technol*. **1998**, *16*, 837–855.

4. Harris, R. K.; Thompson, T. V.; Forshaw, P.; Foley, N.; Thomas, K. M.; Norman, P. R.; Pottage, C. A magic-angle spinning NMR study into the adsorption of deuterated water by activated carbon. *Carbon* **1996**, *34*, 1275–1279.

5. Cosnier, F.; Celzard, A.; Furdin, G.; Begin, D.; Mareche, J. F.; Barres, O. Hydrophobisation of active carbon surface and effect on the adsorption of water. *Carbon* **2005**, *43*, 2554–2563.

6. Kim, P.; Agnihotri, S. Application of water–activated carbon isotherm models to water adsorption isotherms of single-walled carbon nanotubes. *J. Colloid Interface Sci*. **2008**, *325*, 64–73.

7. Sliwinska-Bartkowiak, M.; Jazdzewska, M.; Huang, L. L.; Gubbins, K. E.; Melting behavior of water in cylindrical pores: carbon nanotubes and silica glasses. *Phys. Chem. Chem. Phys*. **2008**, *10*, 4909–4919.

8. Cabrera-Sanfelix, P.; Darling, G. R. Dissociative Adsorption of Water at Vacancy Defects in Graphite. *J. Phys. Chem. C* **2007**, *111*, 18258–18263.

9. Collignon, B.; Hoang, P. N. M.; Picaud S.; Rayez, J. C. Ab initio study of the water adsorption on hydroxylated graphite surfaces. *Chem. Phys. Lett*. **2005**, *406*, 430–435.

10. Ueno, Y.; Muramatsu, Y.; Grush, M. M.; Perera, R. C. C. Configurations of Benzene and Pyridine Molecules Adsorbed on Graphitic Surface of Microporous Carbon. *J. Phys. Chem. B* **2000**, *104*, 7154–7162.

11. Kowalczyk, P.; Ustinov, E. A.; Terzyk, A. P.; Gauden, P. A.; Kaneko K.; Rychlicki, G. Description of benzene adsorption in slit-like pores. Theoretical foundations of the improved Horvath–Kawazoe method. *Carbon* **2004**, *42*, 851–864.

12. Ueno, Y.; Muramatsu, Y. Direct observation of benzene and pyridine molecules adsorbed in microporous carbon using synchrotron-radiation-excited soft X-ray emission spectroscopy. *Carbon* **2000**, *38*, 1939–1942.

13. Birkett G. R.; Do, D. D. Simulation study of water adsorption on carbon black: the effect of graphite water interaction strength. *J. Phys. Chem. C* **2007**, *111*, 5735–5742.

14. Smith, M. R.; Hedges, S. W.; LaCount, R.; Kern, D.; Shah, N.; Huffman, G. P.; Bockrath, B. Selective oxidation of single-walled carbon nanotubes using carbon dioxide. *Carbon* **2003**, *41*, 1221–1230.

15. Marosfoi, B. B.; Szabo, A.; Marosi, G.; Tabuani, D.; Camino G.; Pagliari, S. Thermal and spectroscopic characterization of polypropylene-carbon nanotube composites. *J. Therm. Anal. Calorim*. **2006**, *86*, 669–673.

16. Maniva, Y.; Sato, M.; Kijme, K.; Kozlov, M. E.; Tokumoto, M. Comparative NMR study of new carbon forms. *Carbon* **1996**, *34*, 1287-1291.

17. Darmstad, H.; Roya, C.; Kaliaguinea, S.; Xua, G.; Auger, M.; Tuel, A.; Ramaswamy, V. Solid state C-NMR spectroscopy and XRD studies of commercial and pyrolytic carbon blacks. *Carbon* **2000**, *38*, 1279–1287.

18. Freitas, J. C. C; Emmerich, F. G.; Cernicchiaro, G. R. C.; Sampaio, L. C.; Bonagamba, T. J. Magnetic Susceptibility Effects on ^{13}C MAS NMR Spectra of Carbon Materials and Graphite. *Solid-State Nucl. Magn. Reson.* **2001**, *20*, 61–73.

19. Cluff, K. J.; Blümel, J. Adsorption of ferrocene on carbon nanotubes, graphene, and activated carbon. *Organometallics* **2016**, *35*, 3939−3948.

20. Wibowo, N.; Setyadhi, L.; Wibowo, D.; Setiawan, J.; Ismadji, S. Adsorption of Benzene and Toluene from Aqueous Solutions onto Activated Carbon and its Acid and Heat Treated Forms: Influence of Surface Chemistry on Adsorption. *J. Hazard. Materials* **2007**, *146*, 237–242.

21. Dubinin, M. M.; Polyakov, N. S.; Kataeva, L. I. Basic Properties of Equations for Physical Vapor Absorption in Micropores of Carbon Adsorbents Assuming a Normal Micropore Distribution. *Carbon* **1991**, *29*, 481-488.

22. Chiang, H. L.; Huang, C. P.; Chiang, P. C. The Adsorption of Benzene and Methylethylketone onto Activated Carbon: Thermodynamic aspects. *Chemosphere* **2002**, *46*, 143-152.

23. Hindarso, H.; Ismadji, S.; Wicaksana, F.; Mudjijati, N.; Indraswati, H. Adsorption of Benzene and Toluene from Aqueous Solution onto Granular Activated Carbon. *J. Chem. Eng. Data* **2001**, *46* 788–791.

24. Basso, M. C.; Cukierman, A. L. Arundo Donax Based Activated Carbons for Aqueous Phase Adsorption of Volatile Organic Compounds. *Ind. Eng. Chem. Res*. **2005**, *44*, 2091–2100.

25. Xu, Y.; Watermann, T.; Limbach, H.-H.; Gutmann, T.; Sebastianib, D.; Buntkowsky, G. Water and small organic molecules as probes for geometric confinement in well-ordered mesoporous carbon materials. *Phys. Chem. Chem. Phys.* **2014**, *16*, 9327-9336.

26. Voss, V.; Boddenberg, B. Anisotropic reorientation dynamics of benzene molecules adsorbed on graphite, alumina, and zeolite Y. *Surface Science* **1993**, *298*, 241-250.

27. Kaplan, S.; Resing, H. A.; Waugh, J. S. ^{13}C NMR chemical shift anisotropy for benzene adsorbed on charcoal and silica gel. *J. Chem. Phys*. **1973**, *59*, 5681–5687.

28. Hubbard, P. J.; Benzie, J. W.; Bakhmutov, V. I.; Blümel, J. Ferrocene Adsorbed on Silica and Activated Carbon Surfaces: A Solid-State NMR Study of Molecular Dynamics and Surface Interactions. *Organometallics* **2020**, *39*, 1080−1091.

29. Klomkliang, N.; Do, D. D.; Nicholson, D. Affinity and Packing of Benzene, Toluene, and p-Xylene Adsorption on a Graphitic Surface and in Pores. *Ind. Eng. Chem. Res.* **2012**, *51*, 5320−5329.

30. Harris, P. J. F.; Liu, Z.; Suenaga, K. Imaging the atomic structure of activated carbon. *J. Phys. Condens. Matter* **2008**, *20*, 362201−362206.

31. Kempiński, M.; Śliwińska–Bartkowiak, M.; Kempiński, W. Molecules in the porous system of activated carbon fibers: spin population control. *Rev. Adv. Mater. Sci.* **2007**, *14*, 163−166.

32. Wieckowski, A. B.; Najder-Kozdrowska, L.; Rechnia, P.; Malaika, A.; Krzyzynska, B.; Kozłowski, M. EPR Characteristics of activated carbon for hydrogen production by the thermo-catalytic decomposition of methane. *Acta Phys. Pol. A* **2016**, *130*, 701−704.

33. Schnellbach, M.; Blümel, J.; Köhler, F. H. The Union Carbide Catalyst (Cp_2Cr + SiO_2), Studied by Solid-State NMR. *J. Organomet. Chem.* **1996**, *520*, 227−230.

34. Cluff, K. J.; Blümel, J. Adsorption of Metallocenes on Silica. *Chem. Eur. J.* **2016**, *22*, 16562-16575.

35. Bartuś, K.; Bródka, A. Methane behavior in carbon nanotube as a function of pore filling and temperature studied by molecular dynamics simulations. *J. Phys. Chem. C.* **2017**, *121*, 4066−4073.

36. Bartuś, K.; Bródka, A. Temperature study of structure and dynamics of methane in carbon nanotubes. *J. Phys. Chem. C* **2014**, *118*, 12010−12016.

37. Sun, J.; Hippo, E. J.; Marsh, H.; O'Brien, W. S.; Crelling, J. C. Activated carbon produced from an Illinois basin coal. *Carbon* **1997**, *35*, 341-352.

38. Gonzalez, J.; Devi, R. N.; Tunstall, D. P.; Cox, P. A.; Wright, P. A. Deuterium NMR studies of framework and guest mobility in the metal-organic framework compound MOF-5, Zn_4O-($O_2CC_6H_4CO_2$)$_3$. *Microporous Mesoporous Mater*. **2005**, *84*, 97−104.

39. Gedat, E.; Schreiber, A.; Albrecht, J.; Emmler, T.; Shenderovich, I.; Findenegg, G. H.; Limbach, H.-H.; Buntkowsky, G. Evidence for surface and core phases of benzene-d_6 confined in mesoporous silica SBA-15 as studied with ^{2}H-NMR. *J. Phys. Chem. B* **2002**, *106*, 1977−1984.

40. Gonzalez, J.; Devi, R. N.; Wright, P. A.; Tunstall, D. P.; Cox, P. A. Motion of aromatic hydrocarbons in the microporous aluminum methylphosphonates AlMePO-α and AlMePO- β. *J. Phys. Chem. B* **2005**, *109*, 21700−21709.

41. Xu, J.; Sinelnikov, R.; Huang, Y. Capturing guest dynamics in metal−organic framework CPO-27-M (M = Mg, Zn) by ^{2}H solid-state NMR Spectroscopy. *Langmuir* **2016**, *32*, 5468−5479.

42. Buntkowsky, G.; Breitzke, H.; Adamczyk, A.; Roelofs, F.; Emmler, T.; Gedat, E.; Grunberg, B.; Xu, Y.; Limbach, H.-H.; Shenderovich, I. ^{2}H-Solid-state NMR study of benzene-d_6 confined in mesoporous silica SBA-15. *Phys. Chem. Chem. Phys*. **2007**, *9*, 4843−4853.

43. Xiong, J.; Maciel, G. E. Deuterium NMR studies of local motions of benzene adsorbed on Ca-montmorillonite. *J. Phys. Chem. B* **1999**, *103*, 5543−5549.

44. Aliev, A. E.; Harris, D. M.; Mahdyarfar, A. Dynamics of benzene and pyridine guest molecules in their TOT inclusion compounds: solid-state ^{2}H NMR studies. *J. Chem. Soc., Faraday Trans.* **1995**, *91*, 2017−2026.

45. Zhou, R. *Modeling of Nanotoxicity*, Springer International Publishing, Springer, Cham, 2015, pp. 169−184.

46. Harris, R. K. *Nuclear magnetic resonance, a physicochemical view,* Pitman Publishing Inc. 1983 Toronto, p. 119-122

47. Sinnokrot, M. O.; Valeev, E. F.; Sherrill, C. D. Estimates of the ab initio limit for π-π interactions: the benzene dimer. *J. Am. Chem. Soc*. **2002**, *124,* 10887-10893.

48. Chipot, C.; Jaffe, R.; Maigret, B.; Pearlman, D. A.; Kollman, P. A. Benzene Dimer: A Good Model for for π - π Interactions in Proteins? A Comparison between the Benzene and the Toluene Dimers in the Gas Phase and in an Aqueous Solution. *J. Am. Chem. Soc.* **1996**, *118,* 11217-11224.

49. Tummanapelli, A. K.; Vasudevana, S. Communication: Benzene dimer—The free energy landscape, *J. Chem. Phys*. **2013**, *139,* 201102.

50. Park, Y. C.; Lee, J. S. Accurate ab initio binding energies of the benzene dimer. *J. Phys. Chem. A* **2006**, *110,* 5091−5095.

51. Gielen, M.; Willem, R.; Wrackmeyer, B. *Unusual Structures and Physical Properties in Organometallic Chemistry*, (West Sussex: Wiley) 2002 p.152

52. Fyfe, C. A. *Solid-State NMR for Chemists,* C.F.C. Press, Guelph, Canada, 1983.

CHAPTER III

MOLECULAR DYNAMICS AND SURFACE INTERACTIONS OF NICKELOCENE ON SILICA AS PRECURSOR FOR SINGLE ATOM CATALYST STUDIED BY PARAMAGNETIC SOLID-STATE NMR

Introduction

The adsorption of small molecules on surfaces is important for processes in industry and academia that involve separation sciences and catalysis. However, NMR spectroscopic adsorption studies with solid supports have focused mainly on *liquids* like water, alcohols and benzene.[1] Spectroscopic studies on adsorbed *solids* are more scarce. We reported recently that species like phosphine oxides[2] can be adsorbed on diverse surfaces by dry grinding, and we could demonstrate that they are mobile on silica surfaces.[3-5] Regarding the adsorption of phosphine oxides on silica the interactions with the surface are rather well-defined. The oxygen of the P=O functionality forms hydrogen bonds with surface silanol groups.[2-4] Molecular hydrogen-bonded adducts of P=O groups with silanols,[3,6] hydrogen peroxide,[7,8] and di(hydroperoxy)alkanes[7,9-11] have all been identified by single crystal X-ray diffraction.

Solid-state NMR spectroscopy[12,13] is a powerful tool to investigate surface species, for example, immobilized catalysts on support surfaces.[14] Furthermore, complexes with aromatic ligands have been adsorbed on silica[15] and studied by ^{13}C solid-state NMR.[16]

The two most important anisotropic interactions that occur in the solid state and are utilized in NMR are the Chemical Shift Anisotropy (CSA) and dipolar interactions.[12,13]

The CSA reflects the unsymmetry of the electronic surroundings of a nucleus. The spherically rather symmetric phosphonium salts, for example, have a small ^{31}P CSA in the solid state, while polycrystalline phosphine oxides display a large CSA.[2-4] A large CSA manifests in solid-state NMR spectra in the form of multiple sets of rotational sidebands besides the isotropic line when samples are rotated. The CSA parameters can be derived by simulations from the spectra of rotated samples, or by measuring wideline spectra without spinning. The anisotropic dipolar proton-proton interactions generally lead to a broadening of the signals in the solid state. In solution, both anisotropic interactions are completely averaged out and only the isotropic lines are seen in the spectra. However, in case the mobility is limited and only partial averaging occurs, the residual CSA and dipolar interactions can be used to gain insight into the mobility of an adsorbed molecule, as described for nickelocene in the results and discussion section.

Recently, we discovered that metallocenes of the type Cp_2M (Cp = cyclopentadienyl, C_5H_5) can be adsorbed on silica by dry grinding of the components in the absence of solvents.[17-22] In contrast to the phosphine oxides, hydrogen bonding can be excluded for the interactions of these metallocenes with silica. The interactions with the surfaces must be of a van der Waals type nature, but the orientation of the metallocenes with respect to the surface is not known.

Under an inert atmosphere ferrocene does not undergo chemical reactions even with supports such as silica. In contrast, the important polymerization catalysts of the type Cp_2MCl_2 react readily via the chloride ligands when they are supported on silica,[23] or incorporated into polymers[24] or sol-gel-type materials.[25] But even in the absence of chloride ligands, some of the Cp_2M metallocenes react quickly with oxide surfaces after the adsorption step. On a silica or alumina surface, chromocene forms the important heterogeneous Union Carbide catalyst that is used industrially for olefin polymerization under mild conditions in the absence of a co-catalyst.[26,27] Despite the importance of this catalyst, its structure remains largely unknown. The commonly accepted partial structure of the catalytically active surface species consists of a CpCr(III) moiety that must be bound to a surface siloxide anion, as determined by solid-state NMR,[17] and XPS and IR studies.[26]

The most important incentive to study the interactions of Cp_2M-type metallocenes adsorbed in monolayers with support surfaces is related to the potential creation of single atom catalysts by reducing the metal center.[20] It has been visualized on a cm length scale that nickelocene is translationally mobile in large silica gel specimens.[20] Importantly with respect to a later application in single atom catalysis, when the adsorption is undertaken in the absence of a solvent, well-defined monolayers are formed.[20] No stacking of metallocenes in multiple layers on the surface occurs on any support.[18-21] In case an excess of metallocene is offered, it remains in its polycrystalline form and does not adsorb.

In case nickelocene (Cp_2Ni, $(C_5H_5)_2Ni$, **1**) is adsorbed in a monolayer on silica, it can subsequently be reduced by hydrogen to form a single atom catalyst that is active with respect to the cyclotrimerization of phenylacetylene.[20] Therefore, it is important to gain more insight into the behavior of the nickelocene molecules on the silica surface within the pores. Specifically, the orientation of the nickelocene molecules with respect to the surface, whether they stand upright or lie on their side, should influence their reactivity.

Polycrystalline nickelocene is reasonably stable at ambient temperature under an inert atmosphere and allows its characterization with paramagnetic NMR spectroscopy.[17,28-30] The same accounts for **1** adsorbed on silica.[20]

In this contribution, we apply variable-temperature ^{1}H solid-state NMR and T_1 relaxation time measurements[12] to investigate the behavior of **1** on the surface in the pores of silica on the molecular scale. Both paramagnetic ^{1}H MAS and ^{1}H wideline NMR spectroscopy will be applied at different temperatures. ^{1}H solid-state NMR spectroscopy without sample rotation has, for example, been successfully used recently to investigate the distribution of moisture in polymers.

The new insights gained on the different states of mobility of nickelocene on a silica surface should have major implications for single atom catalysis, as well-defined adsorption is the first step in generating these atom-economic and active heterogeneous catalysts.

Results and Discussion

The most closely related diamagnetic analog of nickelocene (Cp_2Ni, **1**) is ferrocene (Cp_2Fe, **2**). Recently, working in the field of solid-state NMR studies of molecular dynamics on the surface of porous materials, we have found a liquid-like behavior of ferrocene on a silica surface at moderate temperatures.[1] In the context of these studies, the mobility of nickelocene on the same silica surface is of great interest. Furthermore, in our quest to generate a nickel single atom catalyst from nickelocene, knowledge about the interactions with the surface are essential. Most importantly, preliminary results regarding the dry adsorption of nickelocene on a silica surface have to be corroborated and the behavior and orientation of the individual molecules on the surface have to be elucidated. More specifically, for the subsequent reduction of the nickelocene molecules with hydrogen it is important to know whether they stand "upright", or lie on the surface "sideways".

According to preliminary data communicated earlier,[20] according to its ^{1}H NMR spectra compound **1** behaves similarly to ferrocene after adsorption on silica in a submonolayer. As compared to polycrystalline **1**, surface-adsorbed nickelocene displays a diminished Chemical Shift Anisotropy (CSA) of its proton signal.[20] However, the deeper reasons for this behavior and the solid-state characteristics have not been investigated yet.

In this study we apply both variable temperature ^{1}H wideline and MAS NMR to characterize neat polycrystalline nickelocene (**1**) and samples that have been prepared by dry adsorption[20,22] of **1** on a silica surface. The studied samples have been prepared by adsorption of **1** on a silica surface with different loadings. Surface coverages of 70%, 140% and 200% have been obtained by dry grinding of **1** with the corresponding amounts of silica. For simplicity, the samples will be denoted as **1-70**, **1-140** and **1-200** in the following. The targeted surface coverages have been determined as described earlier for ferrocene.[20,22] For comparison, a sample containing ferrocene (**2**) adsorbed on the silica surface with a 70% coverage has also been prepared (**2-70**). ^{1}H and ^{13}C solid-state NMR spectra have been recorded at different temperatures. These studies included ^{1}H T_1 relaxation time measurements performed by inversion-recovery experiments.

Unfortunately, **1** is not stable on the silica surface over prolonged periods of time at room temperature. A broad ^{1}H resonance at about 5 ppm appears in the ^{1}H NMR spectra of static samples, which is growing over 24 hours. This signal most probably belongs to a decomposition product, such as cyclopentadiene or the Diels-Alder product dicyclopentadiene. Nevertheless, using freshly prepared samples, mostly the signals of adsorbed, but not chemically reacted, nickelocene are visible in the spectra.

As outlined above, nickelocene is paramagnetic, with an electron spin S = 1, and therefore its ^{13}C and ^{1}H MAS NMR spectra display paramagnetic, large ^{13}C and ^{1}H chemical shift values that are mainly caused by Fermi-contact electron-nucleus interactions.[28-30,33,34] Due to the Fermi contact contributions, the isotropic ^{13}C resonance of the cyclopentadienyl (C_5H_5, Cp) rings in **1** is observed at a very low magnetic field with δ_{iso} of 1594-1579[28] or 1514[29] ppm. The isotropic ^{1}H resonance is shifted towards high field and shows a $\delta_{iso}(^{1}H)$ value of –257 ppm (Figure 14, top).[28] The exact δ_{iso} of both nuclei in **1** and also their CSA values strongly depend on the measurement temperature,[28,33,34] again due to Fermi-contact interactions. Therewith, the chemical shift and CSA values also depend indirectly on the MAS speed because due to friction the rotors heat up at higher rotational frequencies.[35] In addition, anisotropic interactions, such as spin-dipolar interactions, dipolar diamagnetic interactions, and bulk magnetic susceptibility (BMS) effects result in large chemical shift anisotropies (CSA). They can reach, for example, 2600 ppm in the case of the ^{13}C nuclei in **1**,[28] complicating their experimental detection.

In accordance with the above mentioned literature, the ^{1}H MAS NMR spectrum of polycrystalline **1** (Figure 14), used as a reference molecule, exhibits a spinning sideband pattern with a $\delta_{\text{iso}}(^1\text{H})$ of –248 ppm. Interestingly, the distribution of the spinning sideband intensities in this manifold is very close to that observed for vanadocene.[33]

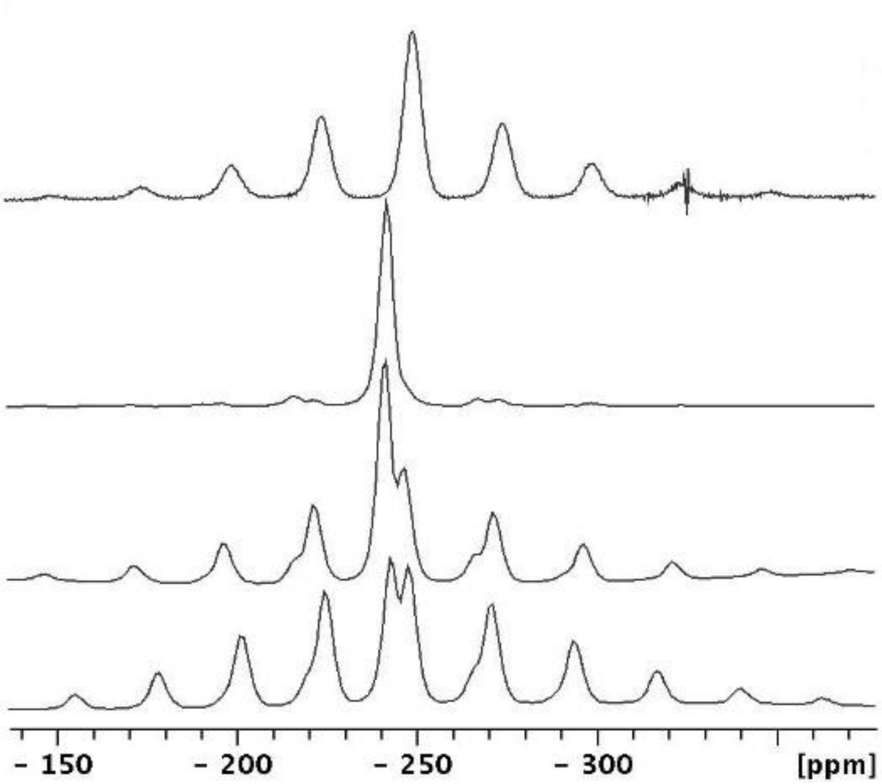

Figure 14. ^{1}H MAS NMR spectra of polycrystalline and adsorbed **1**, recorded at 295 K with a spinning rate of 10 kHz. From top to bottom: compound **1**, and materials **1-70**, **1-140**, and **1-200**.

Since the MAS NMR experiments have been applied in this contribution only for qualitative considerations, we did not make temperature corrections to account for the heating of the samples at high spinning rates (see above).[35] Inversion-recovery experiments, carried out for polycrystalline **1** at 295 K yielded different relaxations for the sidebands and the isotropic resonance in the partially-relaxed ^{1}H MAS NMR spectra. The ^{1}H T_1 time amounts to 0.28 ms for the isotropic resonance and to 0.25 and 0.21 ms for the first order downfield and upfield sidebands, respectively. This result, revealing the presence of a ^{1}H T_1 time distribution in **1** is often observed for paramagnetic systems.[36] Naturally, it complicates the interpretation of T_1 time data. Nevertheless, the measured ^{1}H T_1 times are all very short, in agreement with the assumption that the Fermi-contact interactions are dominant. The latter leads to a scenario where the relaxation of the nuclei depends on the electron relaxation and is independent of molecular dynamics.[5] It is remarkable that the line width $\Delta\nu$ of the Cp resonance in the ^{1}H MAS NMR spectrum of **1** (Figure 14, top) which equals 2.5 kHz at 295 K, gives a ^{1}H T_2 time of 0.12 ms (or 0.40 ms) for a Lorentz (or Gauss) resonance shape, in agreement with the above ^{1}H T_1 time. The $\Delta\nu$ value of the Cp resonance changes with temperature from 3.5 kHz at 283 K to 4.0 kHz (273 K), 4.8 kHz (263 K) and 5.5 kHz (253 K). This feature will be used below for quantitative estimates based on a line shape analysis.

One section of the temperature dependent ^{1}H NMR spectra of a static sample of **1** is shown in Figure 15. The ^{1}H background signal from the probehead has been subtracted for clarity.

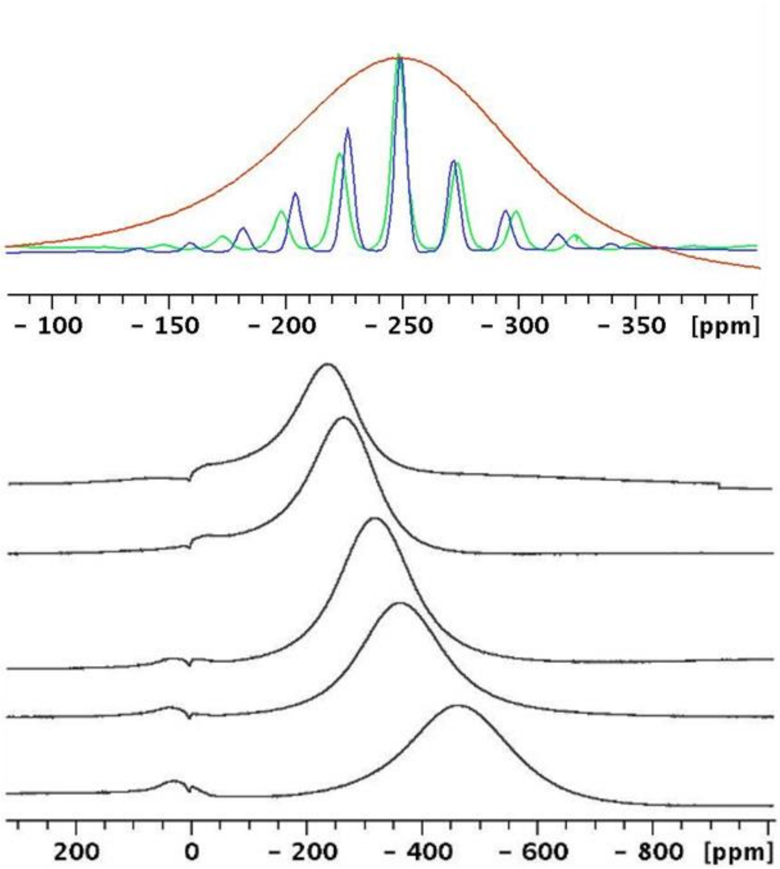

Figure 15. Variable temperature ^{1}H wideline NMR spectra of polycrystalline **1** from top to bottom: 295 K, 273 K, 245 K, 225 K and 185 K. The display on the top shows the static ^{1}H (brown) and MAS NMR spectra of **1** spinning at 10 (green) and 9 (blue) kHz.

As Figure 15 shows, upon cooling the ^{1}H Cp resonance experiences a strong upfield shift. The corresponding values are graphically displayed in Figure 16. This behavior is well documented for nickelocene and vanadocene.[28,34]

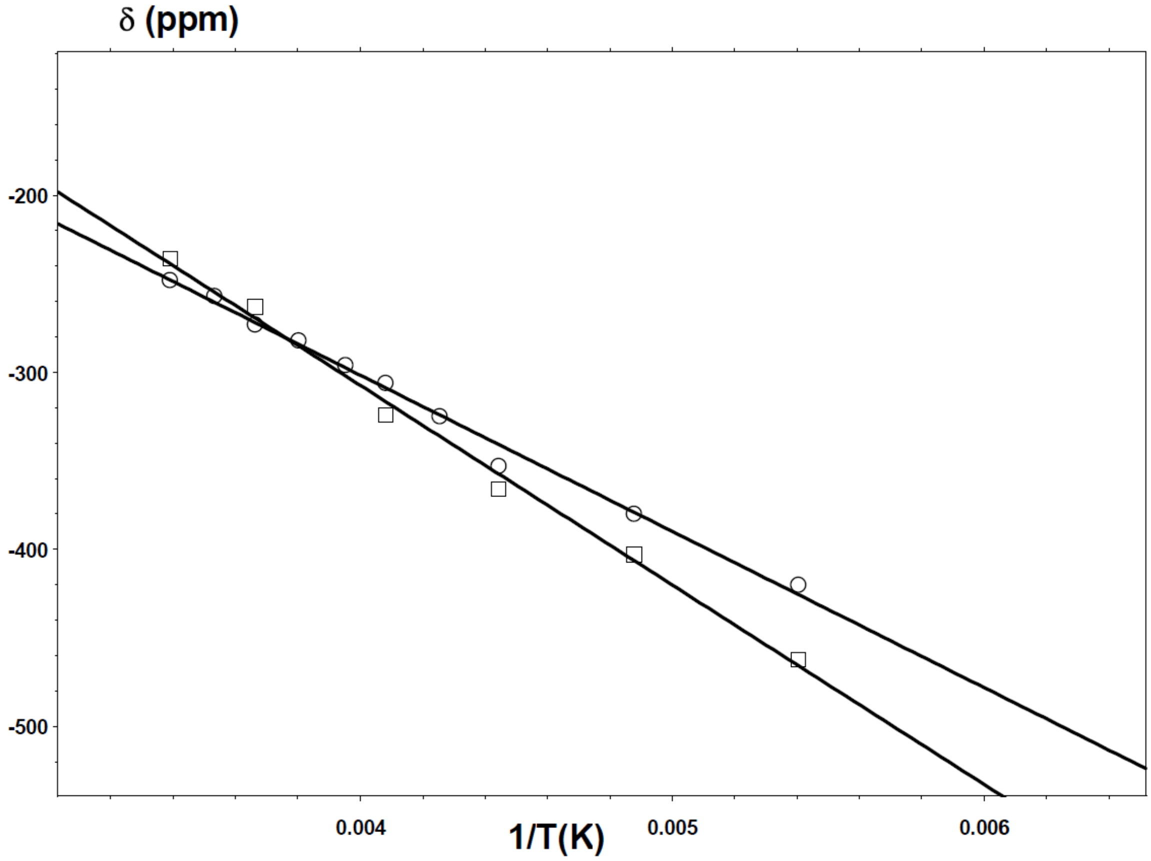

Figure 16. Temperature dependence of the ^{1}H Cp chemical shifts in the NMR spectra of static samples of **1** (□) and **1-70** (O), presented in coordinates of δ versus 1/T.

The observed chemical shift change is accompanied by a moderate increase in the line widths Δν which are summarized in Table 4 and graphically displayed in Figure 17. Correspondingly, as the temperature is lowered, ^{1}H CSA values are growing (Table 5). Both effects, as mentioned above, are already known for **1**.[28] However, in this study, we will use these parameters in order to characterize compound **1** as a reference for an immobile molecule. Hereby, the exceptionally fast rotation of the Cp rings[35,37] is not considered.

Table 4. Linewidths Δν in the static ^{1}H NMR spectra of **1** and **1-70** measured in kHz at different temperatures. The line widths $\Delta\nu_{rot}$ in the ^{1}H MAS NMR spectra of 1 are given for accessible temperatures.

T (K)	**1** **Δν ($\Delta\nu_{rot}$) (kHz)**	**1-70** **Δν (kHz)**
295	41.6 (2.5)	8.4
283	44.9 (3.5)	11.6
273	49.6 (4.0)	18.7
263	50.7 (4.8)	22.4
253	53.6 (5.5)	30.9
245	54.4	46.8
235	55.9	58.9
225	64	79.5
205	68	94.5
185	73.6	116
175		140

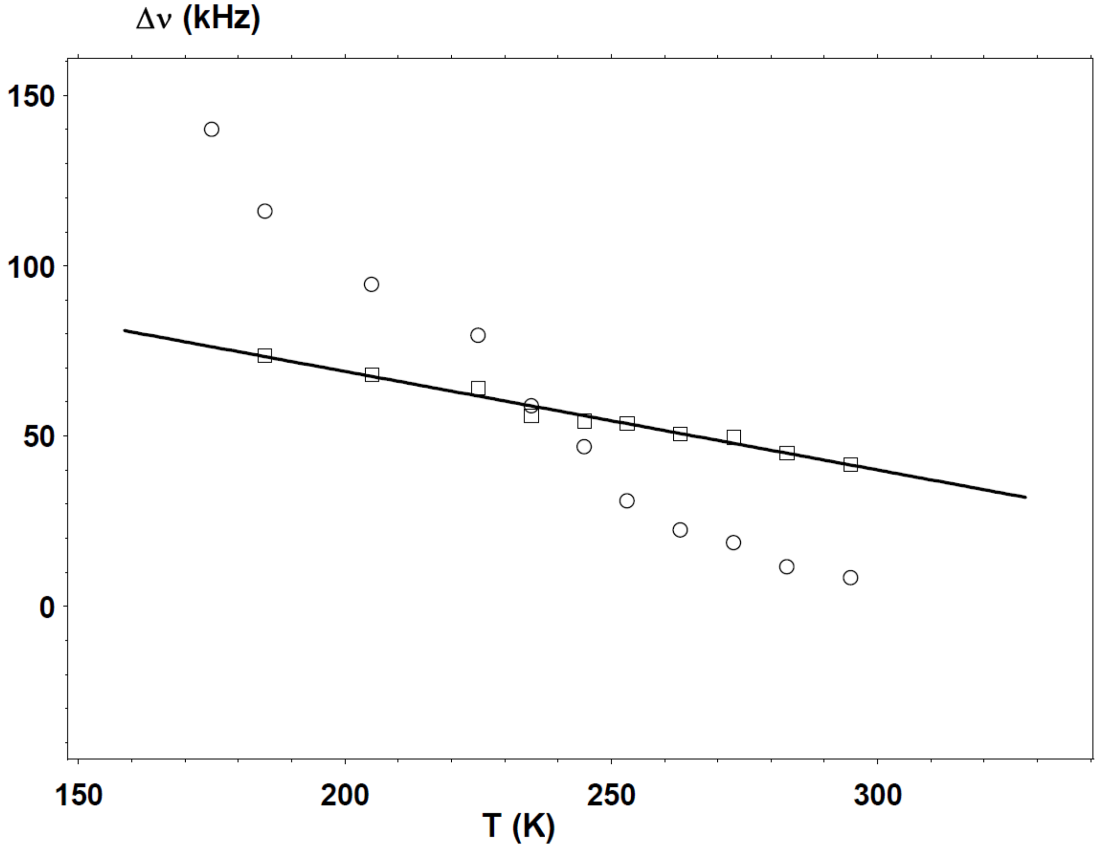

Figure 17. The correlation of Δν with the temperature for polycrystalline **1** (□) and **1-70** (O).

Table 5. Chemical shift anisotropy parameters, ^1H CSA and asymmetry parameter η, obtained by a sideband analysis performed for ^1H MAS NMR spectra of **1** spinning at a rate of 10 kHz in the temperature range between 305 and 263 K.

T (K)	**^1H CSA (ppm)**	**η**
305	52	0.86
295	55.5	0.89
283	57	0.95
273	61	0.90
263	66	0.80

In general, the analysis of the side band patterns in the ^1H MAS NMR spectra of polycrystalline **1** (Figure 15, top display) in order to determine the ^1H CSA values is not trivial. The reason for this is that in solid materials the shift anisotropies are governed by the spin-dipolar interactions, diamagnetic dipolar interactions (proton-proton), BMS effects, sometimes in the presence of an important part due to the contact interactions.[30] This combination of interactions obviously leads to distorted intensities in spinning sideband manifolds. In fact, the ^1H MAS NMR spectrum of polycrystalline **1**, shown in Figure 18, cannot be simulated as a single CSA pattern. However, it can be reproduced by, at least, two sets of sideband patterns with a ^1H CSA of 56 ppm and asymmetry parameter $\eta = 0.9$ (the high intensity manifold) and a ^1H CSA of 127 ppm and $\eta = 0.9$ (the low intensity manifold). It should be emphasized that this approach does not represent the actual situation. It illustrates, however, a poor simulation of the low intensity sidebands when using only the first set of parameters.

Unfortunately, the experimental ^{1}H CSA values for Cp rings in metallocenes are not available. First-principle calculations using relativistic approximations have resulted in a scenario where the CSA of **1** is dependent on the calculation levels: around 105-108 ppm or 64-67 ppm.[38] It is remarkable that the ^{1}H CSA of 64-67 ppm corresponds to the value obtained experimentally at 263 K (Table 5). However, the theoretical calculations[38] were carried out assuming an axially symmetric chemical shift tensor while the experimental sideband manifolds displayed in Figure 15 and Figure 18 do not have this symmetry. The latter is also valid for the ^{1}H MAS NMR of vanadocene.[33] Given this complex situation, in the following we use the CSA of the major component (Table 5) for the interpretations of the temperature dependent ^{1}H line shapes in the spectra of **1** and **1-70**.

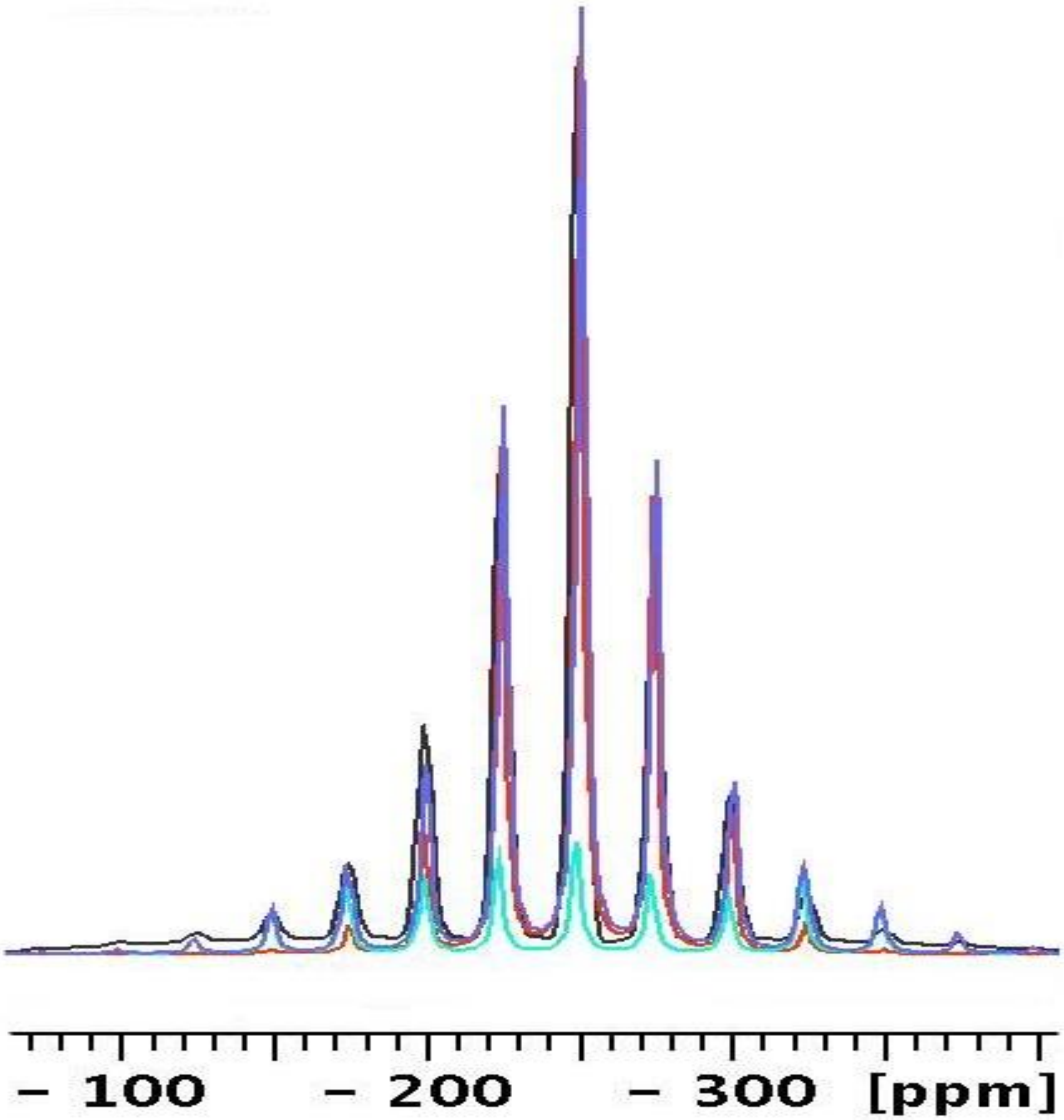

Figure 18. The ^{1}H MAS NMR spectrum of **1** recorded at a spinning rate of 10 kHz (black) and simulated as an intense manifold with a ^{1}H CSA = 56 ppm and η = 0.9 and δ_{iso} = −248.9 ppm (red), and a low intensity pattern with ^{1}H CSA = 127 at η = 0.9 and δ_{iso} = −246.6 ppm (green). The blue line shows the best fitting.

As follows from Figure 14, the ^{1}H MAS NMR spectrum of material **1-70** manifests a resonance at δ_{iso} of −243 ppm with very low intensity sidebands. These sidebands disappear completely in the temperature range from 315 to 325 K. Thus, in a submonolayer coverage, compound **1** behaves like a liquid on the silica surface. In full accordance with this behavior, the ^{13}C MAS NMR spectrum of **1-70**, recorded at 325 K (Figure 19) shows a resonance at 1415 ppm, corresponding to $\delta_{iso}(^{13}C)$,[28] which is not accompanied by spinning sidebands.

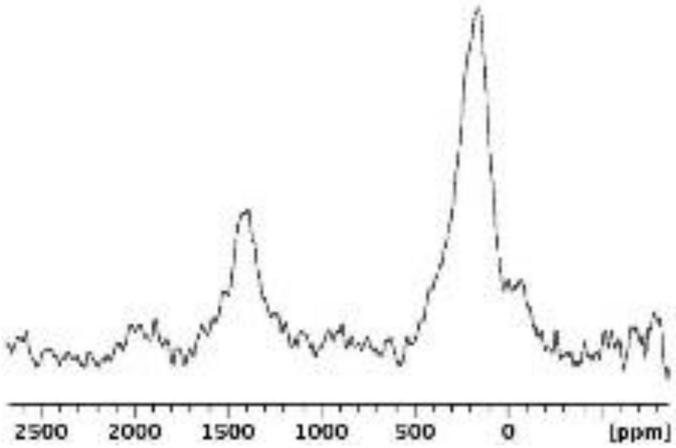

Figure 19. The ^{13}C MAS NMR spectrum recorded at 325 K for a sample of **1-70**, spinning at a rate of 9 kHz. The high-field resonance corresponds to the decomposition product that appears during prolonged accumulation.

In order to characterize the molecular dynamics of the adsorbed nickelocene in **1-70** we applied the static ^{1}H NMR experiments that require no temperature corrections in contrast to MAS NMR.[35] Selected ^{1}H wideline spectra are displayed in Figure 20.

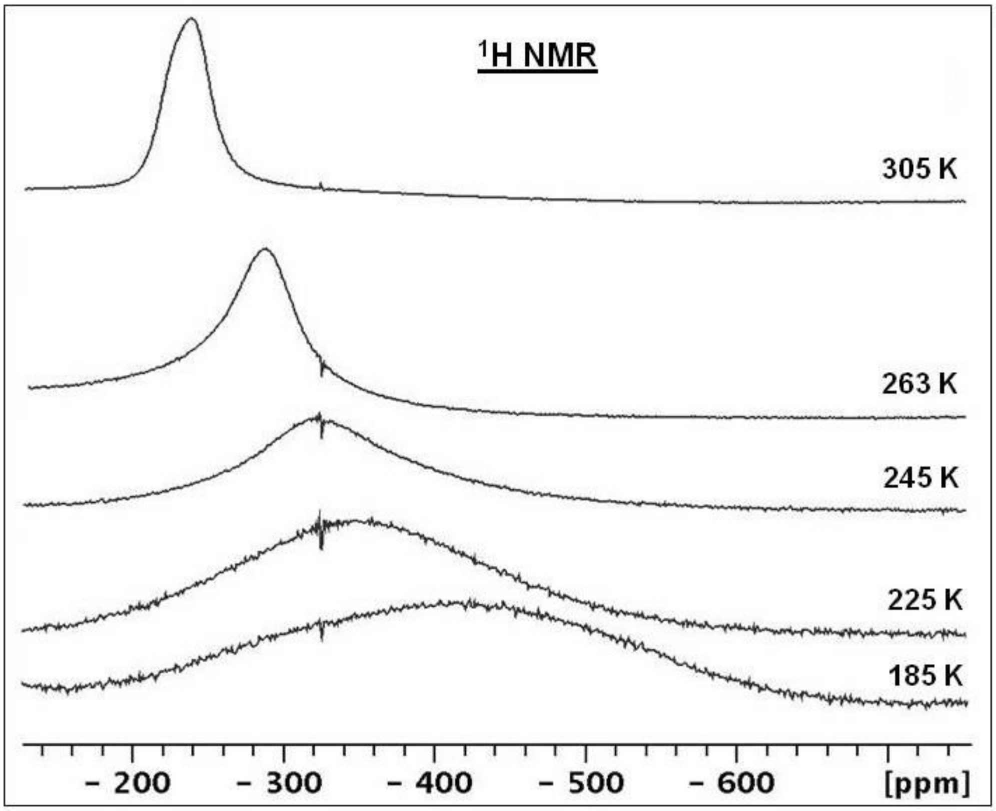

Figure 20. Selected variable temperature ^{1}H wideline NMR spectra of **1-70** obtained without sample rotation at the indicated temperatures.

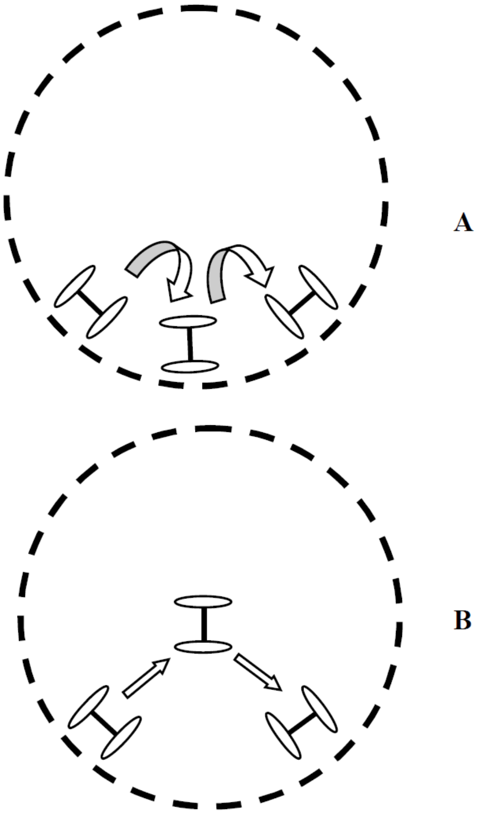

Figure 21. Two motional models leading to a sharp proton resonance of nickelocene on the silica surface.

The wideline spectra clearly show a temperature evolution of the ^{1}H NMR resonance from a liquid-like signal to a very broad line with a line width Δν reaching about 140 kHz at 175 K (Table 4). Note that the ^{1}H T_1 time of the liquid-like signal of **1-70** (0.56 ms) is slightly longer than in **1**. This is probably due to the appearance of a relaxation contribution that is dependent on molecular correlation times.[30] Comparison of the Δν parameters, presented for **1** and **1-70** in Table 4 and Figure 17, reveals that below 225 K the line widths in **1-70** become substantially larger than in **1**, showing a big difference of 42 kHz at 185 K. A formal calculation gives the ^{1}H CSA values of 111 and 162 ppm for

1 and for **1-70**, respectively. Since C_5-rotations of the Cp rings in polycrystalline **1**, as well as in neat ferrocene,[22] are very fast[35,37] and can be detected by NMR only at 110 K, we explain the observed difference by retardation of the Cp–rotations in nickelocene molecules, which are located horizontally on the silica surface. Note that the horizontally-oriented states of the ferrocene on the silica surface were found as the most sable ones in earlier research.[1] It is quite probable that molecule–surface interactions are stronger in the case of **1**, causing the above mentioned retardation at the lowest temperatures.

By analogy with ferrocene (**2**) adsorbed in a submonolayer on the silica surface,[22] the temperature evolution of the ^{1}H resonance in Figure 20 can correspond to two possible motional mechanisms. (a) A chemical exchange on the NMR time scale between liquid-like, truly isotropically-moving states and adsorbed immobile molecules (situation **B** in Figure 21) could take place. (b) Alternatively, consistent motions of the adsorbed molecules along the surface (a "tumbleweed scenario"),[18] which imitates isotropic orientations, could take place. The expected spectral feature of situation **B** is coexistence of the isotropic (sharp) and immobile (broad) resonances in the variable temperature NMR spectra, as it was earlier observed for ferrocene by ^{13}C and ^{2}H NMR.[22] To verify this feature for ferrocene with ^{1}H NMR, the variable-temperature spectra were recorded for sample **2-70** (Figure 22). As can clearly be seen in Figure 22 and the comparison in Figure 23, the spectra of adsorbed ferrocene show this coexistence in contrast to the spectra of **1-70**. Therefore, model **B** with the truly isotropically moving states can be ruled out for adsorbed nickelocene. It should be noted, however, that model **B** can also be realized if the isotropically moving species are intermediates which are not visible in NMR. Under these conditions models **B** and **A** would be *topologically different but spectroscopically identical.*

Finally, as follows from Figure 24, increasing the surface coverage leads to a remarkable decrease in the transformation rate of anisotropic molecular to liquid-like states due to a decrease of the number of free surface sites. Spectroscopically, this corresponds to the strong broadening of the ^{1}H resonance in **1-140**.

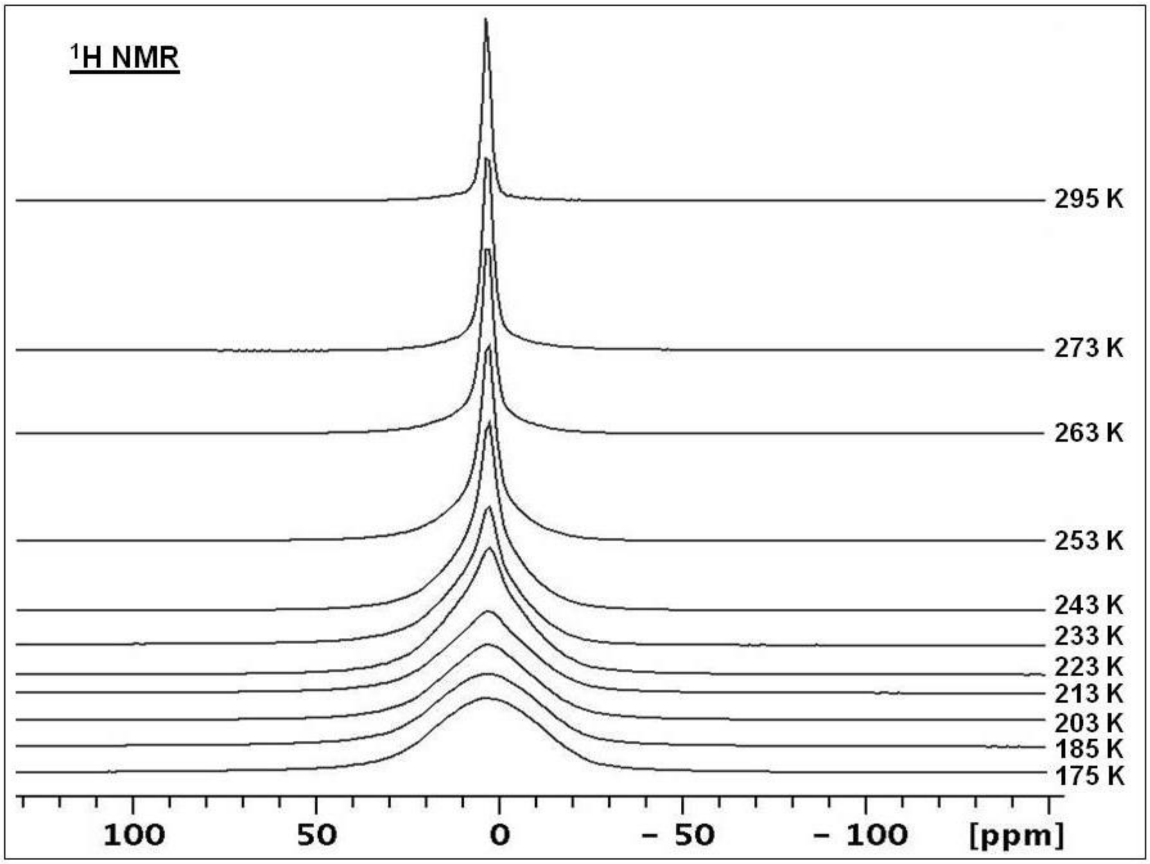

Figure 22. Variable temperature ^{1}H wideline NMR spectra obtained for a static sample of material **2-70** at the indicated temperatures.

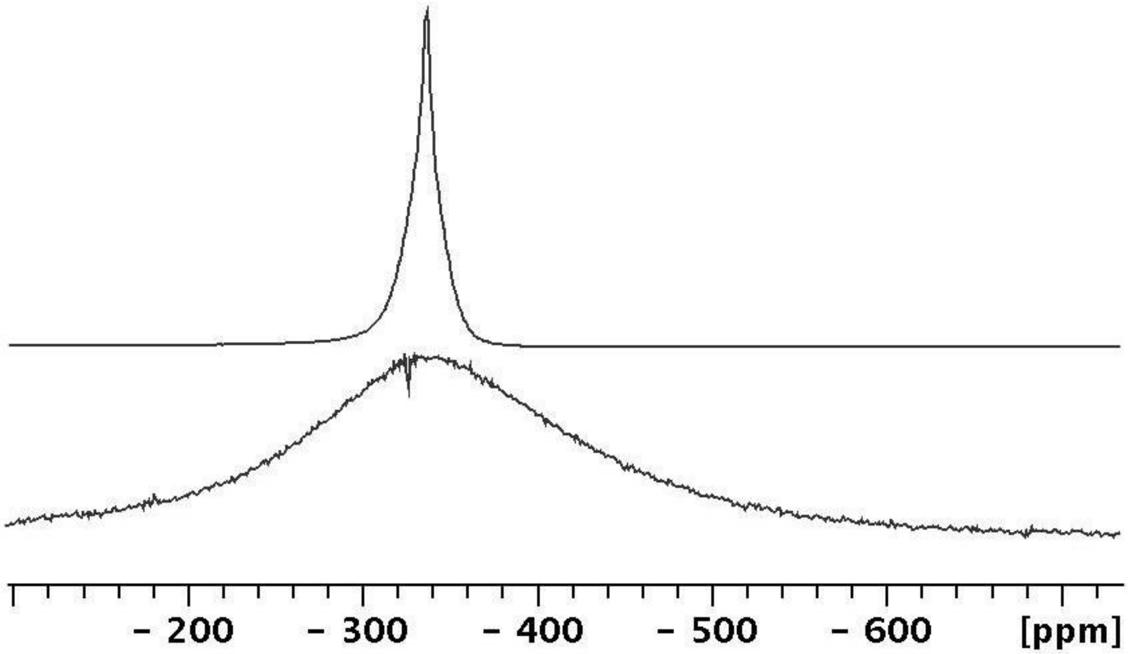

Figure 23. ^{1}H wideline NMR spectra of **2-70** (top) and **1-70** (bottom) recorded at 235 K without sample rotation. The resonance of **2-70** is displayed on top of the resonance of **1-70** for convenience, so the chemical shift scale only accounts for **1-70**.

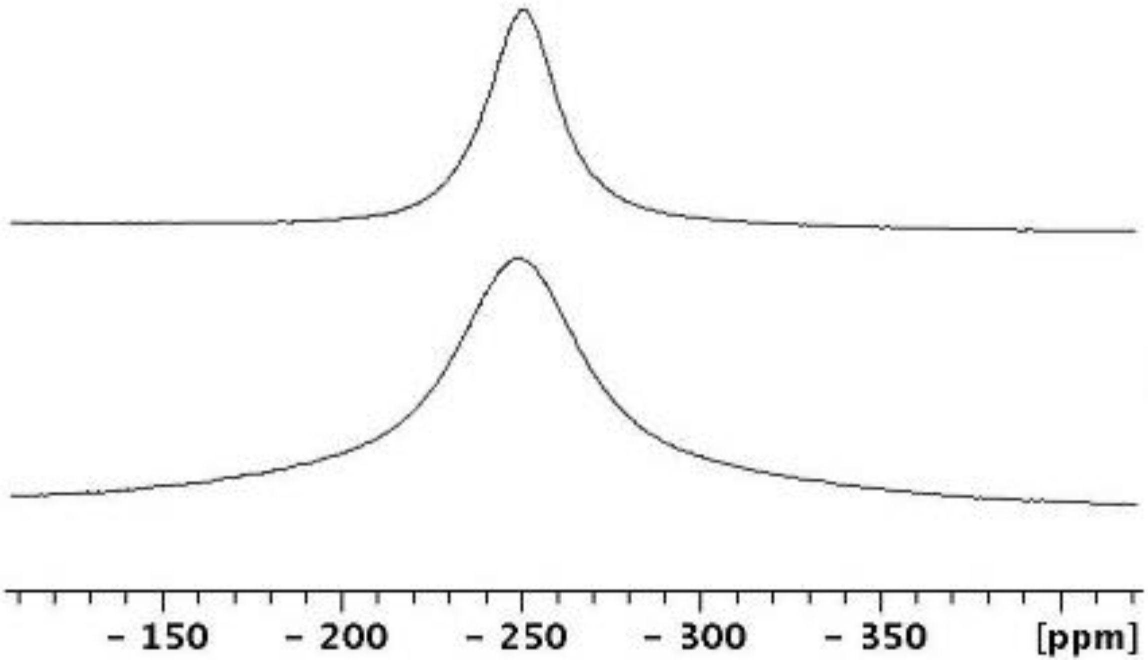

Figure 24. ^{1}H wideline NMR spectra of materials **1-70** (top) and **1-140** (bottom) recorded at 295 K without sample rotation.

The kinetic parameters of the process evolving on the silica surface can be potentially obtained by quantitative treatments of the variable-temperature ^{1}H NMR spectra (Figure 20, where a line-shape analysis plays a central role. However, due to the variety of contributions to the shape of the ^{1}H static signal (anisotropic spin-dipolar interaction, proton-proton dipolar interaction, BMS anisotropy^5), and the impossibility of their accurate separations, such an analysis becomes problematic. In this context, additional information is needed, which can be obtained by considering the ^{1}H MAS NMR spectra in Figure 14, where material **1-70** is compared with **1-140** and **1-200**, containing an excess of **1**. As these ^{1}H MAS NMR spectra show, in contrast to polycrystalline **1** and sample **1-70**, the materials **1-140** and **1-200** exhibit two sets of signals at $\delta_{iso}(^1H) = -243$ ppm and −247 ppm. In both cases, the resonance at −243 ppm, accompanied by spinning sidebands with lower intensities, belongs to more mobile molecules of **1**. It is interesting that the ratio of less mobile to more mobile molecules is determined as 1.3 to 1 and 3.5 to 1 for **1-140** and **1-200**, respectively. Again, lower mobility is found for increased surface coverages, as communicated earlier for adsorbed **2**.[19-21] In addition, there is no exchange between less and more mobile states. This situation can be realized assuming the presence of inhomogeneous distribution of the molecules among silica pores of different sizes. Alternatively, in contrast to **2**,[20] the more firmly adsorbed **1** might prevent rapid exchange between adsorbed and polycrystalline nickelocene on the surface.

The formal sideband analysis of the signals in Figure 14, carried out within the limits of the ^{1}H CSA resulted in the following anisotropy parameters: CSA = 56 ppm at $\eta = 0.9$ for compound **1**; CSA = 16 ppm at $\eta = 0.95$ for material **1-70;** CSA = 32 ppm at $\eta = 0.8$ (-243 ppm) and CSA = 65 ppm at $\eta = 0.95$ (-247 ppm) for material **1-140**; CSA = 35 ppm at $\eta = 0.9$ (-243 ppm) and CSA = 62 ppm at $\eta = 0.9$ (-247 ppm) for material **1-200**. As one can see, at room temperature the materials **1-140** and **1-200** contain immobile nickelocene molecules with CSA values that are close to those of polycrystalline **1**. Additionally, there are mobile molecules with ^{1}H CSA values increasing from 16 ppm (**1-70**) over 32 ppm (**1-140**) to 35 ppm (**1-200**). Thus, this effect illustrates a retardation of the observed motional process by decreasing the number of unoccupied surface sites. This allows us to analyze the VT $^{\mathbf{1}}$H NMR spectra of **1-70** or **1-140** by observing the loss of the CSA with increasing the temperature. Note that the temperature dependent CSA parameters of polycrystalline

1 (Table 5) can be applied as a reference for the immobile compound in the following calculations performed for **1-70**.

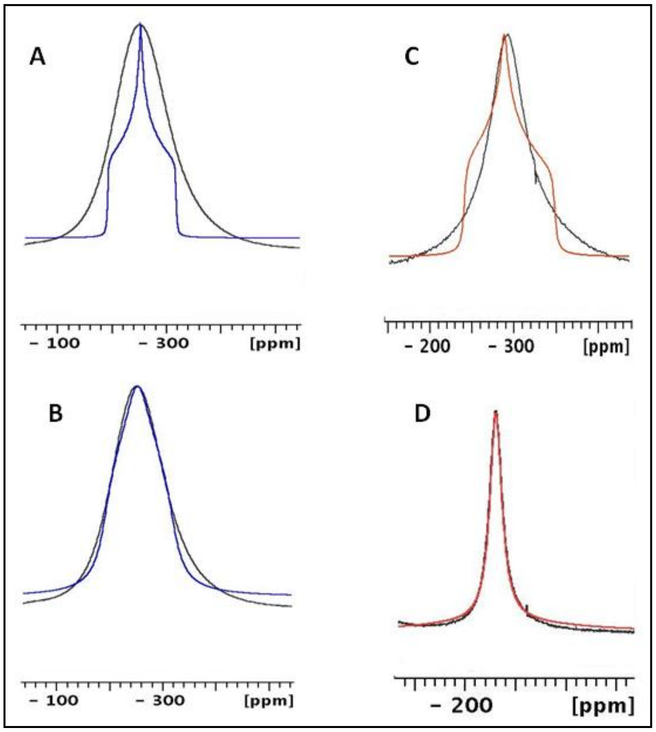

Figure 25. A: Static ^{1}H NMR spectrum of **1** at 295 K (black) and the line shape (blue), calculated with the CSA parameters of **1** on the base of its ^{1}H MAS NMR spectrum. **B**: The line shape of **l** as in A, calculated after addition of 10-12 kHz line broadening to the natural line width, caused by proton-proton dipolar interactions. **C**: Static ^{1}H static NMR spectrum of **1-70** at 263 K (black) and the line shape (brown) calculated for **1** based on the CSA in Table 5. **D**: Best fitting obtained for the ^{1}H NMR spectrum of **1-70** at 283 K.

Figure 25**A** displays the static ^{1}H NMR spectrum of **1** at 295 K, accompanied by a static lineshape. This shape was calculated with the CSA parameters summarized in Table 1, including $\Delta\nu_{rot}$ as the characteristics of a natural line width. Obviously, both line shapes differ substantially. However, the situation changes remarkably when 10-12 kHz are added to the natural line width (Figure 25**B**). This magnitude, representing typical proton-proton dipolar contributions, was estimated from the broad component in the low temperature ^{1}H NMR spectra of the diamagnetic adsorbed ferrocene in sample **2-70** (Figure 22).

Table 1 shows that at T > 245 K the $\Delta\nu$ value in **1-70** is smaller than in **1** by > 10 kHz. Hence, if the rate of molecular motions in **1-70** is > $1{\cdot}10^4$ s^{-1}, the above dipolar proton-proton contribution will be negligible. In other words, quantitative treatments of the ^{1}H NMR spectra of **1-70** are simplified and they can be performed on the basis of the CSA alone. Such a situation is shown in Figure 25**C**, where the ^{1}H static NMR spectrum of **1-70** at 263 K is compared with the line shape calculated for **1** on the basis of the CSA in Table 5. Then, the singularities in this shape, corresponding to chemical shifts δ_{11}, δ_{22} and δ_{33}, can be used within the limits of a three-centered exchange (see, for example, Figure 25**D**) to determine the rate (k) of the loss of the CSA due to motions of **1** on the silica surface. These calculations were carried out using the temperature dependent $\Delta\nu_{rot}$ values for **1** (Table 5), as the natural line widths, and at the constant line width of 7.2 kHz observed for **1-70** at 325 K. The resulting k values were averaged and summarized in Table 6.

Table 6. Temperature dependence of the rate constants k (s-1), obtained by analysis of the static 1H NMR spectra of compound 1-70 (see text).

T (K)	**k·10^3 (s^{-1})**
295	830 / 439[a]
283	582
273	450 / 219[a]
263	341
253	217
245	177

[a] obtained for material **1-140**.

First of all, the obtained data show that, going from **1-70** to **1-140** the motional rate k decreases by approximately two times. Second, the temperature dependencies of the rate k in coordinates of ln(k) versus 1/T (Figure 26), or ln(k/T) versus 1/T (Figure 27), form ideal straight lines that allow the determination of the kinetic parameters $E_{act} = 5.5$ kcal/mol, $A = 1.1 \cdot 10^{10}$, $\Delta H^{\ddagger} = 5.0$ kcal/mol, and $\Delta S^{\ddagger} = -15$ e.u.

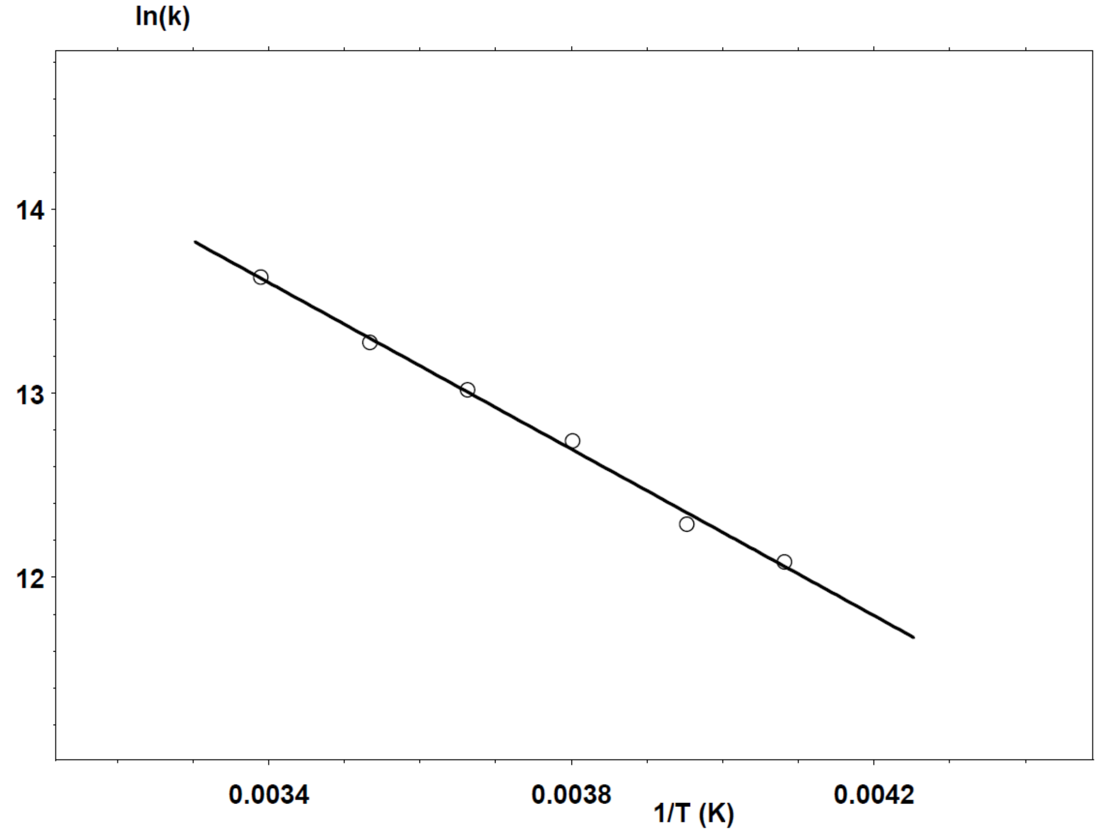

Figure 26. Temperature dependence of the rate constants k obtained for **1** absorbed on the silica surface in a submonolayer (sample **1-70**) in coordinates of ln(k) versus 1/T.

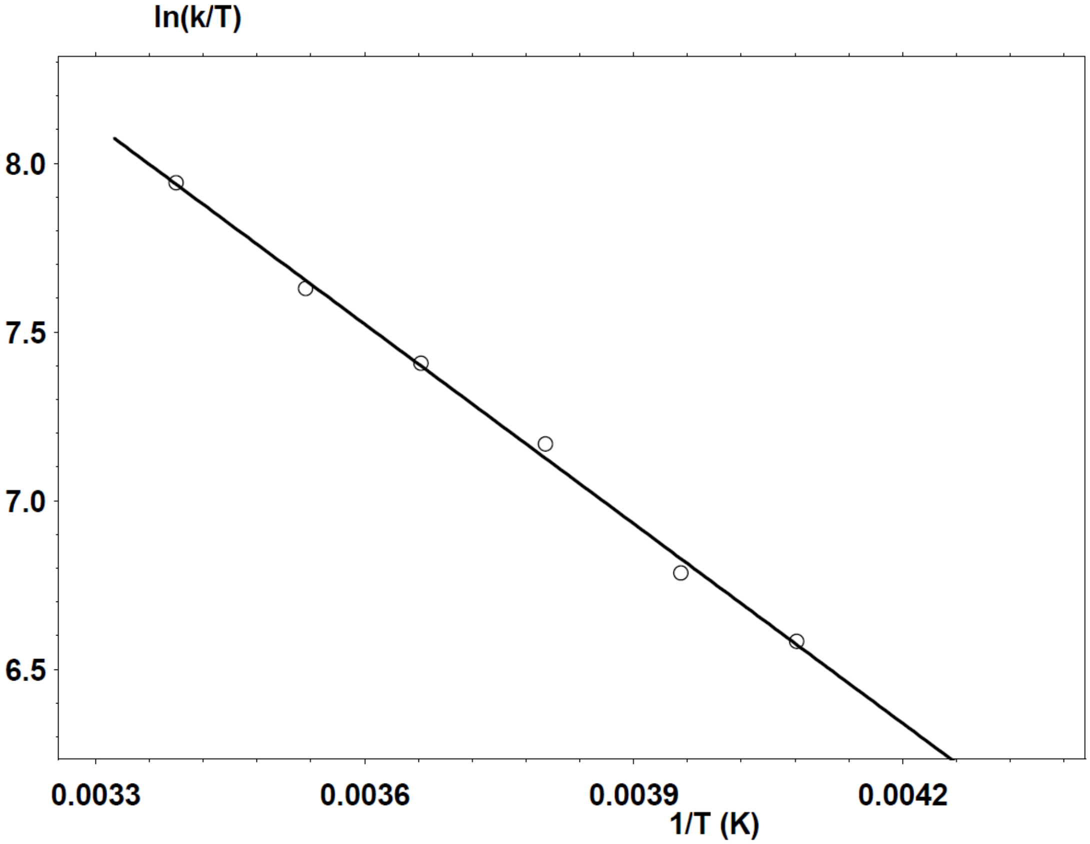

Figure 27. Temperature dependence of the rate constants k obtained for material **1-70** in coordinates of ln(k/T) versus 1/T.

Finally, one can conclude that the dynamics of ferrocene[1] and nickelocene adsorbed in submonolayers on the silica surface and also of triphenylphosphine oxide on alumina[11] are similar and show rates in diapason.

Conclusion

In summary, the results described in this contribution lead to the conclusion that the molecular dynamics of nickelocene on the silica surface is similar to those of ferrocene on silica[22] and triphenylphosphine oxide on alumina.[5] This is in spite of the differences in surface-molecule interactions. The rates of motions are on the same time scales and the motions themselves consist of rotations and jumps, changing the orientation of the rotational axis. It is remarkable that this combination is often considered as interpretation of the molecular dynamics in highly viscous liquids that are investigated theoretically and experimentally by dielectric spectroscopy, and NMR spectroscopy including NMR relaxation.[39-42]

Experimental Section

Materials. The silica (Merck, 40 Å average pore diameter, 0.063-0.2 mm average particle size, specific surface area 750 m^2/g) was dried *in vacuo* at 200° C for 2 days to remove adsorbed water and condense surface silanol groups.[15,43]

Sample preparation. The maximal surface coverage of the silica with **2** has been determined earlier.[20] Since ferrocene and nickelocene have the same foot prints, samples of adsorbed **1** can be prepared using the same molar amounts. Sample **1-70** was prepared by dry grinding of 191.0 mg (1.011 mmol) of Cp_2Ni (**1**) with 256 mg of silica in a glove box for 1.5 minutes using a pestle and mortar. Sample **1-140** was created by dry grinding of **1** (188.0 mg, 0.995 mmol) with 127 mg of silica. The sample **1-200** was generated by dry grinding of 277.0 mg (1.467 mmol) of **1** with 126 mg of silica. All samples of **1** adsorbed on silica displayed a moss green color.

NMR instrumentation and measurements. The $^{13}C\{^{1}H\}$ and ^{1}H MAS and static ^{1}H NMR experiments were carried out with a Bruker Avance 400 solid-state NMR spectrometer (400 MHz for ^{1}H nuclei) equipped with a two-channel 4 mm MAS probe head. The standard single pulse sequences (direct nuclear excitation with a 50° radio frequency pulse) were applied for the nuclei ^{13}C using recycle delays as needed for the corresponding full spin-lattice relaxation estimated based on the inversion-recovery experiments.

The static ^{1}H NMR data were collected with a solid-echo pulse sequence ($90° - \tau - 90°$) with a τ delay of 40 μs, a 90° pulse length of 5.25 μs, and a relaxation delay of 4 s. All samples were densely packed into the insert-free rotors as finely ground powders. Compressed nitrogen was used as both the bearing and drive gas for the MAS measurements.

The variable-temperature ^{13}C and ^{1}H NMR experiments have been performed with a standard temperature unit of the spectrometer calibrated with liquid methanol placed into a 4 mm rotor. The experimental ^{13}C and ^{1}H T_1 relaxation times were measured by inversion-recovery ($180° - \tau - 90°$) experiments, and rf pulses were calibrated and τ delays widely varied to determine rough T_1 estimates. Relaxation (recycle) delays were adjusted to provide full nuclear relaxation in each cycle.

The experimental ^{1}H inversion-recovery data for the displays of signal intensity versus τ time have been treated with a standard nonlinear fitting computer program based on the Levenberg–Marquardt algorithm.[44] The statistical errors of the ^{1}H T_1 time determinations were <15%. The lineshape analysis of the static ^{1}H VT NMR spectra was performed with the program DNMR in the software package of the Bruker spectrometer.

References

1. Benzie, J. W.; Bakhmutov, V. I.; Blümel, J. Benzene Adsorbed on Activated Carbon: A Comprehensive Solid-State NMR Study of Interactions with the Pore Surface and Molecular Motions, *J. Phys. Chem. C* **2020**, *124*, DOI: 10.1021/acs.jpcc.0c06225.

2. Hilliard, C. R.; Bhuvanesh, N.; Gladysz, J. A.; Blümel, J. Synthesis, purification, and characterization of phosphine oxides and their hydrogen peroxide adducts, *Dalton Trans.* **2012**, *41*, 1742-1754.

3. Hilliard, C. R.; Kharel, S.; Cluff, K. J.; Bhuvanesh, N.; Gladysz, J. A.; Blümel, J. Structures and Unexpected Dynamic Properties of Phosphine Oxides Adsorbed on Silica Surfaces, *Chem. Eur. J.* **2014,** *20*, 17292-17295.

4. Kharel, S.; Cluff, K. J.; Bhuvanesh, N.; Gladysz, J. A.; Blümel, J. Structures and Dynamics of Secondary and Tertiary Alkylphosphine Oxides Adsorbed on Silica, *Chem. Asian J*. **2019**, *14*, 2704-2711.

5. Hubbard, P. J.; Benzie, J. W.; Bakhmutov, V. I.; Blümel, J. Disentangling different modes of mobility for triphenylphosphine oxide adsorbed on alumina, *J. Chem. Phys*. **2020**, *152*, 054718.

6. Kharel, S.; Bhuvanesh, N.; Gladysz, J. A.; Blümel, J. New hydrogen bonding motifs of phosphine oxides with a silanediol, a phenol, and chloroform, *Inorg. Chim. Acta* **2019**, *490*, 215-219.

7. Ahn, S. H.; Cluff, K. J.; Bhuvanesh, N.; Blümel, J. Hydrogen Peroxide and Di(hydroperoxy)propane Adducts of Phosphine Oxides as Stoichiometric and Soluble Oxidizing Agents, *Angew. Chem. Int. Ed*. **2015**, *54*, 13341-13345.

8. Arp, F. F.; Bhuvanesh, N.; Blümel, J. Hydrogen peroxide adducts of triarylphosphine oxides, *Dalton Trans*. **2019**, *48*, 14312-14325.

9. Ahn, S. H.; Lindhardt, D.; Bhuvanesh, N.; Blümel, J. Di(hydroperoxy)cycloalkanes Stabilized via Hydrogen Bonding by Phosphine Oxides: Safe and Efficient Baeyer–Villiger Oxidants, *ACS Sustainable Chem. Eng.* **2018**, *6*, 6829-6840.

10. Ahn, S. H.; Bhuvanesh, N.; Blümel, J. Di(hydroperoxy)alkane Adducts of Phosphine Oxides: Safe, Solid, Stoichiometric, and Soluble Oxidizing Agents, *Chem. Eur. J.* **2017**, *23*, 16998-17009.

11. Arp, F. F.; Nattamai Bhuvanesh, N.; Blümel, J. Di(hydroperoxy)cycloalkane Adducts of Triarylphosphine Oxides: A Comprehensive Study Including Solid-State Structures and Association in Solution, *Inorg. Chem*. **2020**, *59*, 13719-13732.

12. Fyfe, C. A., *Solid-State NMR for Chemists*. C.F.C. Press, Guelph, Canada, 1983.

13. Duncan, T. M. *A Compilation of Chemical Shift Anisotropies*. Farragut Press: Chicago, IL, 1990.

14. Guenther, J.; Reibenspies, J.; Blümel, J. Synthesis and characterization of tridentate phosphine ligands incorporating long methylene chains and ethoxysilane groups for immobilizing molecular rhodium catalysts, *Mol. Catal*. **2019**, *479*, 110629.

15. Iler, R. K., *The Chemistry of Silica*, John Wiley, New York, **1979**.

16. Oprunenko, Y.; Gloriozov, I.; Lyssenko, K.; Malyugina, S.; Mityuk, D.; Mstislavsky, V.; Günther, H.; Von Firks, G.; Ebener, M. Chromium tricarbonyl complexes with biphenylene as η^6 ligand: synthesis, structure, dynamic behaviour in solid state and thermal η^6,η^6-haptotropic rearrangements. Experimental (NMR) and theoretical (DFT) studies, *J. Organomet. Chem*. **2002**, *656*, 27-42.

17. Schnellbach, M.; Blümel, J.; Köhler, F. H. The Union Carbide catalyst ($Cp_2Cr + SiO_2$), studied by solid-state NMR, *J. Organomet. Chem.* **1996**, *520*, 227-230.

18. Cluff, K. J.; Schnellbach, M.; Hilliard, C. R.; Blümel, J. The adsorption of chromocene and ferrocene on silica: A solid-state NMR study, *J. Organomet. Chem.* **2013**, *744*, 119-124.

19. Cluff, K. J.; Blümel, J. Adsorption of ferrocene on carbon nanotubes, graphene, and activated carbon, *Organometallics* **2016**, *35*, 3939−3948.

20. Cluff, K. J.; Blümel, J. Adsorption of Metallocenes on Silica, *Chem. Eur. J.* **2016**, *22*, 16562-16575.

21. Cluff, K. J.; Bhuvanesh, N.; Blümel, J. Adsorption of Ruthenium and Iron Metallocenes on Silica: A Solid-State NMR Study, *Organometallics* **2014**, *33*, 2671-2680.

22. Hubbard, P. J.; Benzie, J. W.; Bakhmutov, V. I.; Janet Blumel, J., Ferrocene adsorbed on silica and activated carbon surfaces: a solid-state NMR study of molecular dynamics and surface interactions, *Organometallics* **2020**, *39*, 1080–1091.

23. Li, K.-T.; Yang, C.-N. Uniform rod-like self-assembly of polymer nanofibrils produced via propylene polymerization on Stober silica nuclei supported metallocene catalysts, *Mater. Today Commun*. **2019**, *19*, 80-86.

24. Estrada-Ramirez, A. N.; Ventura-Hunter, C.; Vitz, J.; Díaz-Barriga Castro, E.; Peralta-Rodriguez, R. D.; Schubert, U. S.; Guerrero-Sánchez, C.; Pérez-Camacho, O. Poly(n-alkyl methacrylate)s as Metallocene Catalyst Supports in Nonpolar Media, *Macromol. Chem. Phys*. **2019**, *220* (19), 1900259.

25. Bernardes, A. A.; Scheffler, G. L.; Radtke, C.; Pozebon, D.; dos Santos, J. H. Z.; da Rocha, Z. N. Supported metallocenes produced by a non-hydrolytic sol-gel process: Application in ethylene polymerization, *Colloids Surf. A Physicochem. Eng. Asp*. **2020**, *584*, 124020.

26. McKenna, W. P.; Bandyopadhyay, S.; Eyring, E. M. FT-IR/PAS Investigation of Chromocene Supported on Silica, *Applied Spectrosc*. **1984**, *38*, 834-837, and references cited.

27. Karol, F. J.; Karapinka, G. L.; Wu, C.; Dow, A. W.; Johnson, R. N.; Carrick, W. L. *J. Polym. Sci. A1* **1972**, *10*, 2621.

28. Heise, H.; Frank H. Köhler, F. H.; Xie, X. Solid-state NMR spectroscopy of paramagnetic metallocenes, *J. Magn. Reson*. **2001**, *150*, 198–206.

29. Pritchard, B. P.; Simpson, S.; Zurek, E.; Autschbach, J. Computation of chemical shifts for paramagnetic molecules: a laboratory experiment for the undergraduate curriculum, *J. Chem. Educ*. **2014**, 91, 1058−1063.

30. Pell, A. J.; Pintacuda, G.; Grey, C. P.; Paramagnetic NMR in solution and the solid state, *Progr. Nucl. Magn. Reson. Spectr*. **2019,** *111*, 1–271.

31. Pope, J.; Sue, H.-J.; Bremner, T.; Blümel, J. High-temperature steam-treatment of PBI, PEEK, and PEKK polymers with H_2O and D_2O: A solid-state NMR study, *Polymer* **2014**, 55, 4577-4585.

32. Pope, J. C.; Sue, H.-J.; Bremner, T.; Blümel, J. Multinuclear solid-state NMR investigation of the moisture distribution in PEEK/PBI and PEKK/PBI blends, *J. Appl. Polym. Sci.* **2015**, *132*, 1804-1816.

33. Köhler, F. H.; Xie, X.; Vanadocene as a temperature standard for ^{13}C and ^{1}H MAS NMR and for solution-state NMR Spectroscopy, *Magn. Reson. Chem*. **1997**, *35*, 487-492.

34. Martin, B.; Autschbach, J. Temperature dependence of contact and dipolar NMR chemical shifts in paramagnetic molecules, *J. Chem. Phys*. **2015**, *142*, 054108.

35. Blümel, J.; Hiller, W.; Herker, M.; Köhler, F. H. Solid-State Paramagnetic NMR Spectroscopy of Chromocenes, *Organometallics* **1996**, *15*, 3474-3476.

36. Bakhmutov, V. I.; Strategies for solid-state NMR studies of materials: from diamagnetic to paramagnetic porous solids, *Chem. Rev*. **2011**, *111*, 530–562.

37. Narankiewicz, Z.; Blumenfeld, A. L.; Bondareva, V. L.; Mamedyarova, I. A.; Nefedova, M. N. Sokolov, Molecular motions and the structure of β-cyclodextrin inclusion complexes with ferrocene, (3)-Ferrocenophane-l,3-dione and ruthenocene. *J. Inclusion Phenom. Mol. Recognit. Chem*. **1991**, *11*, 233−245.

38. Rouf, S. A.; Mares, J.; Vaar, J.; Relativistic approximations to paramagnetic NMR chemical shift and shielding anisotropy in transition metal systems, J. Chem. Theory Comput. 2017, 13, 8, 3731–3745.

39. Meier, R.; Kahlau, R.; Kruk, D.; Rossler, E. A.; Comparative studies of the dynamics in viscous liquids by means of dielectric spectroscopy and field cycling NMR, *J. Phys. Chem. A*, **2010,** *114*, 7847–7855.

40. Kruk, D.; Mielczarek, A; Korpala, A.; Kozlowski, A.; Earle, K. A.; Moscicki, J.; Sensitivity of ^{2}H NMR spectroscopy to motional models: proteins and highly viscous liquids as examples, *J. Chem. Phys*. **2012**, *136*, 244509.

41. Polimeno, A.; Freed, J. H.; A many-body stochastic approach to rotational motions in liquids: complex decay times in highly viscous fluids, *Chem. Phys. Letters*. **1990**, *16*, 481-488.

42. Rossler, E.; Taucher, J.; Eiermann, P. Cooperative reorientations, tranlsation motions, and rotational jumps in viscous liquids, *J. Phys. Chem.* **1994**, *98*, 8173-8180.

43. Blümel, J. Reactions of Ethoxysilanes with Silica: A Solid-State NMR Study, *J. Am. Chem. Soc*. **1995**, *117*, 2112-2113.

44. Levenberg, K. A Method for the Solution of Certain Non-Linear Problems in Least Squares, *Quart. Appl. Math.* **1994**, *2*, 164-168.

CHAPTER IV

METALLOCENES ADSORBED ON SILICA SURFACES MIMICKING HIGHLY VISCOUS LIQUIDS IN SOLID-STATE NMR

Introduction

Investigations of small guest molecules such as water, alcohols, carbonic acids or protein solutions located in pores of different materials, are of great interest. This concerns particularly the characterization of their dynamics on the surface. These studies provide a deeper understanding of how the pores are populated by the guest molecules and how different pore surfaces interact with them. Understanding these interactions is important because they affect the phase states of the adsorbed molecules, which in turn influence thermophysical processes, such as freezing and melting points, and glass transitions.[1] For example, the depression of melting points is well-known for guest molecules in porous materials.[2] It should be noted that the melting point depression depends on the pore size and that this effect can be significant.[3] In other words, a solid in its bulk phase can become a liquid when this solid is confined inside pores.[1] All of the above aspects are very important for numerous processes in industry and academia that involve separation sciences and catalysis.

Recently, we have reported that molecules of ferrocene (Cp_2Fe, $(C_5H_5)_2Fe$, **2**)[4,5] and nickelocene (Cp_2Ni, $(C_5H_5)_2Ni$, **1**)[6] perform fast reorientations on silica surfaces. These motions can only be stopped on the NMR time scale by lowering the temperature. According to these studies, the molecular reorientations represent a combination of rotational motions and jumps, which change the orientation of the rotational axis. In general, such combinations are often considered when interpreting molecular dynamics in highly viscous liquids. The latter are well-studied theoretically and experimentally by dielectric and NMR spectroscopy, as well as NMR relaxation.[7-10]

In the context of studies that involve metallocenes adsorbed on silica surfaces it was important to establish the phase state of the absorbed molecules that are solids with high melting points in the neat, polycrystalline state. To clarify this question, in the presened work we investigate material **1-200**, which contains double the amount of nickelocene that would be needed for a monolayer with 100% surface coverage. We assume that sample **1-200** assumes a double-layer surface coverage, as depicted in Figure 28. This material is compared to the samples **1-70** and **1-140** with 70% and 140% surface coverages.[6] In addition, the mutual influence of **1** and **2** on each other has been studied by NMR experiments using the materials **1-40-2-40** and **1-20-2-20** that contain both **1** and **2** with equal sub-monolayer amounts on the same silica surface. As in the previous communications,[5,6] the most powerful method for the studies was variable temperature ^{1}H and ^{13}C wideline and MAS NMR, including the ^{1}H T_1 time measurements.

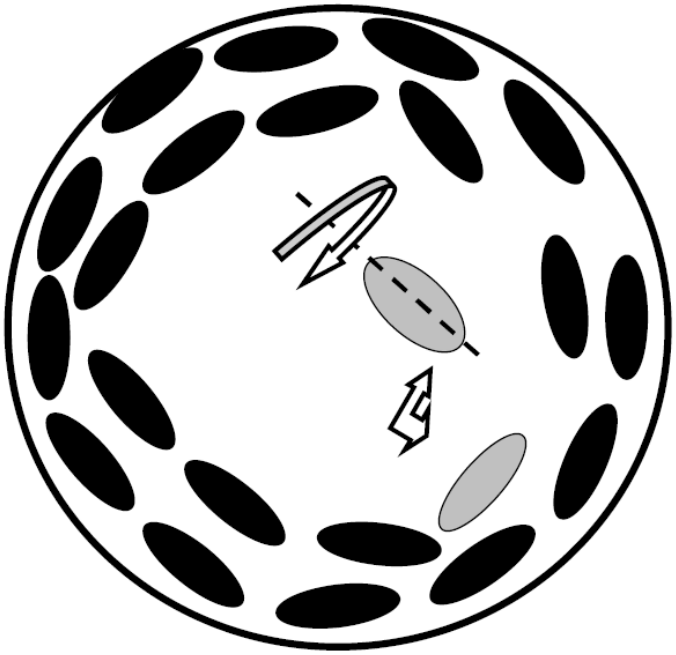

Figure 28. An idealized pore of the silica, where metallocene molecules form a double layer experiencing rotations and jumps, mimicking a liquid on the surface.

Results and Discussion

Figure 29 shows the ^{1}H MAS NMR spectra of material **1-200**, in comparison with polycrystalline **1** and samples **1-70** and **1-140**, recorded at 295 K with a spinning rate of 10 kHz at 295 K.

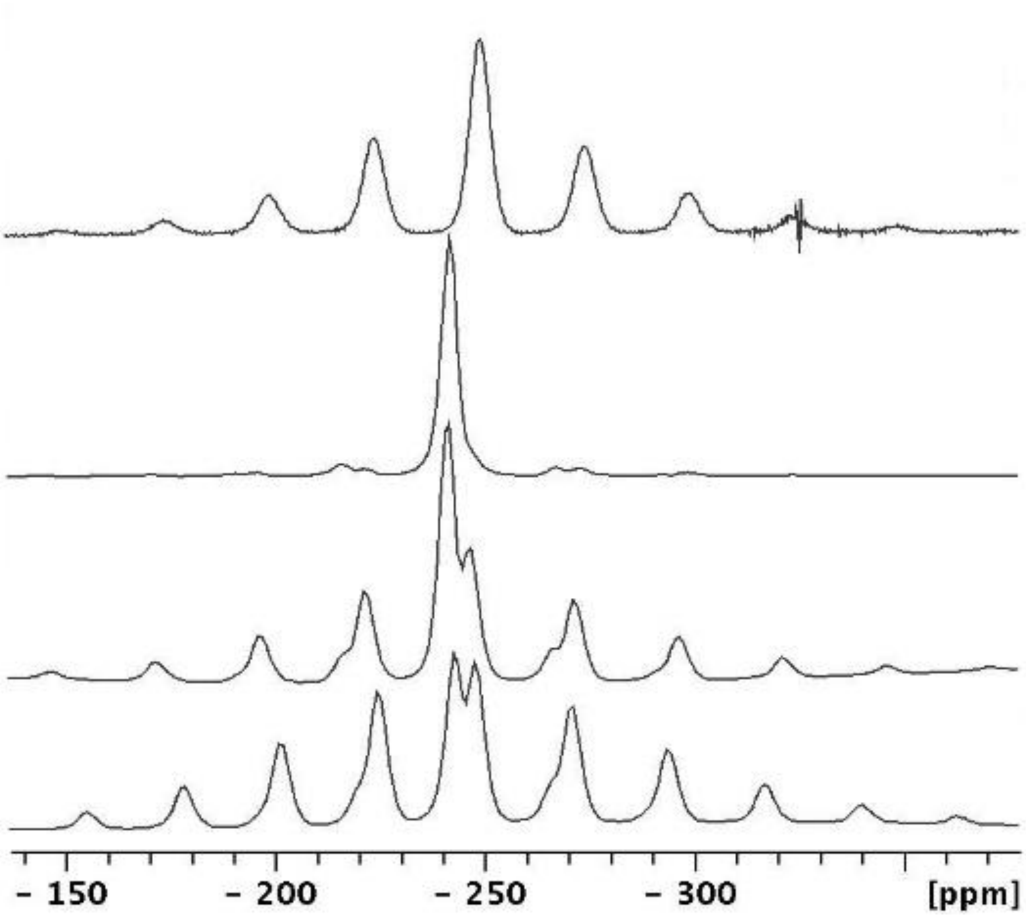

Figure 29. ^{1}H MAS NMR spectra, recorded at 295 K with a spinning rate of 10 kHz. From top to bottom: compound **1**, sample **1-70**, **1-140**, and **1-200**.

As the spectra show, in contrast to polycrystalline **1** and material **1-70**, the samples **1-200** and **1-140** exhibit two signals with spinning sideband patterns. The ^{1}H isotropic resonances are located at δ_{iso} = -243 ppm and -247 ppm. It is also obvious that the resonance at -243 ppm in materials **1-70**, **1-140** and **1-200** is accompanied by less intense spinning sidebands. As reported earlier,[6] this resonance belongs to more mobile molecules of **1**, the relative content of which decreases substantially when proceeding from **1-140** to **1-200**. Finally, it should be emphasized that, since the signals in the spectra are sharp, chemical exchange between these two states of the molecules does not take place. This situation can be realized, when a distribution of the molecules between pores of different sizes on the silica that is not homogeneous, is taken into account.

Since the intensities of the sidebands are remarkably different for all of the materials (Figure 29), their ^{1}H MAS NMR spectra have been used in a sideband analysis[6] to calculate chemical shift anisotropies (CSA) characterizing the Cp ring protons of each state. The following parameters were obtained: ^{1}H CSA = 56 ppm (η = 0.9) for polycrystalline **1**; ^{1}H CSA = 16 ppm (η = 0.95) for material **1-70**; ^{1}H CSA = 32 ppm (η = 0.8) for the signal -243 ppm and ^{1}H CSA = 65 ppm (η = 0.95) for the signal at -247 ppm in material **1-140**; ^{1}H CSA = 35 ppm (η = 0.9) for the signal at -243 ppm and ^{1}H CSA = 62 ppm (η = 0.9) for the signal at -247 ppm in material **1-200**. As follows from these parameters, materials **1-140** and **1-200** contain at room temperature *immobile* nickelocene molecules with CSA values that are close to those of polycrystalline **1**, and *mobile* molecules with ^{1}H CSA values that increase from **1-70** to **1-140** and **1-200** (16, 32 and 35 ppm, respectively).

Among the materials presented in this work, the dynamics of **1** in material **1-200** with a double-layer surface coverage is most interesting. The variable temperature ^{1}H MAS NMR experiments performed on a sample of **1-200** are presented in Figure 30. The sideband intensities, accompanying the isotropic resonances, decrease upon heating the materials. Thus, in spite of the double-layer pore coverage in material **1-200**, the molecules of **1** are still moving and their mobility increases significantly at higher temperatures. This means that nickelocene does not behave as a polycrystalline solid in the pores of the silica, but it is experiencing again rotations and jumps.[6] This conclusion is supported by the ^{13}C MAS NMR spectra of **1-200**, presented in Figure 31. As it can be seen, at 295 K the spectrum shows an isotropic resonance of mobile molecules at 1531 ppm[11,12] and a lower intensity spinning sideband pattern belonging to less mobile molecules. Upon heating, the isotropic resonance shifts to lower field. The chemical shifts of 1432 ppm at 315K and 1340 ppm at 335 K illustrate the well-known temperature effect on paramagnetic chemical shifts.[13,14]

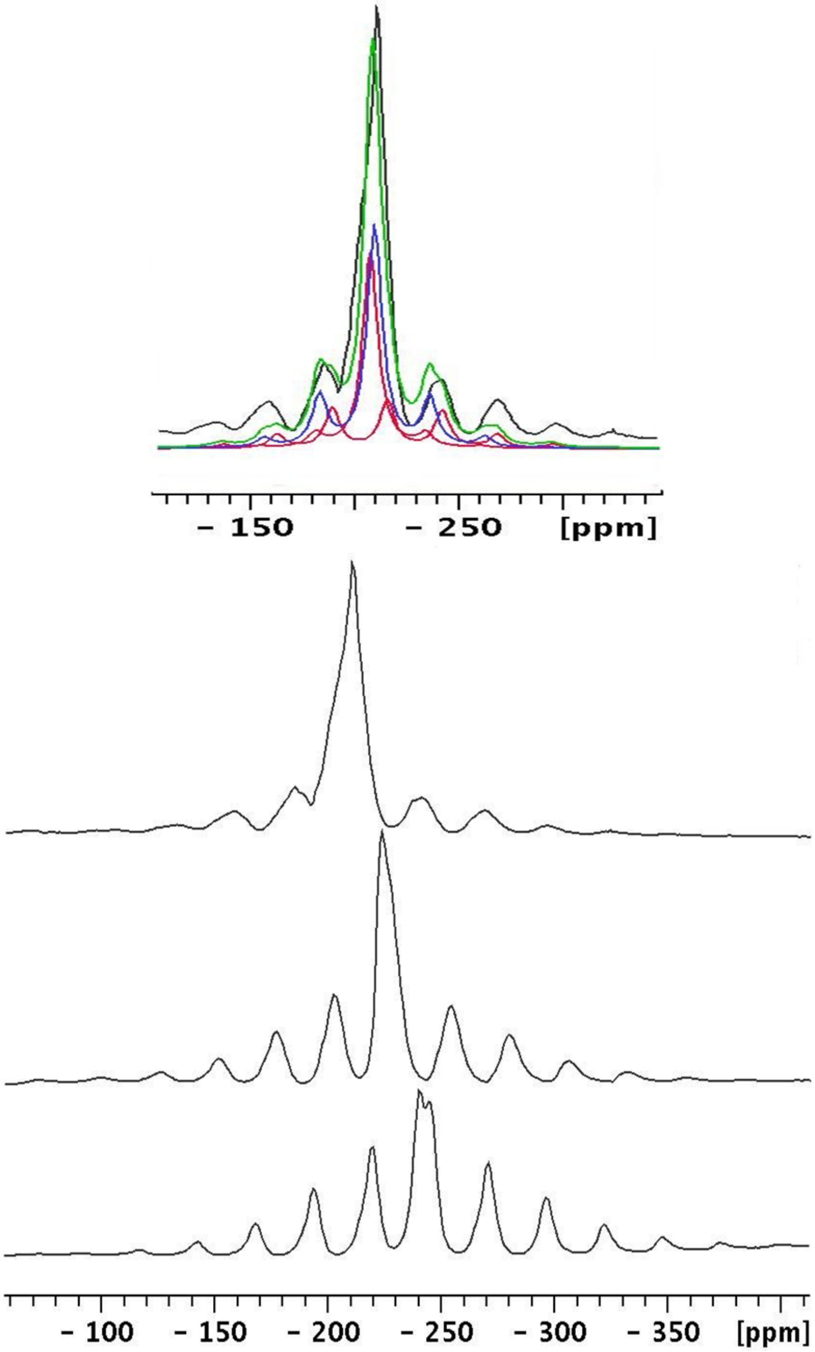

Figure 30. ^{1}H MAS NMR spectra of **1-200** recorded at a spinning rate of 10 kHz. From top to bottom: 335 K, 315 K, 295 K. Top trace: simulation of the 335 K ^{1}H MAS NMR spectrum of **1-200**.

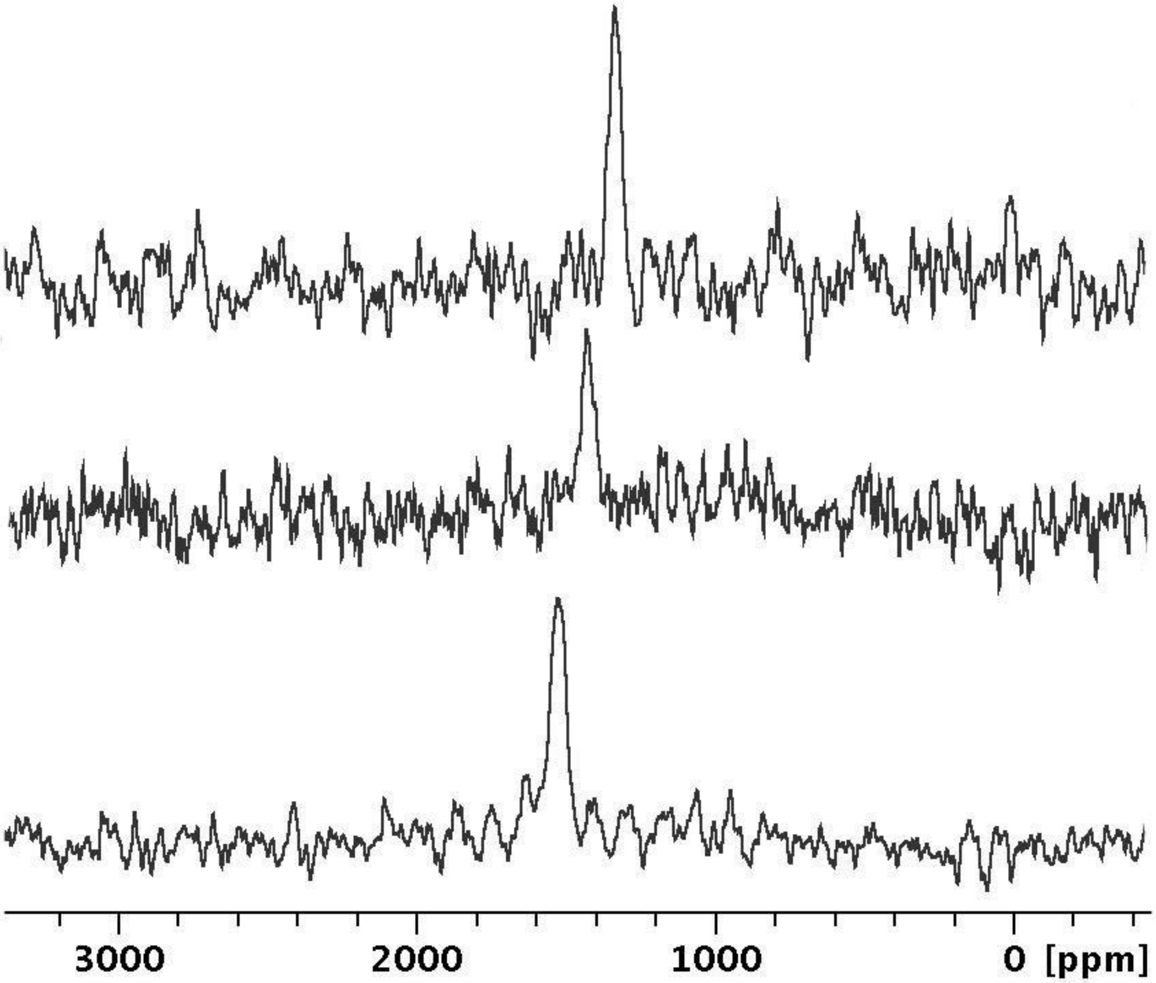

Figure 31. ^{13}C Hahn-echo MAS NMR spectra of material **1-200**, recorded at a spinning rate of 10 kHz. From top to bottom: 335 K, 315 K and 295 K. The spectra were collected with a frequency carrier located at the δ value of 1500 ppm.

In order to render our considerations more quantitative, we performed simulations of the sideband patterns, observed at 335 K in the ^{1}H MAS NMR spectrum of **1-200** (Figure 30). These cannot be carried out within the frameworks of a single site. The simulations give three subspectra with ^{1}H CSA of 23 ppm ($\eta = 0.94$) for δ_1(iso) of -206 ppm, ^{1}H CSA of 40 ppm ($\eta = 0.94$) for δ_2(iso) = -208.0 ppm and ^{1}H CSA of 69 ppm ($\eta = 0.94$) for the low intensity pattern with δ_3(iso) = -214 ppm. The chemical shift and CSA values provide the obvious assignments: the highest field resonance belongs to immobile polycrystalline nickelocene. These molecules, estimated to represent about 20%, are probably located outside of the pore space. Two lower-field signals correspond to mobile molecules, located in pores of different sizes and moving at different rates. At room temperature material **1-70** contains only fast moving molecules of adsorbed **1** and the rates of their motions have been determined earlier.[6] We characterized this material additionally by the ^{1}H CSA obtained from the ^{1}H MAS NMR spectra between 253 and 295 K (Table 7), when the molecular motions occur on the NMR time scale.[6]

Table 7. Temperature dependence of ^{1}H CSA values calculated from ^{1}H MAS NMR experiments on sample **1-70** spinning at a rate of 10 kHz versus motion correlation times of **1** (τ_C) on the silica surface of **1-70** obtained from rate constants k[6] as τ_C = 1/k.

T (K)	**$\tau_C \cdot 10^{-6}$ (s)**	**CSA (ppm) with η = 0.9**
295	1.2	16
283	1.7	29
273	2.2	42
263	2.9	46
253	4.5	54

Then, by using the τ_C – CSA correlation of Table 7, the components moving faster and slower in material **1-200** with ^{1}H CSA of 23 and 40 ppm at 335 K correspond to τ_C = $1.6 \cdot 10^{-6}$ s and $2.2 \cdot 10^{-6}$ s, respectively. Generally, the molecular motion correlation times even in liquids are often described by τ_C distributions. For example, the NMR spectra of benzene-d_6 in tricresyl phosphate at 208 K were well reproduced theoretically in the presence of a Gaussian distribution, where τ_C values were of the order of tenths of μs or less.[8] For objective reasons, the NMR experiments performed here cannot provide information about a τ_C distribution. Nevertheless, the τ_C values, obtained above for material **1-200** could correspond to the center of a distribution. By using these values, we can calculate the viscosity η for a double-layered phase state of nickelocene on the silica surface at 335 K via the Stokes-Einstein-Debye equation **(6)**.

$$\textbf{(6)} \qquad \tau_C = 4\,\pi\,a^3\,\eta\,/\,3\,kT$$

Here, the molecular radius (a) for **1** can be assumed to be 3.5 Å and k is the Boltzmann constant. The viscosity is calculated by using τ_C of $1.6 \cdot 10^{-6}$ s to $2.2 \cdot 10^{-6}$ s as 41 to 57 Pa·s. As it is well known, the η magnitudes between 10^1 and 10^3 Pa·s are typical for pastes, gels, and other *semisolids*, but not for solids.[8] The observed behavior of nickelocene molecules adsorbed on the surface within silica pores could in principle be attributed to the depression of the melting point.[1] However, the depression of > 110 K in the case of nickelocene or ferrocene, melting at 444-445 K, seems way too large. We believe that the phase state of nickelocene molecules within the silica pores of material **1-200** with a double-layer coverage can be accepted as a highly viscous liquid with motions depicted in Figure 28. One can imagine that this phase state can be realized, when the nickelocene−surface interactions are stronger than the intermolecular interactions within the layers.

In general, we interpret the observed phenomenon as Highly Viscous Liquid Model (HVLM), where the viscosity depends on the strength of the surface−molecule interactions and the number of free surface sites. Developing this concept, we also investigated mixed systems containing paramagnetic **1** and diamagnetic **2** in the materials **1-40-2-40** (40% for each component to account for a total surface coverage of 80%) and **1-20-2-20** (20% for each component to result in a total coverage of 40%). The room temperature the ^{1}H NMR spectra of **1-40-2-40**, recorded in static and spinning regimes are shown in Figure 32. Two isotropic resonances in a 1 : 1 ratio are observed at 5.1 and -250.6 ppm for compounds **2** and **1**, respectively. The ^{1}H T_1 times of the signals, determined in spinning and static samples by inversion-recovery experiments performed at two carrier frequencies centered at positions of both resonances are given in Table 8. The very short ^{1}H T_1 time of paramagnetic **1** in material **1-40-2-40** does not depend on the spinning rate or on the temperature, in agreement with the dominance of the Fermi-contact relaxation mechanism for the Cp protons of **1**.[15,16] The ^{1}H T_1 time of the diamagnetic compound **2** is substantially longer, slightly diminished upon cooling and it depends on the spinning rate. This dependence indicates the spin-diffusion relaxation mechanism,[15,16] that is effective for the diamagnetic compound **2**.

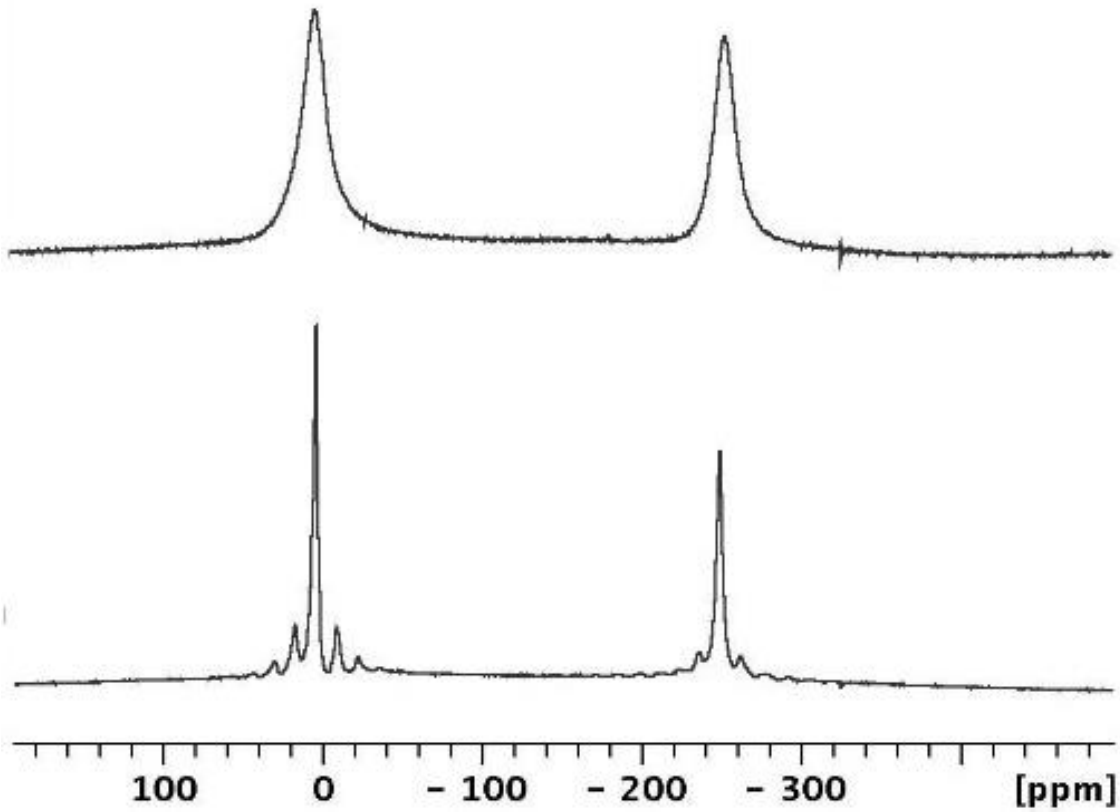

Figure 32. ^{1}H solid-state NMR spectra of material **1-40-2-40** recorded at 295 K in the static (top) and spinning (5 kHz) regime (bottom).

Table 8. ^{1}H T_1 relaxation times (ms) measured for compound **1** and **2** in static (st) and spinning (sp) material **1-40-2-40**.

T (K)	**2** **T_1(st) / T_1(sp)**	**1** **T_1(st) / T_1(sp)**
305	12 / 12.6 (8 kHz)	0.43 / 0.44 (8 kHz)
295	9.8 / 14.0 (5 kHz)	0.45 / 0.42 (5 kHz)
283	9.1 / 14.0 (5 kHz) 16.8 (8 kHz)	0.36 / 0.35 (5 kHz)
273	8.4	0.35
263	7.0	-
253	-	0.32
243	-	0.35
223	-	0.42

The obtained data show that molecules of **1** and **2** are neighboring in the pores of **1-40-2-40**, where they are mixing on the molecular level. The spin-diffusion effective for compound **2** is caused by strong proton-proton dipolar coupling between these molecules. It is remarkable that the spin-diffusion relaxation is effective for protons of **2** in spite of the relatively narrow signals in the ^{1}H NMR spectra in Figure 32 showing molecular reorientations of both components. Again, the observed behavior is not simple liquid-like because fast mutual molecular reorientations should destroy proton-proton dipolar coupling interactions between molecules of **1** and **2**.

The temperature evolution of the ^{1}H static NMR spectra of **1-40-2-40** and the increase in the spinning sideband intensities in the ^{1}H MAS spectra upon cooling correspond to retarding molecular dynamics of both compounds **1** and **2** on the NMR time scale[5,6] (Figure 33).

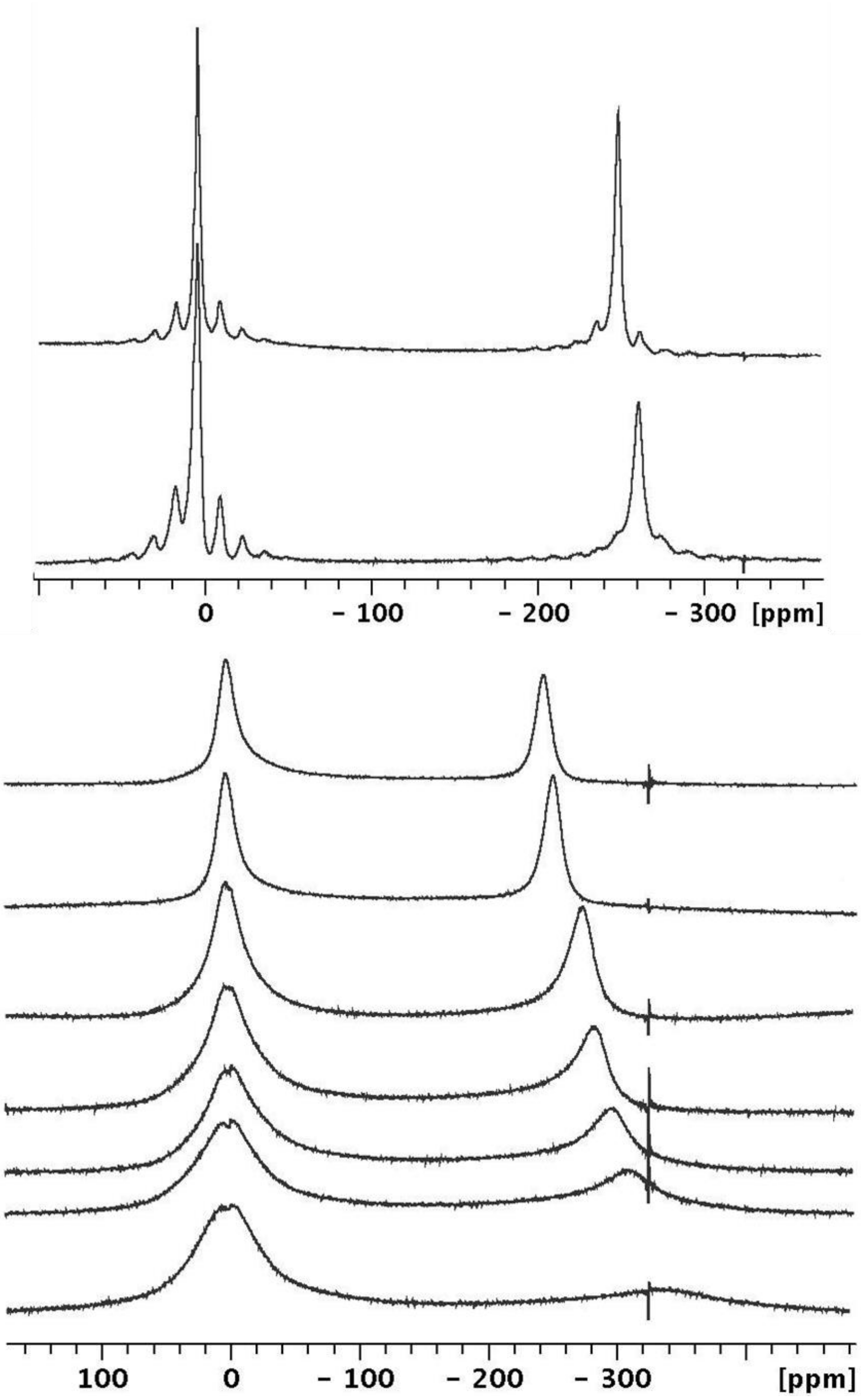

Figure 33. Temperature-dependent ^{1}H NMR spectra of the static sample **1-40-2-40**. From top to bottom: 305, 295, 273, 263, 253, 243, 223 K. The top two traces show the ^{1}H MAS NMR spectra of **1-40-2-40** recorded at a spinning rate of 5 kHz at 295 K (top) and 283 K (bottom).

An important feature of these spectra (Figure 33) should be noted: the line width of the ^{1}H resonance observed for **2** practically does not change from 253 to 223 K. It does remain, however, much larger than that of the ^{1}H resonance in material **2-70** at 203 K, when the molecular motions of **2** are already slow on the NMR time scale.[6] We assume that this broadening effect originates from π-π interactions between the Cp rings of paramagnetic **1** and diamagnetic **2** at low temperatures. At the same time, in the higher temperature ^{1}H MAS spectra of **1-40-2-40**, the resonance of **2** is relatively sharp. Moreover, the ^{1}H T_1 time, determined for compound **2** in material **1-40-2-40** at 295 K as 9.8 ms, could correspond to a line width Δν of 32 or 102 Hz for Lorentz or Gauss resonance shapes. However, the observed line width of Δν = 6.2 kHz is much more larger, thus reflecting molecular dynamics of **2** at least at higher temperatures.

The variable temperature static ^{1}H NMR spectra of material **1-20-2-20** in Figure 34 are similar to those of **1-40-2-40**. They show again the retardation of motions for both compounds upon cooling. In addition, the ^{1}H T_1 times, determined at 295 K for **2** and **1** in material **1-20-2-20** as 11.2 and 0.42 ms, respectively, are again similar to those in material **1-40-2-40**.

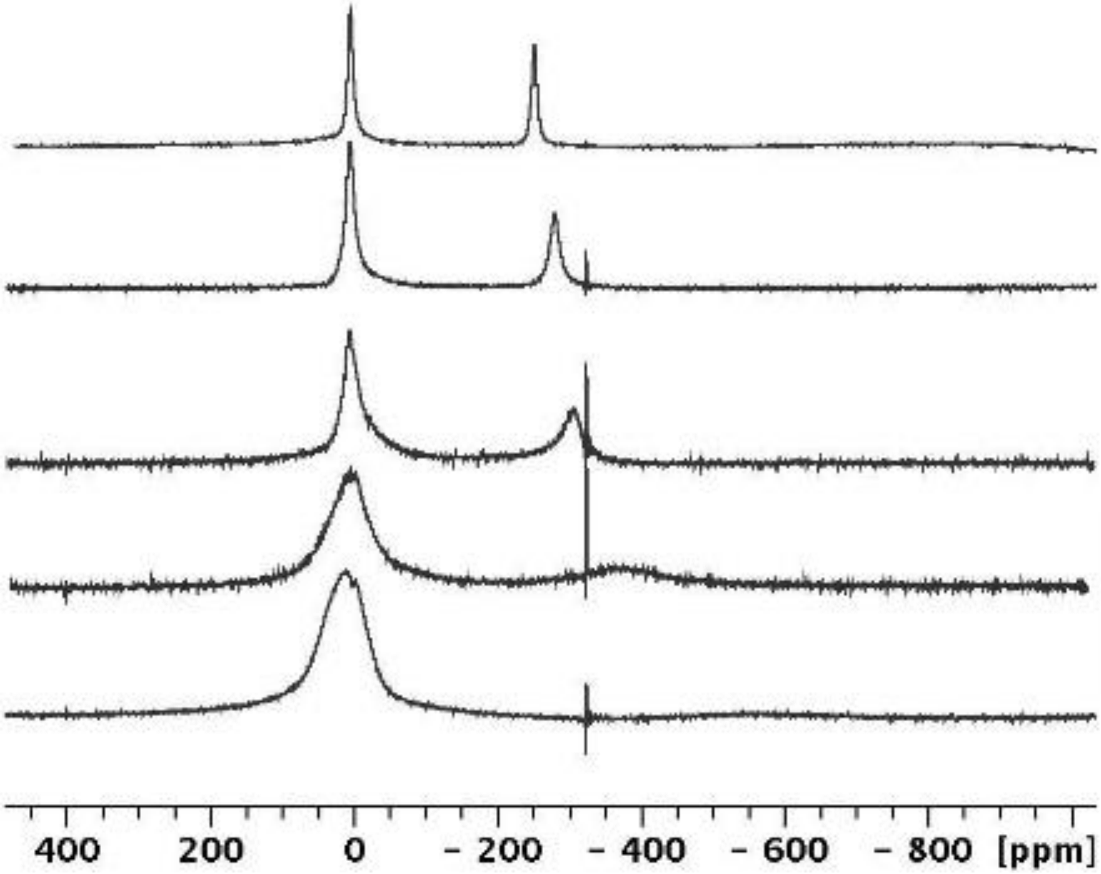

Figure 34. Temperature-dependent ^{1}H NMR spectra of static **1-20-2-20**. From top to bottom: 295, 273, 253, 223 K and 185 K.

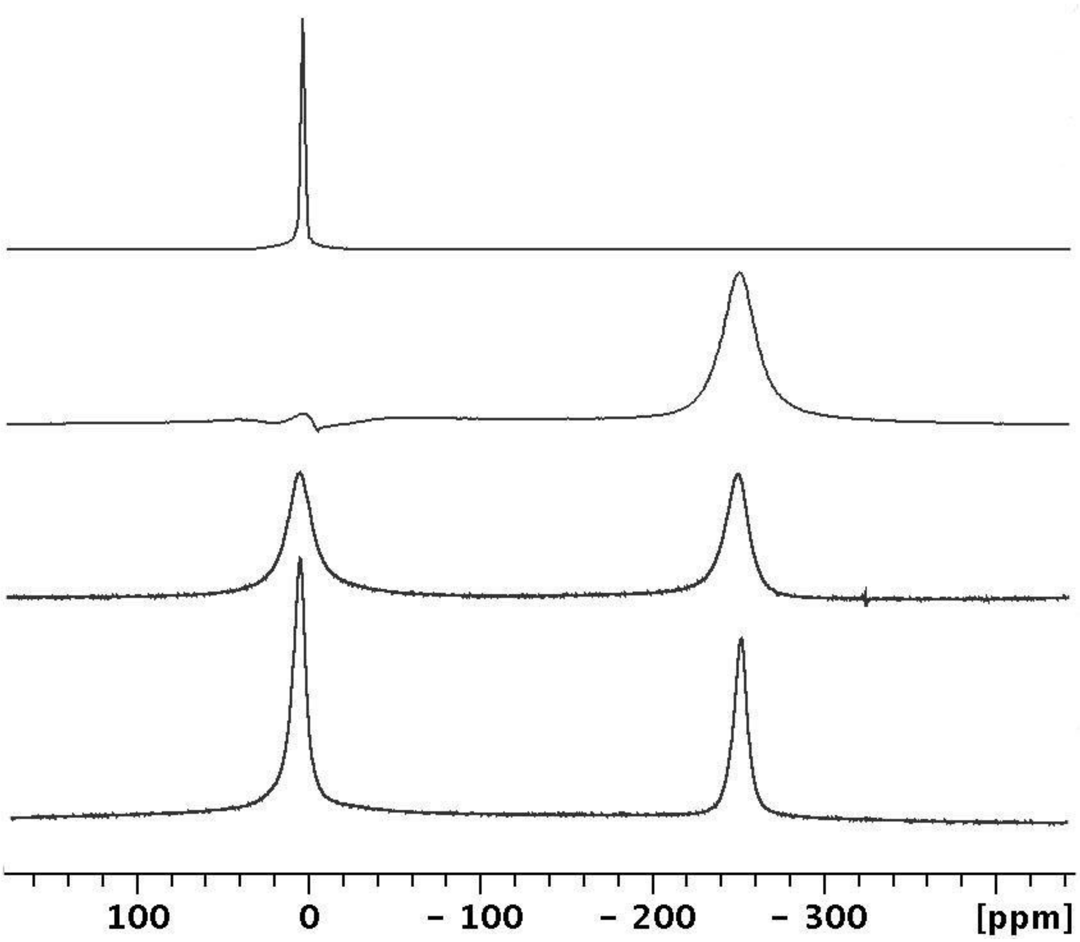

Figure 35. Static ^{1}H NMR spectra obtained at 295 K after subtracting the background signal from the NMR probe head. From top to bottom: **2-70**, **1-70**, **1-40-2-40** and **1-20-2-20**.

The room temperature static ^{1}H NMR spectra of materials **1-70**, **2-70**, **1-40-2-40** and **1-20-2-20** are compared in Figure 35. In spite of the similar total surface coverages in the materials **1-70**, **2-70** and **1-40-2-40** (i.e. similar number of free surface sites), the molecular motions in material **1-40-2-40** are *faster* for compound **1** (its resonance in **1-40-2-40** is narrower than that in **1-70**) but *slower* for compound **2**. Therefore, we observe an opposite mutual influence of the components when theiy are mixed on the surface.

Quantitatively this effect is shown for compound **1** in Table 9, where the rate constants characterizing the motions were obtained by the line-shape analysis as described previously.[6] We believe that this non-trivial result can be interpreted within the limits of the HVLM.

Table 9. Comparing the rate constants k (s^{-1}), obtained from the signal of adsorbed 1 by an analysis of the static ^{1}H NMR spectra of materials **1-20-2-20, 1-40-2-40** and **1-70** at 295 and 273 K.

T (K)	**Material**	**k·10^3 (s^{-1})**
295	**1-20-2-20**	3500
	1-40-2-40	1250
	1-70	830
273	**1-20-2-20**	1720
	1-40-2-40	900
	1-70	450

In fact, according to previous results,[5,6] the variable temperature ^{13}C, ^{2}H, and ^{1}H NMR spectra of individual ferrocene molecules within the pores of silica have shown *the simultaneous presence of isotropically- and anisotropically-moving ferrocene molecules*, i.e. the free and absorbed states of **2** co-exist on the surface. This is not observed for compound **1**, most probably due to stronger interactions of **1** with the silica surface. Within the realm of the HVLM model, the effect observed in **1-40-2-40** can be rationalized as *mixing two highly-viscous liquids* with different viscosities, where **2** on the silica surface plays the role of a component with lower viscosity. Finally, the ^{1}H NMR spectra in Figure

35 show clearly an acceleration of the motions for both molecular components when going from **1-40-2-40** to **1-20-2-20**. It is obvious that within the boundaries of the HVLM model this can be explained by an increase of free surface sites within the silica pores.

Conclusion

The comprehensive solid-state NMR study of paramagnetic nickelocene and diamagnetic ferrocene adsorbed on a silica surface has provided important insights into the dynamic processes on the surface. Materials with different surface coverages, including systems with mixed components on the surface, have allowed us to determine the phase states of metallocene molecules on the silica surface. The adsorbed metallocenes **1** and **2** are mixing on the molecular level on the surface and can be described as highly viscous liquids.

Experimental Section

Materials. The silica (Merck, 40 Å average pore diameter, 0.063-0.2 mm average particle size, specific surface area 750 m^2/g) was dried *in vacuo* at 200° C for 2 days to remove adsorbed water and condense surface silanol groups.

Sample preparation. The maximal surface coverage of the silica with **2** has been determined earlier.[4] Since ferrocene and nickelocene have the same foot prints, samples of adsorbed **1** can be prepared using the same molar amounts. Sample **1-70** was prepared by dry grinding of 191.0 mg (1.011 mmol) of Cp_2Ni (**1**) with 256 mg of silica in a glove box for 1.5 minutes using a pestle and mortar. Sample **1-140** was created by dry grinding of **1** (188.0 mg, 0.995 mmol) with 127 mg of silica. The sample **1-200** was generated by dry grinding of 277.0 mg (1.467 mmol) of **1** with 126 mg of silica. For sample **1-40-2-40** 0.500 g of silica was grinded together with 0.113 g (0.607 mmol) of Cp_2Fe, and 0.116 g (0.614 mmol) of Cp_2Ni in a glove box. Sample 1-20-2-20 was prepared analogously by using the same amounts of Cp_2Fe and Cp_2Ni together with 1.00 g of silica. All samples of **1** adsorbed on silica displayed a moss green color, materials with adsorbed **1** and **2** were lime green.

NMR measurements. The ^{13}C, ^{1}H MAS and static NMR experiments were carried out with a Bruker Avance 400 solid-state NMR spectrometer (400 MHz for ^{1}H nuclei) equipped with a two-channel 4 mm MAS NMR probe head. The standard single-pulse and Hahn-echo sequences were applied for ^{1}H and ^{13}C nuclei, correspondently. The Hahn-echo experiments were synchronized with spinning rates.

The ^{1}H T_1 times were determined by inversion−recovery (180°−τ−90°) experiments with well calibrated rf- pulses with relaxation (recycle) delays corresponding to full nuclear relaxation in each cycle. In the mixed systems due to the large chemical shift difference for **1** and **2** the relaxation times were obtained at two carrier frequencies centered at positions of both resonances.

The variable-temperature ^{1}H NMR data have been collected with a standard temperature unit of the spectrometer calibrated with liquid methanol placed into a 4 mm rotor.

The side-band analysis to determine ^{1}H CSA values and the line-shape analysis of the static ^{1}H NMR spectra were performed with the corresponding programs in the software package of the Bruker spectrometer.

All samples were densely packed into the insert-free rotors as finely ground powders. Compressed nitrogen was used as both the bearing and drive gas for the MAS measurements.

References

1. Buntkowsky, G.; Vogel, M. Small molecules, non-covalent interactions, and confinement, *Molecules* **2020**, *25*, 3311, 1-32.

2. L. D. Gelb, K. E. Gubbins and R. Radhakrishnan, Rep. Prog. Phys., 1999, 62(12), 1573–1659.

3. Le Bideau, J.; Gaveau, P.; Bellayer, S.; Neouze, M.A.; Vioux, A. Effect of confinement on ionic liquids dynamics in monolithic silica ionogels: H-1 NMR study. Phys. Chem. Chem. Phys. **2007**, 9, 5419–5422.

4. Cluff, K. J.; Blümel, J. Adsorption of metallocenes on silica, *Chem. Eur. J.* **2016**, *22*, 16562 – 16575.

5. Hubbard, P. J.; Benzie, J. W.; Bakhmutov, V. I.; Blümel, J. Ferrocene adsorbed on silica and activated carbon surfaces: a solid-state NMR study of molecular dynamics and surface interactions, *Organometallics* **2020**, *39*, 1080–1091.

6. Benzie, J. W.; Bakhmutov, V. I.; Blümel, J., *in preparation*.

7. Meier, R.; Kahlau, R.; Kruk, D.; Rossler, E. A. Comparative studies of the dynamics in viscous liquids by means of dielectric spectroscopy and field cycling NMR, *J. Phys. Chem. A*, **2010,** *114*, 7847–7855.

8. Kruk, D.; Mielczarek, A; Korpala, A.; Kozlowski, A.; Earle, K. A.; Moscicki, J. Sensitivity of ^{2}H NMR spectroscopy to motional models: proteins and highly viscous liquids as examples, *J. Chem. Phys*. **2012**, *136,* 244509.

9. Polimeno, A.; Freed, J. H. A many-body stochastic approach to rotational motions in liquids: complex decay times in highly viscous fluids, *Chem. Phys. Letters*. **1990**, *16*, 481-488.

10. Rossler, E.; Tauchert, J.; Eiermann, P. Cooperative reorientations, translation motions, and rotational jumps in viscous liquids, *J. Phys. Chem.* **1994**, *98*, 8173-8180.

11. Heise, H.; Köhler, F. H.; Xie, X. Solid-state NMR spectroscopy of paramagnetic metallocenes, *J. Magn. Reson*. **2001**, *150***,** 198–206.

12. Pritchard, B. P.; Simpson, S.; Zurek, E.; Autschbach, J. Computation of chemical shifts for paramagnetic molecules: a laboratory experiment for the undergraduate curriculum, *J. Chem. Educ*. **2014**, *91*, 1058−1063.

13. Köhler, F. H.; Xie, X. Vanadocene as a temperature standard for $^{\mathbf{13}}$C and $^{\mathbf{1}}$H MAS NMR and for solution-state NMR Spectroscopy, *Magn. Reson. Chem*. **1997**, *35*, 487-492.

14. Martin, B.; Autschbach, J. Temperature dependence of contact and dipolar NMR chemical shifts in paramagnetic molecules, *J. Chem. Phys*. **2015**, *142*, 054108.

15. Pell, A. J.; Pintacuda, G.; Grey, C. P. Paramagnetic NMR in solution and the solid state, *Progr. Nucl. Magn. Reson. Spectr*. **2019,** *111*, 1–271.

16. Bakhmutov, V. I. Strategies for solid-state NMR studies of materials: from diamagnetic to paramagnetic porous solids, *Chem. Rev*. **2011**, *111*, 530–562.

CHAPTER V

CONCLUSION

The adsorption studies that were performed have provided fundamental knowledge about the interactions of organic and metallocenes molecules adsorbed on to the surfaces of silica and activated carbon, as well as providing insight highly viscous liquid-like nature of mixed metallocenes on silica. First, three different states of benzene on the surface of **AC** have been found: isotropically moving molecules, bound molecules, and intermediates between these states have been found. Different surface coverages, from a dilute sub-monolayer to a more densely packed monolayer were produced. These samples were studied via multinuclear ^{2}H and ^{13}C variable temperature solid-state NMR techniques. The stationary molecules are stabilized through π-p interactions with the **AC** surface, experience fast in-plane C_6 rotations. Benzene-d_6 in semibound states, are similar to T-complexes in benzene dimers, rotating perpendicularly to the surface. The adsorption enthalpy $-\Delta H^0$ for benzene on the pore surface was determined to be 4.6 kcal/mol, with this value being larger than the π- π binding interactions in benzene dimers calculated in the gas phase, but smaller than the adsorption enthalpy found for horizontally oriented ferrocene molecules on the pore surface of **AC**. The exchange between semibound and isotropically moving benzene molecules is fast, only requiring a low activation energy.

Nickelocene was adsorbed within pores on the surface of silica by dry grinding in absence of solvents at room temperature. Using paramagnetic variable temperature ^{1}H solid-state NMR and T_1 relaxation time measurements, the dynamics of nickelocene within these pores has been quantitatively characterized on the molecular scale. The obtained data indicates that nickelocene molecules exhibits liquid-like behavior on the surface. Fast exchange between isotropically moving molecules and surface-attached molecular states of nickelocene has been found in a sample with sub-monolayer surface coverage. The surface-attached molecular states have been quantified. The temperature dependencies of the rate k in coordinates of ln(k) versus 1/T and ln(k/T) versus 1/T form ideal straight lines that allow the determination of the kinetic parameters $E_{act} = 5.5$ kcal/mol, $A = 1.1 \cdot 10^{10}$, $\Delta H^{\ddagger} = 5.0$ kcal/mol, and $\Delta S^{\ddagger} = -15$ e.u.

Finally nickelocene on silica is further investigated utilizing paramagnetic variable temperature ^{1}H solid-state NMR and T_1 relaxation time measurements. Using samples with additionally adsorbed ferrocene, and different surface coverages, have allowed us to determine the phase states of metallocene molecules on the silica surface. It could be proven that both metallocenes mix on the molecular level on the surface. The phase states of both components can be described as highly viscous liquids.

APPENDIX A

CHAPTER II SUPPLEMENTAL DATA

This supporting information contains **Figures S1−S7** and **Table S1**.

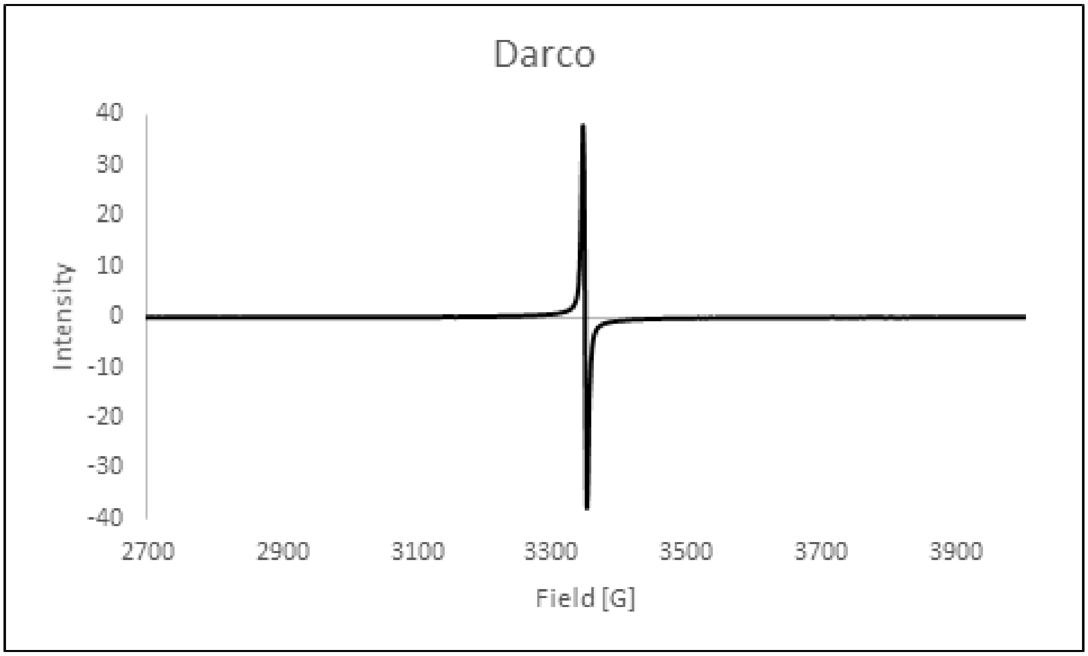

Figure S1. Single-scan ESR spectrum of **AC** at room temperature.

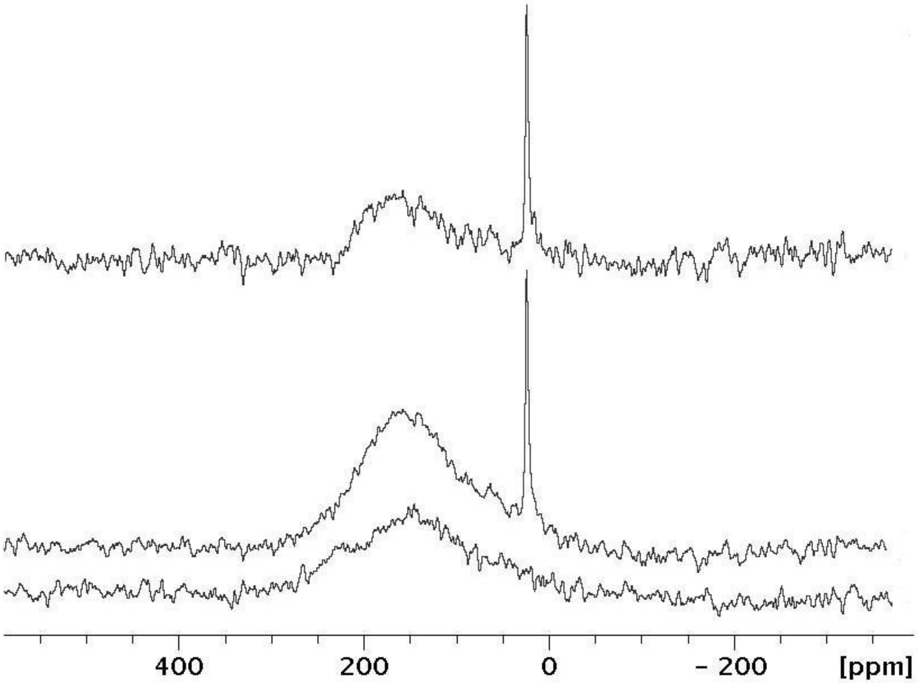

Figure S2. The room-temperature $^{13}C\{^1H\}$ NMR spectra recorded without rotation under the same conditions for **AC-C$_6$D$_{12}$-55** (middle) and the empty rotor (bottom). The difference spectrum (top) shows the broad **AC** signal and the isotropic benzene resonance. The relative intensities of both signals can be determined from the top spectrum.

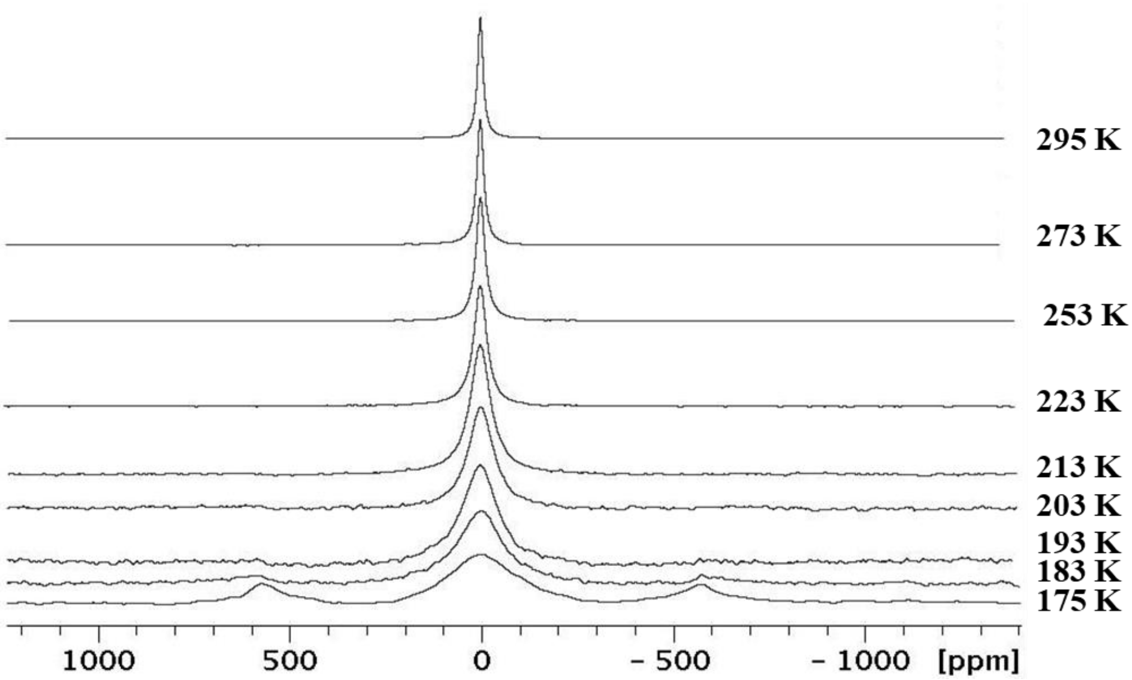

Figure S3. VT ^{2}H NMR spectra obtained for the static sample **AC-C$_6$D$_6$-620** with the Hahn-echo (90°-τ-180°-τ) pulse sequence.

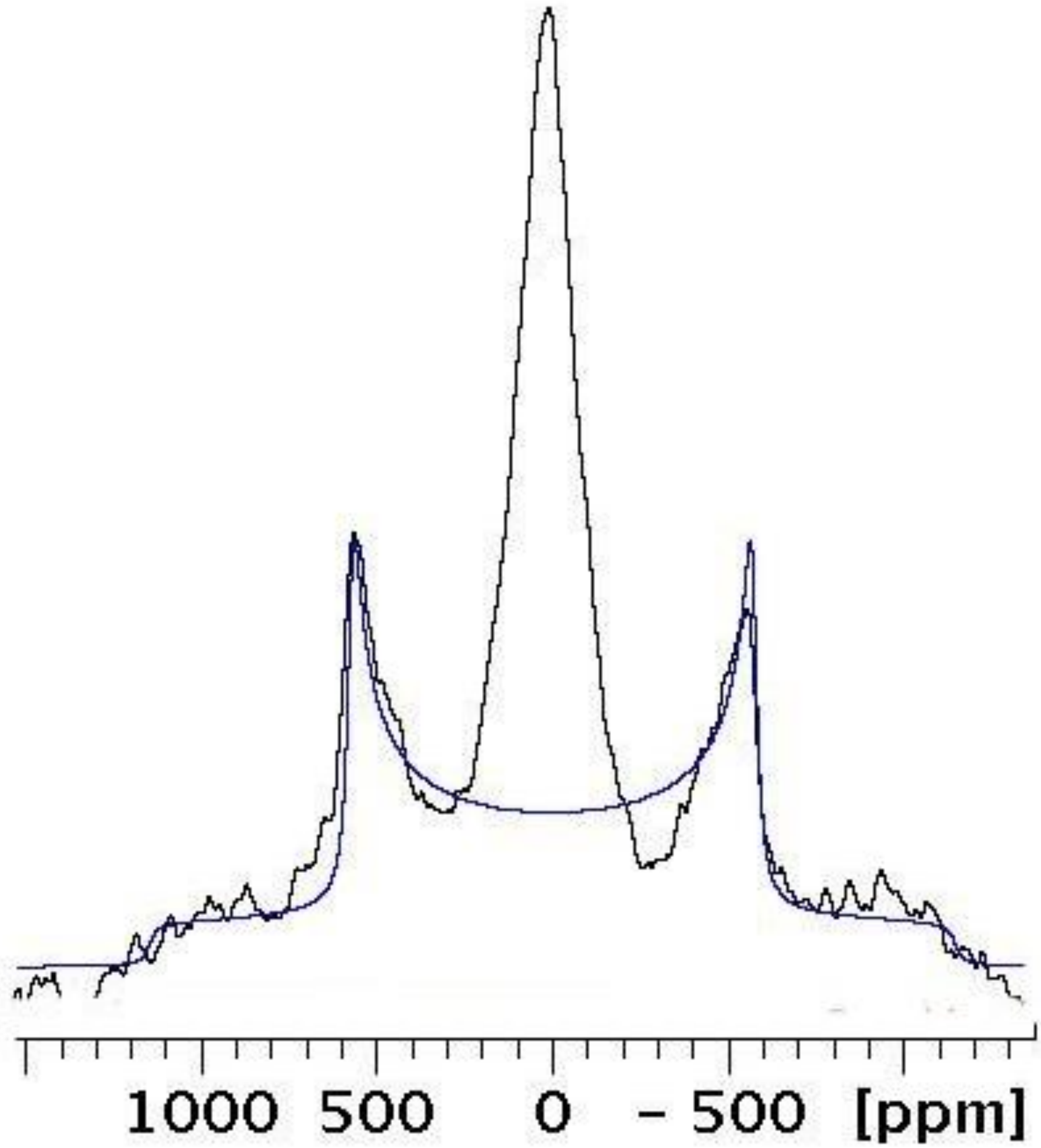

Figure S4. Quadrupolar ^{2}H Pake pattern of stationary benzene molecules observed for sample **AC-C$_6$D$_6$-620** at 175 K, corresponding to a deuterium quadrupolar coupling constant (C_Q) of 92 ± 3 kHz with an asymmetry parameter $\eta = 0.0$.

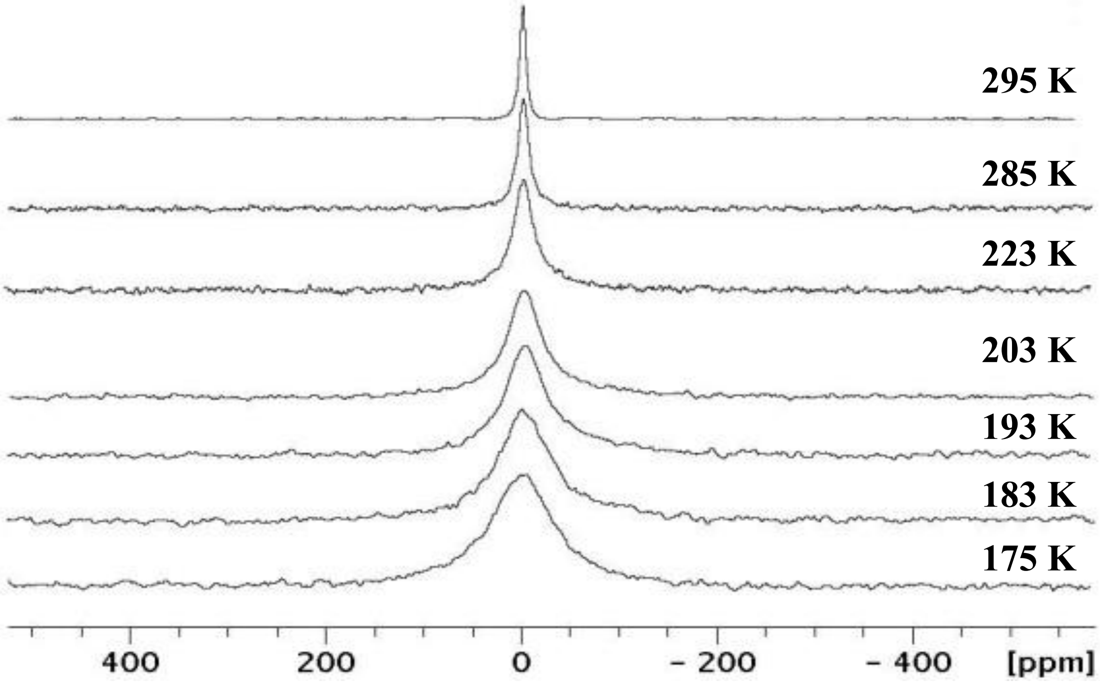

Figure S5. Hahn-echo ^{2}H NMR spectra obtained from a static sample of **AC-C_6D_{12}-55** at the indicated temperatures.

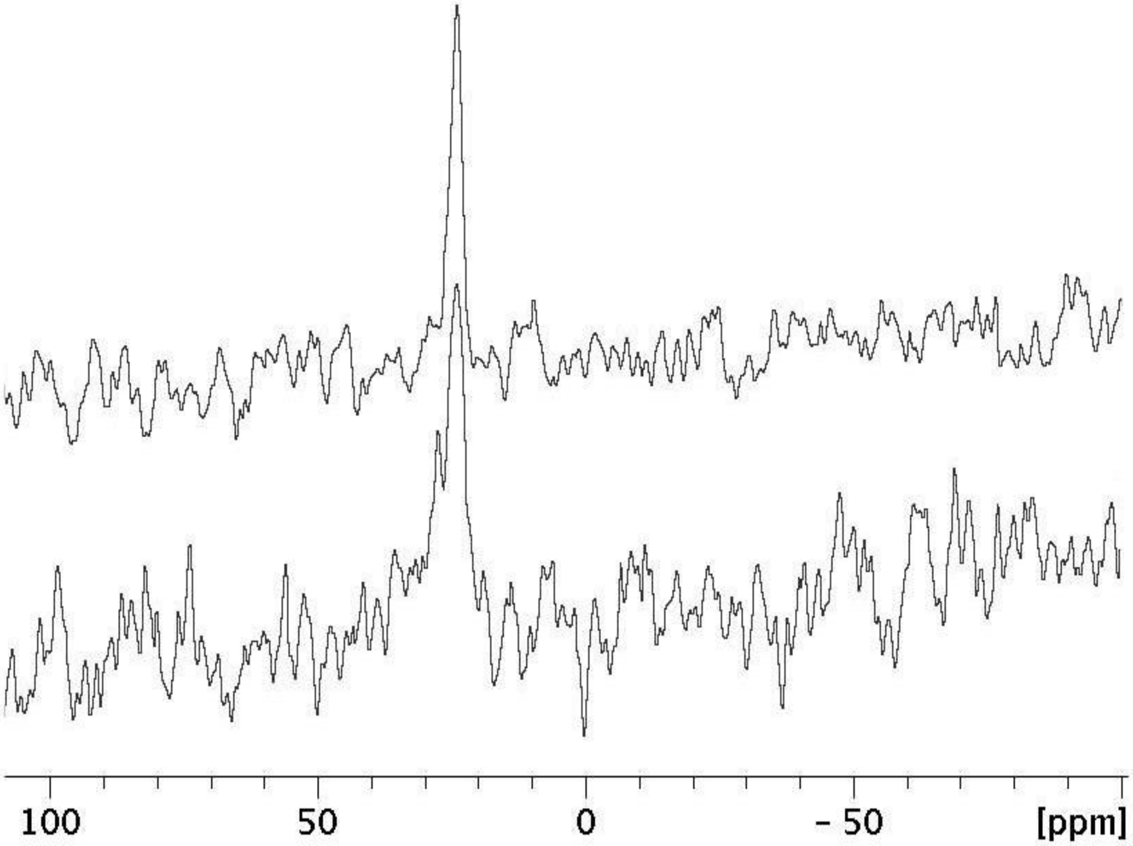

Figure S6. $^{13}C\{^{1}H\}$ NMR spectra of the static sample **AC-C$_6$D$_{12}$-55** at 295 K (top) and 175 K (bottom).

Table S1. The temperature dependence of the halfwidths (Δν) for the central components of the ^{2}H signals observed for the static samples **AC-C_6D_6-370**, and **AC-C_6D_{12}-55.**

AC-C_6D_6-370		**AC- C_6D_{12}-55**	
Δν (kHz)	T (K)	Δν (kHz)	T (K)
1.2	295	0.7	295
1.5	273	0.9	285
1.8	253	1.6	223
2.3	233	2.5	203
3.9	213	3.0	193
4.6	203	3.9	183
6.2	193	4.7	175
8.3	185		
12.6	175		

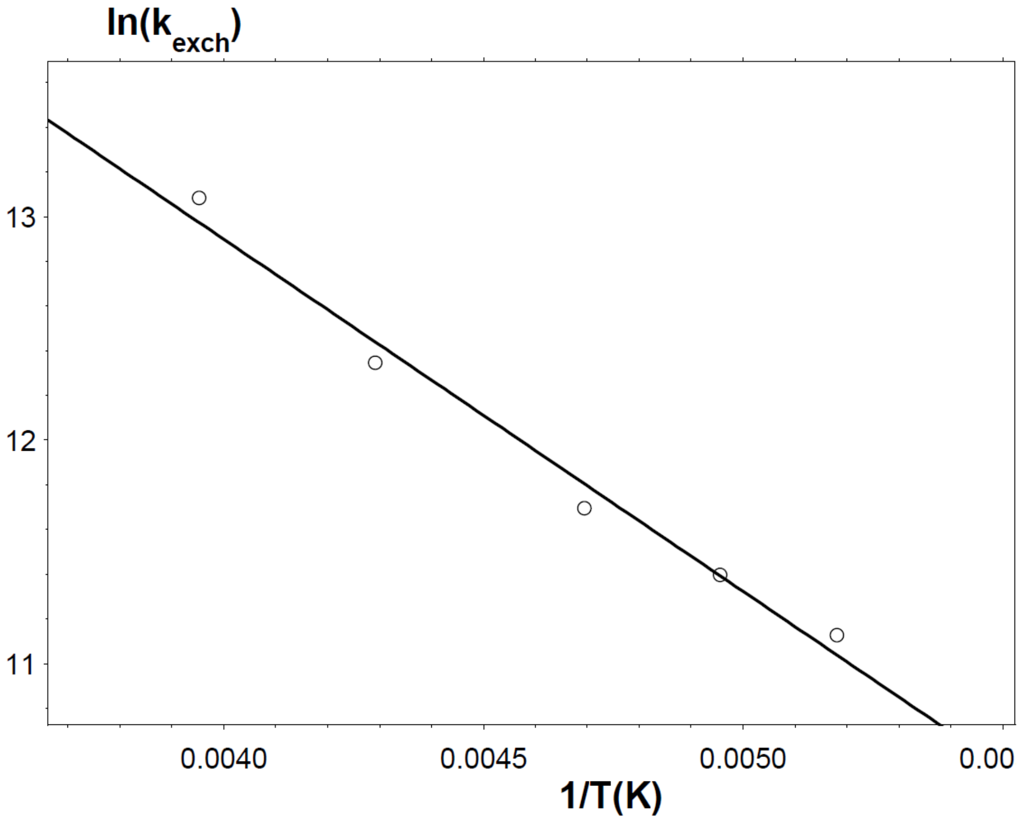

Figure S7. The temperature dependence of the rate constants k_{exch} in Table 2, obtained from the central component in the ^{2}H NMR spectra of **AC-C_6D_6-370**, presented in the coordinates $\ln(k_{exch})$ versus 1/T.